Aus dem Institut für Pathologie

der Medizinischen Fakultät Mannheim

(Direktor: Prof. Dr. med. Christoph Brochhausen-Delius)

Long-term response to trastuzumab in patients with HER2-positive advanced gastric or gastroesophageal adenocarcinoma

Inauguraldissertation

zur Erlangung des Doctor scientiarum humanarum (Dr. sc. hum.)

der

Medizinischen Fakultät Mannheim

der Ruprecht-Karls-Universität

zu

Heidelberg

vorgelegt von

Isabel Porth

aus

Darmstadt

2023

Dekan: Prof. Dr. med. Sergij Goerdt
Referent: Prof. Dr. med. Timo Gaiser

Preliminary remark

Partial results of the presented thesis have been published:

Porth I, Hirsch D, Ceribas Y, Weidner P, Weichert W, Götze TO, Perner S, Luley K, Heyer CM, de la Torre C, Hofheinz RD, Lorenzen S, Gaiser T. Comprehensive biomarker analysis of long-term response to trastuzumab in patients with HER2-positive advanced gastric or gastroesophageal adenocarcinoma. Eur J Cancer. 2023 Apr;183:119-130. doi: 10.1016/j.ejca.2023.01.022. Epub 2023 Feb 3. PMID: 36848831

TABLE OF CONTENT

LIST OF FIGURES

LIST OF TABLES

LIST OF ABBREVIATIONS

5FU	5-fluorouracil
ACRG	Asian Cancer Research Group
ADC	antibody-drug conjugates
AF	allele frequency
CEP17	centromere chromosome 17 probe
ChT	chemotherapy
CI	confidence interval
CIN	chromosomal instability
CN	copy number
CNV	copy number variant
CPS	combined positive score
CYT	cytolytic activity
DAB	3,3N-Diaminobenzidine Tertrahydrochloride
DAPI	4′,6-diamidino-2-phenylindole
DEG	differential expressed genes
DP	read depth
EBV	Epstein-Barr virus
EMA	European Medicines Agency
EMT	epithelial-mesenchymal transition
ERBB	epidermal growth factor receptor
ERBB2	human epidermal growth factor receptor 2 (gene)
ERBB2:CEP17	ratio of ERBB2 to CEP17 signals
ERBB2d16	ERBB2 deletion of exon 16
EtOH	ethanol
FDA	US Food and Drug Administration
FFPE	formalin-fixed paraffin-embedded
FISH	fluorescence in situ hybridization
FLO	5FU/leucovorin/oxaliplatin
FLOT	5FU/leucovorin/oxaliplatin/docetaxel
GC	gastric cancer
GEJ	gastroesophageal junction
GEJC	gastroesophageal junction adenocarcinoma
GEO	Gene Expression Omnibus
GS	genomically stable
GZMA	granzyme A

H&E	hematoxylin and eosin
HER2	human epidermal growth factor receptor 2 (protein)
HR	hazard ratio
HRP	horseradish peroxidase
IHC	immunohistochemistry
ISH	in situ hybridization
Mb	megabase
mGEJ	metastatic or advanced gastric cancer
mGEJC	metastatic or advanced gastroesophageal junction adenocarcinoma
MSI	microsatellite instability
MSS	microsatellite stable
mut/Mb	somatic mutations per megabase
ND	not determined
NGS	next-generation sequencing
OCA	Oncomine comprehensive assay
ORR	objective response rate
OS	overall survival
PCR	Polymerase-chain reaction
PD-L1	programmed death-ligand 1
PFS	progression-free survival
PLF	cisplatin/leucovorin/5FU
PoN	panel of normals
PRF1	perforin 1
RT	room temperature
RTK	receptor tyrosine kinase
SISH	silver in situ hybridization
SNV	single nucleotide variant
TAS	targeted amplicon sequencing
TCGA	The Cancer Genome Atlas
Tcm	T-cell central memory
T-DM1	trastuzumab emtansine
T-Dxd	trastuzumab deruxteca
Tem	T-cell effector memory
TMB	tumor mutational burden
TML	Tumor Mutation Load
TP53	tumor protein P53
UDG	uracil-DNA glycosylase

WES	whole exome sequencing
WGS	whole genome sequencing
WHO	World Health Organization
PD-1	programed death protein 1

1 Introduction

1.1 Gastric and gastroesophageal adenocarcinoma

1.1.1 Epidemiology

With over 1 million new cases and over ¾ million entity specific deaths in 2020, gastric cancer (GC) has the fifth-highest incidence and is the fourth leading cause of cancer-related deaths worldwide [1]. However, incidence rates vary significantly depending on the location, age at diagnosis and gender. Approximately 60% of GC cases worldwide are diagnosed in East Asia, while less than 10% occur in Europe [2]. According to the European Cancer Information System, GC accounts for 2.8% of cancers diagnosis in Europe and has led to 4.1% of cancer-related mortality in 2020 [3]. GC affects men approximately twice as often as women, resulting in a global male-to-female rate of 2.24 [4,5]. In general, GC is uncommon in adults under 50 years, but its incidence increases with age in both sexes and reaches a plateau between 55 and 88 years [5,6]. The 5-year survival rate for GC is approximately 30-35%, reflecting the fact that a high proportion of cases (40-70%) are diagnosed at metastatic stage [7-9]. However, when GC is diagnosed at an early resectable stage (T1a), the 5-year survival rate increases to 44-90% [10,11]. The high number of advanced stage diagnoses can be attributed to the lack of specific symptoms during the early stages of GC and missing screening programs. Common symptoms of advanced-stages GC include weight loss, indications of upper intestinal bleeding and dysphagia [12].

Overall the incidence of GC is steadily declining in the western population, while an increase in esophageal adenocarcinoma, including gastroesophageal junction (GEJ) carcinoma, which occurs in close proximity to the stomach, has been reported [13,14]. Several factors have contributed to the decrease in GC incidence, such as the treatment of *Helicobacter pylori* infection, improved hygiene standards, improved food preservation and storage, and reduced tobacco consumption [15]. In Northern Europe and Northern America, adenocarcinoma account for more than 60% of esophageal cancers [4]. Increased body weight and gastroesophageal reflux disease may have contributed to the increase in esophageal adenocarcinoma cases in the Western world [16].

1.1.2 Pathology

The majority of GCs are adenocarcinomas (>90%) [17]. Approximately 18% of GC occur in the cardia, which is in close proximity to the GEJ and the esophagus (Figure 1) [4]. There are two

main histologic subtypes of esophageal cancer: squamous cell carcinomas, predominantly located in the upper two-thirds of the esophagus, and adenocarcinomas, typically found in the lower third of the esophagus [18]. Molecular analysis revealed that esophageal adenocarcinomas are more closely related to GC than to esophageal squamous cell carcinoma [19]. It has been suggested that GEJ adenocarcinomas (GEJC) and GC can be considered as a single entity, at least on the molecular level [19]. The anatomical classification of GEJC consists of three Siewert types (Siewert type I-III), which describe the distance of the tumor epicenter to the GEJ (Figure 1) [20]. Siewert type I cancers have the epicenter located 1-5 cm above the GEJ. Siewert type II cancers span the GEJ and are located 1 cm above or 2 cm below the GEJ. Tumors located 2-5 cm aboral of the GEJ in the gastric cardia are classified as Siewert Type III. The Siewert types are relevant for the selection of the appropriate surgical procedure [21]. Carcinomas of the GEJ are not considered a separate entity according to the TNM-classification system and are staged as either esophageal or gastric carcinoma. By definition, a GEJ adenocarcinoma is staged as esophageal if the epicenter is located within 2 cm of the gastric cardia [22]. If the tumor is located lower than 2 cm in the gastric cardia, it is staged as GC.
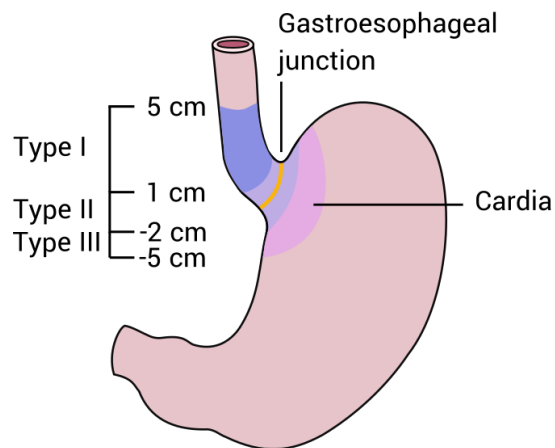
Figure 1 | Siewert classification of gastroesophageal junction carcinoma
Gastroesophageal junction carcinoma are classified according to the distance to the gastroesophageal junction (orange) into three Siewert Types.

The leading histologic classification systems for GC are the Lauren classification and the World Health Organization (WHO) classification. The Lauren classification system was developed in 1965 and categorizes GC into three major subtypes: Intestinal, diffuse or mixed type [23]. The intestinal type is characterized by cohesive tumor cells arranged in tubular or glandular formations, and it is the most common subtype, particularly among males and older patient [23,24]. This subtype is also associated with overexpression of the human epidermal growth factor receptor 2 (HER2) and microsatellite instability (MSI) [25,26]. In contrast, the diffuse

subtype is characterized by discohesive tumor cells, which leads to infiltration of single tumor cells or cell groups into the stroma [23]. The incidence of diffuse type GC is higher in younger and female patients [27]. In addition, the diffuse and mixed type are associated with lymph node metastasis [28]. On the contrary, the WHO classification describes five histologic subtypes (papillary, tubular, mucinous, singlet-ring cell and mixed) [29]. The papillary, tubular and mucinous types are comparable with the Lauren intestinal type, while the signet-ring cell type is similar to the Lauren diffuse type. Although the WHO classification system does not have direct clinical relevance, the Lauren classification subtypes have an impact on the recommended resection margins according to the German S3 guideline. Intestinal subtype GC is resected with a margin of 5 cm and diffuse GC with a margin of 8 cm [21].

1.1.3   Therapy

Therapy for GC is based on TNM tumor staging, tumor location and the presence of biomarkers. The evaluation of the biomarkers HER2, programmed death-ligand 1 (PD-L1) and microsatellite status is recommended [17].

In cases of localized GC (stage IA-III), the primary treatment modality is surgical resection. The type of surgical procedure, gastrectomy (subtotal or total), a distal esophagectomy or endoscopic mucosal resection, is chosen according to the tumor location and depth of tumor invasion. For stage IB to stage III, it is recommended to combine the resection with perioperative systemic chemotherapy, whereby surgery alone remains an option for stage IB [17]. The commonly used regimen in perioperative treatment for GC and GEJC is the triplet chemotherapy known as FLOT, which includes 5-fluorouracil (5FU), oxaliplatin, leucovorin, and docetaxel. FLOT has demonstrated superior overall survival compared to therapy with 5FU/capecitabine with cisplatin and epirubicin [30]. In advanced or metastatic stages, chemotherapy is administered alone or in combination with targeted therapy if the tumor is positive for the treatment-specific biomarker (Figure 2). Chemotherapy usually consists of a platinum compound and a fluoropyrimidine [17].
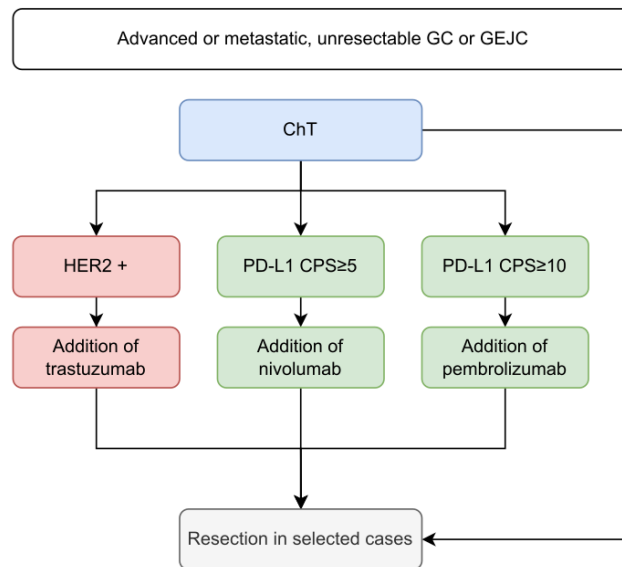
Figure 2 | First-line therapy recommendations for advanced or metastatic unresectable gastric and gastroesophageal cancer (GC/GEJC).
Platinum-fluoropyrimindine chemotherapy (blue) can be combined with immunotherapies, marked in green, or HER2-targeting therapy, displayed in red, when biomarker requirements are met. Adapted from Lordick et al. 2022 [17]. ChT, chemotherapy; CPS, combined positive score; PD-L1, programmed death-ligand 1;

In cases with HER2-positive status, the HER2-targeting antibody trastuzumab is added to chemotherapy since 2010 [31]. Since 2021, immunotherapeutic agents nivolumab or pembrolizumab are combined with chemotherapy, depending on the PD-L1 combined positive score (CPS) [32,33]. The CPS describes the expression of PD-L1 on tumor and immune cells relative to total number of tumor cells. A CPS≥5 or CPS≥10 is required for treatment with nivolumab or pembrolizumab, respectively. In case of good response to chemotherapy, tumor resection may be considered even in advanced stages [17]. Treatment decisions for advanced GEJC follow the same guidelines as those for gastric cancer, as described above [17,34].

1.2   HER2 as target in gastric cancer therapy

1.2.1   ERBB receptor family

HER2 is a member of the epidermal growth factor receptor (ERBB) family and is encoded by the *ERBB2* gene on chromosome 17q21 [35,36]. The ERBB family consists of four transmembrane receptor tyrosine kinases (RTKs): *EGFR* (HER1, ERBB1), *ERBB2* (HER2), *ERBB3* (HER3) and *ERBB4* (HER4) [36]. All members of the receptor family share common structural elements such as the intracellular and extracellular domain, a transmembrane region, and a carboxy-terminal region. The extracellular region of the RTKs is composed of

four subdomains with domain I and III forming the ligand binding site, and domain II mediating dimerization [37].The active center of the tyrosine kinase is located in the intracellular domain. ERBB3 is an exception, as it has no intrinsic tyrosine kinase activity and requires dimerization with another receptor of the ERBB family for phosphorylation [38-40]. Binding of a ligand, like the epidermal growth factor or heregulin, induces conformational changes in the extracellular domain and allows the formation of homo- or heterodimers [37]. This leads to mutual phosphorylation of the cytoplasmic tyrosine residues of the receptors. The phosphorylated tyrosine residues serve as binding sites for signaling molecules that subsequently activate downstream signaling cascades such as PI3K/Akt or Ras/MAPK [41,42]. ERBB signaling has versatile functions and is involved in cell proliferation and survival [43]. Interestingly, there is no known ligand for HER2, yet its extracellular domain has an active confirmation that enables dimerization even without ligand binding [44]. The HER2/HER3 heterodimer is the most effective dimer in terms of interaction, receptor tyrosine phosphorylation and signaling cascade activation [40,45]. Spontaneous formation of HER2 homodimers can occur when HER2 is overexpressed, leading to continuous signaling activation, which contributes to invasiveness and increased cell proliferation [46,47].

1.2.2 HER2-targeting in gastric cancer

HER2 overexpression is caused by amplification of the *ERBB2* gene region or by amplification of the whole chromosome 17 (polysomy) and occurs in various cancers such as breast, gastric, lung and ovarian cancer [48-53]. In gastric cancer, HER2 overexpression was first observed in 1986 through immunohistochemistry (IHC), occurring in approximately 12-20% of GC cases and 10-30% of GEJC cases [51,54-56].

Yet in 2000, HER2 was proposed as a potential therapeutic target for GC [57]. Trastuzumab, the first humanized monoclonal HER2-targeting antibody, was developed in 1990 [58]. By binding to the extracellular domain III of HER2, trastuzumab prevents the activation of downstream signaling cascades [58,59]. In addition, trastuzumab induces antibody-dependent cell-mediated cytotoxicity by recruiting immune cells to the tumor [60].

The ToGA study, a phase III trial completed in 2010, evaluated the combination of trastuzumab with chemotherapy in patients with HER2-positive metastatic or advanced GC of GEJC (mGC/mGEJC). The study demonstrated that the addition of trastuzumab to chemotherapy significantly improved overall survival (OS) by 2.7 months compared to chemotherapy alone (hazard ratio (HR) = 0.74; 95%-CI: 0.60-0.91; p=0.0046) [31]. The chemotherapy regimen used in the ToGA trial consisted of cisplatin with either capecitabin or 5FU. Subsequent clinical trials further validated the efficacy and safety of trastuzumab in combination with various chemotherapy regimens for HER2-positive advanced GC and GEJC [61-64]. After combinational

therapy with trastuzumab and chemotherapy, the treatment is often continued without the platinum-based agent as trastuzumab maintenance therapy. Studies have shown that trastuzumab maintenance therapy, either as monotherapy or in combination with a fluoropyrimidine like 5FU, is both safe and effective [65-67].
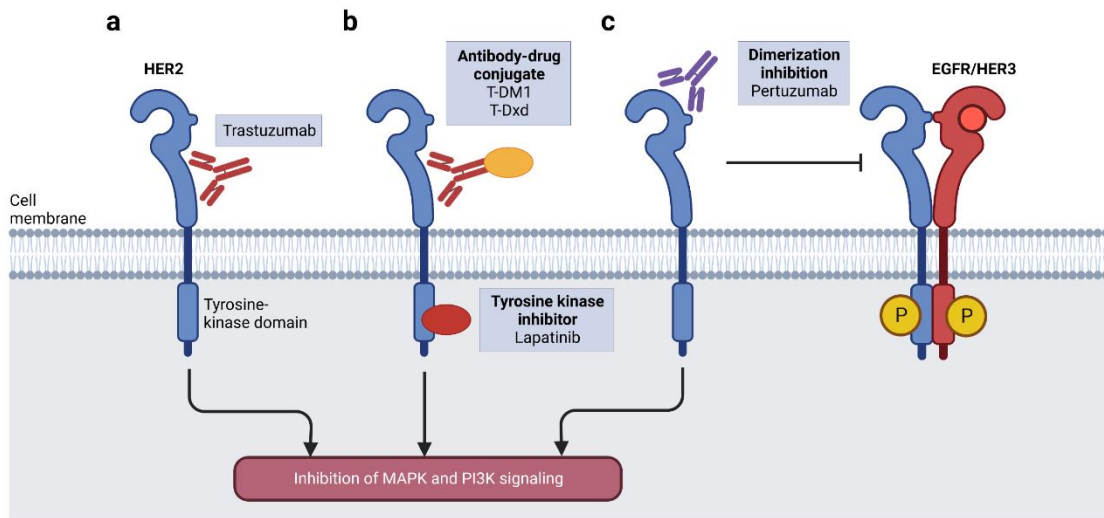
Figure 3 | Mechanisms of action of HER2-targeting therapeutics.
A: Trastuzumab binding to the extracellular domain of HER2. This causes antibody-dependent cell-mediated cytotoxicity but also inhibits downstream signaling. **B:** Anti-body drug conjugates like trastuzumab emtansine (T-DM1) and trastuzumab deruxtecan (T-Dxd) carry a cytotoxic agent coupled to trastuzumab, interfering with signaling activity and inducing drug related apoptosis. Small tyrosine kinase inhibitors like lapatinib block the kinase domain and consequently downstream signaling. **C:** Pertuzumab targets the dimerization domain of HER2 and prevents the formation of signaling active dimers of HER2 with other ERBB family receptors like HER3 and EGFR [68]

Following the tremendous success of the ToGA trial, other HER2-targeting therapies have been explored (Figure 3). Several antibody-drug conjugates (ADCs), such as trastuzumab emtansine (T-DM1) and trastuzumab deruxtecan (T-Dxd), have been developed to improve the efficacy of trastuzumab and overcome resistance by delivering cytotoxic agents to the tumor site. T-DM1 combines trastuzumab with maytansine, an antitubulin molecule that induces apoptosis [69]. However, the combination of T-DM1 with chemotherapy as second-line treatment for HER2-positive metastatic GC and GEJ patients who progressed on trastuzumab treatment, did not result in prolonged survival in the GATSBY trial [70]. Recently, T-Dxd, an ADC of trastuzumab linked to a DNA topoisomerase inhibitor, has gained increasing attention [71]. The DESTINY-Gastric01 and DESTINY-Gastric02 trials evaluated T-Dxd monotherapy as a second-line treatment for patients with HER2-positive advanced GC or GEJ who progressed on first-line treatment. The objective response rate (ORR) to T-Dxd was 41.8 % in the DESTINY-Gastric02 trial and 40.5 % in the DESTINY-Gastric01 trial, compared to an ORR of 11.3% with single-agent chemotherapy [72-74]. This led to the approval of T-Dxd monotherapy as a second-line treatment for HER2-positive advanced or metastatic GC and GEJC by the European Medicines Agency (EMA) in December 2022 [74]. Additional studies with T-Dxd are

ongoing, including a trial investigating the combination of T-Dxd with chemotherapy in the first-line setting (DESTINY-Gastric03, NCT04379596) [75].

Because dimerization is critical for HER2 signaling activity, the recombinant humanized antibody pertuzumab was developed to bind to the dimerization domain of HER2 and inhibit the formation of homo- or heterodimers [76]. The JACOB trial evaluated the efficacy of the combination of trastuzumab, pertuzumab and chemotherapy in metastatic GC or GEJC and compared it to trastuzumab plus chemotherapy. A survival benefit could not be demonstrated in this trial (HR=0.84; 95%-CI 0.71-1.00; p=0.057) [77].

Another strategy to target HER2 functionality involves inhibiting the RTK domain to disrupt phosphorylation and downstream signaling. In the TRIO-013/LOGiC trial, the tyrosine kinase inhibitor lapatinib was combined with chemotherapy and compared to placebo plus chemotherapy as first-line treatment in HER2-positive metastatic GC, GEJC and esophageal adenocarcinoma. However, no survival benefit was observed (median OS 12.2 vs. 10.5 months; p=0.349) [78].

To date, trastuzumab is the only HER2-targeting first-line therapy approved in Europe for HER2-positive advanced or metastatic GC or GEJC. Although the therapy improves patient survival, it remains unsatisfactory with a median OS of 13.8 months and a median progression-free survival (PFS) of 6.7 months [31]. Nonetheless, a subset of patients with long-term response to trastuzumab has been described in small studies and case reports. However, a biomarker that can distinguish between long-term responders from rapidly progressing patients has not yet been identified [65,79-81].

1.2.3 HER2 assessment in gastric cancer

A positive HER2 status is the requirement for the treatment of advanced GC and GEJC with trastuzumab [17]. The HER2 status is determined by IHC and/or *in situ* hybridization (ISH) techniques (Figure 4). IHC is graded from 0 to 3+ based on a combination of the HER2 staining pattern and the percentage of stained cells (Table 1). A score of 0 or 1+ indicates a HER2-negative status, characterized by absent or weak membranous staining in less than 10% of tumor cells, respectively. Conversely, an IHC score of 3+ signifies a HER2-positive status, reflecting strong staining of the entire membrane in more than 10% of tumor cells [82,83]. The IHC score 2+ is assigned when there is a perceptible weak to moderate staining intensity at the complete basolateral or lateral membrane in more than 10% of tumor cells.

In this case, the HER2 IHC score is ambiguous and final result depends on the amplification status of the HER2 gene (*ERBB2*). Gene copy number can be assessed using ISH techniques such as silver or fluorescence *in situ* hybridization (FISH/SISH). The number of signals from the *ERBB2* probe and the centromere chromosome 17 probe (CEP17) must be evaluated in

at least 20 tumor cells. If the ratio of *ERBB2* to CEP17 signals (*ERBB2*:CEP17) is ≤2 or there are on average more than six *ERBB2* gene copies in the tumor cells, *ERBB2* is considered amplified indicating a positive HER2 status. If the ratio is <2, the HER2 status is negative (Table 2) [82,83]. It is important to note that the IHC scoring criteria differ between biopsies and resection specimens. The criteria described above apply specifically to resection specimens. For biopsy material, the staining intensity and location criteria remain the same, but the scoring is based on the staining of tumor cell clusters rather than the percentage of stained tumor cells (Table 1) [82]. In biopsies, the presence of five stained coherent tumor cells is sufficient to assign the corresponding score and the 10% rule does not apply [83].
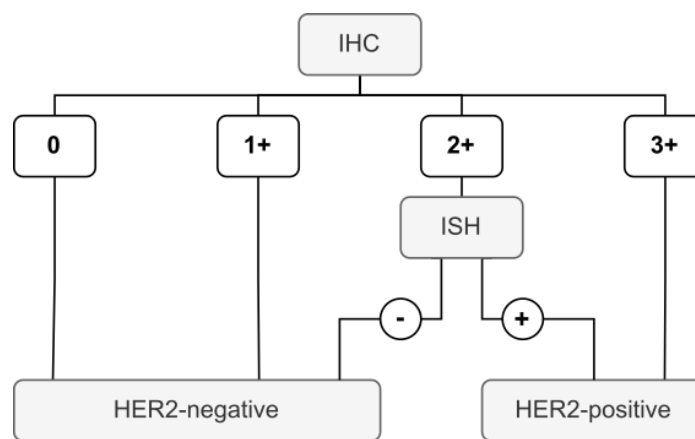
Figure 4 | Algorithm of HER2 testing in advanced gastric and gastroesophageal adenocarcinoma. IHC, immunohistochemistry; ISH, *in situ* hybridization, adapted from Lordick et al. 2017 [83]

The majority of GC cases are diagnosed at unresectable stages. Accordingly, it is more common to assess the HER2-status based on a tumor biopsy. Due to the highly heterogeneous nature of GC and the larger size of tumors in advanced stages, it is critical to obtain a sufficient number of biopsies for HER2 diagnostics. At least five tumor-containing biopsies from different areas of the tumor are recommended for robust HER2 status assessment [83].

Table 1 | HER2 IHC scoring criteria for gastric cancer
(adapted from Rüschoff et al. 2012 [82])

IHC Score	Surgical specimen-staining pattern	Biopsy specimen-staining pattern	HER2 status
0	No reactivity or membranous reactivity in <10% of tumor cells	No reactivity or no membranous reactivity in any tumor cell	negative
1+	Faint/barely perceptible membranous reactivity in ≥10% of tumor cells; cells are reactive only in part of their membrane	Tumor cell cluster with a faint/barely perceptible membranous reactivity irrespective of percentage of tumor cells stained	negative
2+	Weak to moderate complete, basolateral, or lateral membranous reactivity in ≥10% of tumor cells	Tumor cell cluster with a weak to moderate complete, basolateral, or lateral membranous reactivity irrespective of percentage of tumor cells stained	equivocal
3+	Strong complete, basolateral, or lateral membranous reactivity in ≥10% of tumor cells	Tumor cell cluster with a strong complete, basolateral, or lateral membranous reactivity irrespective of percentage of tumor cells stained	positive

Table 2 | Evaluation criteria for *ERBB2* amplification using in situ hybridization.

HER2 status	Description
positive	*ERBB2*:CEP17≥2 or >6 *ERBB2* copies/cell, after evaluation of 20 non-overlapping tumor cells
negative	*ERBB2*:CEP17<2 after evaluation of 20 non-overlapping tumor cells. In case of borderline negative result (ratio 1.8-2.0) after evaluation of 20 non-overlapping tumor cells, analysis of further 20 non-overlapping tumor cells is recommended

1.3 Trastuzumab therapy response and resistance in GC

The addition of trastuzumab to chemotherapy ameliorates the survival of HER2-positive mGC/mGEJC but the outcome remains poor. Several biomarkers such as tumor heterogeneity, level of *ERBB2* amplification, specific genomic alterations or the tumor mutational burden have been associated with improved or impaired response to trastuzumab [84-87].

1.3.1 Heterogeneity

GC is a highly heterogeneous disease. Intratumoral heterogeneity arises during tumor development when genomic alterations are accumulated sequentially in single cells, leading to the presence of distinct tumor subclones with unique molecular characteristics [88]. This heterogeneity has significant implications, particularly in the context of trastuzumab treatment, as it is frequently discussed as a potential cause of therapy resistance [84,89,90]. Intratumoral heterogeneity of HER2 protein expression, as determined by IHC, occurs in 25-60% of the HER2-positive cases, underlining the importance of multiple location testing [55,84,91]. Several studies have demonstrated that patients with homogeneous HER2 expression exhibit improved response to trastuzumab treatment [84,91,92]. In response to trastuzumab, HER2 amplified cells undergo apoptosis, which may lead to changes in clonal composition of the tumor [93]. Several studies have reassessed HER2 status in patients who progressed on trastuzumab. A conversion from HER2-positive to HER2-negative status was observed in 29-32% of the cases, indicating an acquired resistance mechanism [94,95].

Additionally, GCs are heterogeneous between individuals (inter-patient heterogeneity). This heterogeneity is reflected in numerous proposed histologic (see chapter 1.1.2) and molecular classification systems, which utilize genomic, transcriptomic, and DNA methylation analyses to categorize GCs into distinct subtypes [96-100]. The most widely accepted molecular classifications have been presented by The Cancer Genome Atlas (TCGA) and the Asian Cancer Research Group (ACRG) [96,97]. The TCGA classification integrates multiple types of molecular data, including genomics, transcriptomics, proteomics, and DNA methylation, to define four main subtypes: chromosomal instability (CIN), Epstein-Barr virus (EBV), MSI, and genomically stable (GS). The CIN subtype is the most common and is characterized by intestinal histology, tumor protein P53 (TP53) mutations and RTK activation [96].

The four ACRG subtypes include one MSI type and three microsatellite stable (MSS) types. The MSS subtypes are further subdivided according to TP53 activity or loss of function (MSS/TP53+; MSS/TP53-) and the expression of genes associated with the epithelial-mesenchymal transition (EMT; MSS/EMT) [97]. Both classification systems include the MSI

subtype. In addition, the MSS/TP53- subtype shares molecular features with the CIN subtype, such as the TP53 mutations and RTK signaling activation. The remaining subtypes have no similarities. Notably, HER2-amplified tumors do not represent a distinct subtype in either classification system. In the TCGA system, the majority of HER2-positive cases are associated with the CIN subtype, while in the ACRG system, HER2-amplified cases are primarily found in the MSS/TP53- subtype [96,97]. Although none of the molecular classification systems have demonstrated significant clinical relevance thus far, the TCGA classification holds a dominant position in the scientific literature. These classification systems serve as valuable frameworks for understanding the molecular diversity of GC and provide a basis for further research and potential clinical implications in the future.

1.3.2   Genomic mutations and copy number variations

Next-generation panel sequencing in clinical practice

Over the past decade, next-generation sequencing (NGS) has become more affordable and is increasingly utilized in clinical practice. NGS can be used to analyze the sequence of the entire genome (whole genome sequencing, WGS), all protein-coding regions (whole exome sequencing, WES), or a specific panel of selected genes (targeted-panel sequencing). The amount of DNA required for sequencing depends on the sequencing technique, the enrichment method and the size of the DNA region being analyzed [101]. There are two main target-enrichment strategies for panel sequencing. The first is hybrid-capture enrichment, in which DNA is fragmented, hybridized with oligonucleotides at target regions and then captured using magnetic beads or an array-based approach. The second strategy is amplicon-based target enrichment, where polymerase-chain reaction (PCR) is utilized to amplify the target prior to sequencing [102].

In a clinical setting, sample availability is often limited. DNA is commonly isolated from formalin-fixed paraffin-embedded (FFPE) samples that have been previously used for diagnostic techniques such as IHC or ISH. Besides sample size, factors such as tissue processing and cellularity are other critical factors affecting DNA yield and quality [103]. Therefore, a sequencing technique with minimal DNA input, such as panel sequencing, is advantageous. Most targeted DNA panels used in clinical practice require around 10-20 ng of DNA, whereas WES or WGS often require 1 µg of DNA. Further, panel sequencing is less time consuming and cheaper, compared to WGS or WES [104]. The genes included in a panel are typically selected based on their relevance to the disease or due to the availability of a treatment that targets the proteins encoded by those genes. Focusing on disease-relevant genes facilitates the analysis and treatment decisions [105].

NGS-determined *ERBB2* copy number as improved biomarker for trastuzumab response

NGS allows the exact quantification of *ERBB2* copy number (CN) and thus could be an alternative to ISH methods for assessing *ERBB2* amplification. The NGS-determined *ERBB2* CN has been proposed as an improved biomarker for predicting the response to trastuzumab therapy in mGC [85]. However, this opens the debate about the optimal *ERBB2* CN threshold for defining *ERBB2* amplification and identifying trastuzumab-responsive patients. An average of six *ERBB2* copies is sufficient for a HER2-positive status determined by ISH in mGC/mGEJC. Nevertheless, studies have shown that higher levels of *ERBB2* amplification correlate with improved response to trastuzumab therapy [106-110]. This suggests that setting a higher *ERBB2* CN threshold could ameliorate the identification of trastuzumab-sensitive patients. Studies have demonstrated that an *ERBB2* CN cut-off ranging from 11 to 25 may be associated with prolonged survival in patients undergoing trastuzumab containing-therapy [107-109]. However, these proposed thresholds have not been investigated in larger patient cohorts and may exclude patients from treatment that – despite only moderate copy number elevation of ERBB2 – benefit from an HER2 targeting treatment.

Genetic alterations linked to trastuzumab response

Aside from gene amplification, the presence of *ERBB2* mutations can affect trastuzumab treatment response. One frequently observed mutation is the amino acid substitution S310F, which is located in the extracellular domain of HER2. The formation of HER2 homo and heterodimers cannot be inhibited by trastuzumab when this mutation is present [111]. In general, *ERBB2* single nucleotide variations are rare in *ERBB2*-amplified GC and GEJC [112,113]. Another notable genomic alteration is the deletion of exon 16 in the juxta transmembrane domain of *ERBB2* (ERBB2d16). In a study by Wang et al., ERBB2d16 was detected in 48% of 110 examined HER2-positive mGC samples. A high ratio of ERBB2d16 to *ERBB2* was correlated with an increased risk of tumor progression [114].

NGS has been used to identify additional genomic alterations beyond *ERBB2* that are associated with trastuzumab response. In the AMNESIA case-control study, a panel of five genes was proposed to determine response to trastuzumab in GC. Cases showing resistance to trastuzumab harbored mutations in at least one of the candidate genes, including *EGFR*, *MET*, *KRAS*, *PI3K* and *PTEN* or an amplification in *EGFR*, *MET* or *KRAS* [86]. Other studies have confirmed the relevance of certain co-amplifications and mutations within the AMNESIA panel in determining trastuzumab sensitivity, while also highlighting the importance of genetic alterations in other genes such as *CCNE1* [106,107,115].

1.3.3 Tumor mutational burden

The tumor mutational burden (TMB) is an emerging biomarker frequently discussed in relation to the response to immunotherapies like pembrolizumab. TMB is defined as the number of somatic mutations per megabase (mut/Mb) [116]. Various NGS techniques such as WGS, WES and panel sequencing are suitable for determining TMB. However, panel sequencing requires covering a minimum genomic size of 0.8-1 Mb for accurate TMB assessment [117,118]. The types of mutations used to calculate the TMB are not consistent across studies. While most studies focus on the number of non-synonymous mutations, which induce an amino acid exchange, others additionally include synonymous, frameshift and nonsense mutations in their TMB assessment [119]. In addition, the threshold for identifying TMB-high tumors varies among studies. Goodman et al. utilized a three-category system: TMB-high (≥20 mut/Mb), TMB-intermediate (6-19 mut/Mb), and TMB-low (1-5 mut/Mb) [120]. Others have defined two TMB groups, TMB-high and TMB-low, with a TMB-high threshold between 10 and 20 mut/Mb [116,121-123]. Alternatively, the TMB-high threshold can be determined based on the median TMB of the cohort or the top 20% of the cohort's TMB [124,125]. Although the calculation of TMB and the definition of TMB-high is heterogeneous, the FDA approved pembrolizumab for the treatment of TMB-high (≥10 mut/Mb) solid tumors [126].

A genomic mutation can induce a change in the protein sequence, resulting in potential neo-antigens that may be immunogenic. A higher number of mutations also increases the likelihood of having an immunogenic mutation that activates a T-cell mediated immune response [119,127]. Several studies have investigated the prognostic relevance of TMB in GC. It has been observed that GC patients with high TMB tend to have a better therapy response and improved survival rates [123,128]. This was also found in the context of trastuzumab treatment. For instance, a study by Kim et al demonstrated that high TMB (≥10 mut/Mb) was associated with an improved response to trastuzumab [87].

1.4   Objectives

Trastuzumab prolongs the life of patients with HER2-positive mGC/mGEJC but the OS remains poor, and resistance to trastuzumab occurs frequently. While a subpopulation of patients with long-term response to trastuzumab-based treatment has been described in case reports and small studies, it is challenging to identify reliable biomarkers that distinguish between patients with short-term and long-term benefits, beyond the HER2 status alone [65,79-81]. Previous studies have proposed other biomarkers, such as genetic variations and a homogeneous HER2 expression pattern, but a definitive biomarker for long-term responsive remains elusive [84,86].

To address this gap, a retrospective study was conducted, involving a cohort of HER2-positive mGC/mGEJC patients from four German clinical centers. All patients received a trastuzumab-containing therapy. The availability of follow-up data and a tumor sample prior to trastuzumab treatment was required. The patients were divided into two groups based on PFS on trastuzumab-containing therapy: a short-term responder group (PFS<12 months) and a long-term responder group (PFS≥12 months). A comprehensive analysis was performed to investigate potential biomarkers for long-term response to trastuzumab-based treatment in HER2-positive mGC/mGEJC patients. The routinely assessed, established biomarkers HER2, PD-L1 and MSI were analyzed. In addition, NGS panel sequencing and Affymetrix gene expression analysis were applied to evaluate the impact of genetic alterations and pathway activity in the patient cohort.

Therefore, the objectives of this thesis were to address the following key questions:

- Do routinely assessed biomarkers for mGC/mGEJC have prognostic relevance in context of trastuzumab treatment?
- Can the NGS-determined *ERBB2* CN improve the detection of patients with long-term response to trastuzumab compared to the HER2 status alone?
- Does HER2 expression heterogeneity affect the response to trastuzumab?
- Are somatic mutations, copy number alterations, or the TMB involved in primary resistance to trastuzumab?

2 Material

2.1 Reagents

Table 3 | List of reagents

Reagent	Supplier
Absolute Ethanol for Analysis	Merck, Darmstadt, Germany
Ambion™ Nuclease-Free Water	Thermo Fisher Scientific, Waltham, MA, USA
Ampuwa 1000 ml Plastipur	Fresenius Kabi Deutschland GmbH
Antibody diluent	Zytomed Systems, Berlin, Germany
Antibody, HER2, poly clonal, Dako (#A0485)	Agilent, Santa Clara, CA, USA
Antibody, PD-L1, clone CAL10 (#ACI3171)	Biocare Medical, Den Haag, Netherlands
Dako REAL™ Peroxidase-Blocking Solution	Agilent Technologies, Glostrup, Denmark
Dapi Vectashield	LINARIS Biologische Produkte GmbH, Dossenheim, Germany
Eosin	Dr. K. Hollborn & Söhne, Leipzig, Germany
Epitope Retrieval Solution (10x Concentrate), pH 6	Leica Biosystems Nussloch GmbH, Nussloch, Germany
Ethanol (EtOH) 80 %	S.A.R Plus, Böckheim, Germany
EtOh 96 %	S.A.R Plus, Böckheim, Germany
EtOH 99 %	S.A.R Plus, Böckheim, Germany
Fixogum Rubber Cement	Marabu GmbH & Co. KG, Bietigheim-Bissingen, Germany
Hämalaun sauer nach Mayer	Dr. K. Hollborn & Söhne, Leipzig, Germany
Hydrochloric Acid in Ethanol (0.7 %/ 59 %)	Otto Fischar GmbH & Co. KG, Saarbrücken, Germany
IHC wash buffer (20x)	DCS Innovative Diagnostik Systeme, Hamburg, Germany
Mayers Hämalaunlösung	Merck, Darmstadt, Germany
PERTEX®	MEDITE Medical GmbH, Burgdorf, Germany
Uracil-DNA Glycosylase, heat-labile	Thermo Fisher Scientific, Waltham, MA, USA

VENTANA Her2 Dual ISH DNA probe Cocktail	Roche Diagnostics GmbH, Mannheim, Germany
VENTANA INFORM EBER (Epstein-Barr-Virus Early RNA) probe	Roche Diagnostics GmbH, Mannheim, Germany
Xylole	S.A.R Plus, Böckheim, Germany
Zyto Light SPEC CEN 17/ERBB2 Dual Color Probe (#Z-2077-50)	ZytoVision GmBH, Bremerhaven, Germany

2.2   Consumables

Table 4 | List of consumables

Consumable	Supplier
Centrifuge plates	Thermo Fisher Scientific, Waltham, MA, USA
Coverglass 24 x 60 mm	MEDITE Medical GmbH, Burgdorf, Germany
DNA LoBind Tubes, 1.5 mL PCR clean	Eppendorf SE, Hamburg, Germany
PCR SingleCap 8-SoftStrip 0.2 mL	Biozym, hessisch Oldendorf, Germany
Pipette Tips, epT.I.P.S.	Eppendorf SE, Hamburg, Germany
Qubit™ Assay Tubes	Thermo Fisher Scientific, Waltham, MA, USA
Rnase-Free Elution Tube	Thermo Fisher Scientific, Waltham, MA, USA
SuperFrost Plus™ Microscope Slide	R. Langenbrinck GmbH, Emmerdingen, Germany
SuperFrost™ Microscope Slides	Thermo Fisher Scientific, Waltham, MA, USA
SuperFrost™ Microscope Slides ISO 8037/1, ground 45° blue	Epredia, Braunschweig, Germany

2.3   Kits

Table 5 | List of kits

Kit	Supplier
DAKO Real™ Envision Kit	Agilent, Santa Clara, CA, USA
FISH-Tissue Implementation Kit	ZytoVision GmBH, Bremerhaven, Germany
GeneChip® Hybridization, Wash and Stain Kit	Thermo Fisher Scientific, Waltham, MA, USA

GeneChip® WT Plus Reagent Kit	Thermo Fisher Scientific, Waltham, MA, USA
GeneChipTM Human Transcriptome 2.0 Arrays	Thermo Fisher Scientific, Waltham, MA, USA
Idylla MSI Test	Biocatis, Mechelen, Belgium
Ion 540 Chip Kit 4 Pack	Thermo Fisher Scientific, Waltham, MA, USA
Ion 540 Kit-Chef (2/INIT)	Thermo Fisher Scientific, Waltham, MA, USA
Oncomine™ Comprehensive Assay v2M	Thermo Fisher Scientific, Waltham, MA, USA
Oncomine™ TML Assay Chef Kit	Thermo Fisher Scientific, Waltham, MA, USA
OptiView DAB Detection kit	Roche Diagnostics GmbH, Mannheim, Germany
Qubit™ 1X dsDNA HS Assay-Kit	Thermo Fisher Scientific, Waltham, MA, USA
Qubit™ RNA HS Assay kit	Thermo Fisher Scientific, Waltham, MA, USA
RecoverAll™ Multi-Sample RNA/DNA Isolation Workflow	Thermo Fisher Scientific, Waltham, MA, USA
VENTANA ISH iview Blue Detection Kit	Roche Diagnostics GmbH, Mannheim, Germany
VENTANA Red ISH DIG Detection Kit	Roche Diagnostics GmbH, Mannheim, Germany
VENTANA Silver ISH DNP Detection Kit	Roche Diagnostics GmbH, Mannheim, Germany

2.4   Technical equipment

Table 6 | List of devices

Device	Supplier
Centrifuge 5810 R	Eppendorf SE, Hamburg, Germany
Eppendorf Research® plus Pipettes (0.1-2.5 µl, 0.5-10 µl, 2-20 µl, 10-100 µl, 20-200 µl, 100-1000 µl)	Eppendorf SE, Hamburg, Germany
Galaxy Mini Centrifuge	Thermo Fisher Scientific, Waltham, MA, USA
GeneChip Fluidics Station 450	Affymetrix, High Wycombe, UK
GeneChip Hybridization oven 640	Affymetrix, High Wycombe, UK
GeneChip Scanner 3000	Affymetrix, High Wycombe, UK
Glasware	Carl Roth GmbH + Co. KG, Karlsruhe, Germany

Heraeus™ Pico™ 17 centrifuge	Thermo Fisher Scientific, Waltham, MA, USA
HT01 hotplate	Harry Gestigkeit GmbH, Düsseldorf, Germany
Hybridizer	Agilent Technologies Germany GmbH & Co. KG, Waldbronn, Germany
Invitrogen™ Qubit™ 3 Fluorometer	Thermo Fisher Scientific, Waltham, MA, USA
Ion Chef Instrument	Thermo Fisher Scientific, Waltham, MA, USA
Ion GeneStudio™ S5 Prime SQNCR	Thermo Fisher Scientific, Waltham, MA, USA
LAUDA Hydro H16 waterbath	Lauda Dr. R. Wobser GmbH & Co. KG, Lauda-Königshofen, Germany
Leica CV5030 cover slipper	Leica Biosystems Nussloch GmbH, Nussloch, Germany
Liquid-repelling slide marker pen	Science Scerives GmbH, München,Germany
M8 Microscope amd Scanner	PreciPoint GmbH, Freisingen, Germany
neoPipette Controller	neoLab Migge GmbH, Heidelberg, Germany
Olympus BX41TF microscope	Olympus, Tokyo, Japan
Olympus BX51TF microscope	Olympus, Tokyo, Japan
Oven	BINDER GmbH, Tuttlingen, Germany
peqSTAR 96Universal PCR cycler	VWR International, Darmstadt, Germany
Precision™ Water Bath GP05	Thermo Fisher Scientific, Waltham, MA, USA
Sliding Microtome	Leica Biosystems Nussloch GmbH, Nussloch, Germany
ThermoMixer F1.5	Eppendorf SE, Hamburg, Germany
Tissue-Tek Cryo Console	Sakura Finetek USA, Inc., Torrance, CA, USA
TST 44 tissue stainer	MEDITE Medical GmbH, Burgdorf, Germany
UPlanSApo 60x objective	Olympus, Tokyo, Japan
VENTANA BenchMark ULTRA tissue stainer	Roche Diagnostics GmbH, Mannheim, Germany
VF2 vortex	IKA GmbH & CO. KG, Staufen, Germany

2.5   Software

Table 7 | List of software

Name	Distribution	Reference
ANNOVAR	https://annovar.openbioinformatics.org/en/latest/	[129]
bcftools (v1.11)	http://www.htslib.org/doc/1.0/bcftools.html	
bwa (v0.7.17)	https://github.com/lh3/bwa	[130]
CNVkit	https://cnvkit.readthedocs.io	[131]
Conda (v22.9.0)	https://docs.conda.io/en/latest/	
CovCopCan	https://git.unilim.fr/merilp02/CovCopCan	[132]
gatk4 (v.4.1.9.0-0)	https://gatk.broadinstitute.org/hc/en-us	[133]
GraphPad Prism 9	https://www.graphpad.com/	
Integrative Genomics Viewer (v2.8.13)	https://software.broadinstitute.org/software/igv/	[134]
IonReporter (v5.16.0.2)	Thermo Fisher Scientific, Waltham, MA, USA	
Oncocnv (v6.9)	https://github.com/BoevaLab/ONCOCNV	[135]
picard tools (v.2.23.8-0)	https://broadinstitute.github.io/picard/	
python 3 (v3.7.6)	https://www.python.org/	
Rstudio (v2022.07.1)	https://www.rstudio.com/	
Rtools (v4.0.0.28)	https://cran.r-project.org/	
samtools (v1.7)	http://www.htslib.org/	[136]
SAS JMP15 Genomics (v10)	SAS Institute, Cary, NC, USA	
Snakemake (v5.30.1)	https://snakemake.github.io/	[137]
tabix (v0.2)	http://www.htslib.org/doc/tabix.html	
Torrent Suite (v5.18.1)	Thermo Fisher Scientific, Waltham, MA, USA	
vardict-java (v.1.8.2-0)	https://github.com/AstraZeneca-NGS/VarDictJava	
vcflib (v1.0)	https://github.com/vcflib/vcflib	

vcftools (v0.1.16)	https://vcftools.github.io
ViewPoint Light (v1.0.0.9628)	PreciPoint GmbH, Freisingen, Germany

Table 8 | List of R packages

R package	Distribution	Reference
limma	https://bioinf.wehi.edu.au/limma/	[138]
progeny	https://github.com/saezlab/progeny	[139]
dorothea	https://github.com/saezlab/dorothea	[140]
estimate	https://CRAN.R-project.org/package=estimatr	[141]
maftools	https://github.com/PoisonAlien/maftools	[142]
ComplexHeatmap	https://github.com/jokergoo/ComplexHeatmap	[143]
pheatmap	https://CRAN.R-project.org/package=pheatmap	
gtsummary	https://CRAN.R-project.org/package=gtsummary	
IonCopy	https://CRAN.R-project.org/package=ioncopy	[144]
CNVPanelizer	https://github.com/biostuff/CNVPanelizer	

3 Methods

3.1 Patient cohort
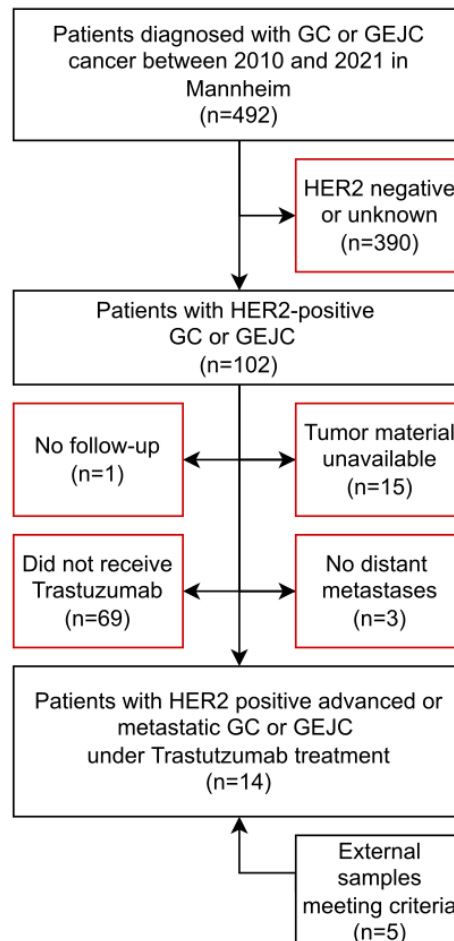
Figure 5 | Flowchart of patient selection criteria for the retrospective cohort
Exclusion criteria are framed in red. FFPE, Formalin-fixed paraffin-embedded; GC/GEJC, gastric and gastroesophageal junction cancers

This retrospective study comprises samples derived from patients diagnosed with HER2-positive locally advanced, recurrent, and/or metastatic gastric or gastroesophageal junction adenocarcinomas from different sources: University Medical Center Mannheim (n=14), Nord-West Krankenhaus Frankfurt (n=2), Technical University Munich (n=1), and University of Lübeck (n=2). Patients who received a platinum- and 5-FU-based chemotherapy in combination with trastuzumab were considered. A treatment overview is shown in Supplementary table 1. Additional selection criteria included the availability of FFPE tumor-containing paraffin block prior to trastuzumab treatment as well as follow-up data (Figure 5). Survival and treatment information of patients were provided by the Department of Medicine II, Medical Faculty Mannheim (Dr. med. Philip Weidner), the Institute of Clinical Cancer Research, Krankenhaus Nordwest, UCT-University Cancer Center Frankfurt (Prof. Dr. med.

Oliver Götze), Clinic for Hematology and Oncology, University Hospital Schleswig-Holstein-Campus Luebeck (Dr. med. Kim Luley) and Medical Clinic III, Klinikum rechts der Isar, Technical University of Munich (Prof. Dr. med. Sylvie Lorenzen). The histology of all samples was reviewed by Prof. Dr. med. Timo Gaiser and tumor areas were marked. This study was approved by the ethics committee of the Medical Faculty Mannheim of Heidelberg University (2016-080R-MA).

The patients were divided into two groups according to PFS under trastuzumab-based therapy. The first group included patients with long-term response to trastuzumab (PFS≥12 months), while patients with short-term response (PFS<12 months) were in the grouped in the second. (Table 9).

A total of 14 tumor-adjacent normal tissue samples and healthy gastric mucosa FFPE samples from the Institute of Pathology of the University Medical Center Mannheim were used as control samples for NGS and Affymetrix gene expression microarray experiments.

For experimental validation of CNV calling, FFPE samples of patients diagnosed with gastric cancer were retrieved from the archive of the Institute of Pathology of the University Medical Center Mannheim (n=4). Two samples with positive HER2 status and two with negative HER2 status were selected. To capture the range of sample ages in our cohort, one aged sample, from 2010 or 2011, and another sample from 2019 was taken for each HER2 status.

Table 9 | Overview of patient, control and validation samples

	ID	Gender	Age at diagnosis	Location	PFS	HER2 status	Sample Year
Long-term responder	Pat1	m	59	GEJ	72	3+	2008
	Pat2	m	45	stomach	38	2+	2017
	Pat3	m	56	GEJ	19	3+	2010
	Pat4	m	61	GEJ	19	2+	2019
	Pat5	m	62	stomach	43	3+	2017
	Pat6	m	59	stomach	14	3+	2017
	Pat7	m	74	stomach	22	3+	2019
Short-term responder	Pat8	m	73	stomach	4	2+	2011
	Pat9	m	70	GEJ	9	3+	2011
	Pat10	m	71	stomach	4	3+	2010
	Pat11	m	72	stomach	10	3+	2017
	Pat12	m	67	GEJ	5	2+	2011
	Pat13	m	77	stomach	4	3+	2015
	Pat14	f	75	GEJ	11	3+	2015
	Pat15	f	72	stomach	6	2+	2019
	Pat16	m	51	GEJ	9	3+	2013
	Pat17	m	59	GEJ	3	3+	2014
	Pat18	f	59	GEJ	9	2+	2018
	Pat19	f	64	GEJ	1	2+	2021

	ID	Gender	Age at diagnosis	Location	PFS	HER2 status	Sample Year
Control Samples	Nor1	m	61	stomach	ND	ND	2019
	Nor2	f	61	stomach	ND	ND	2019
	Nor3	m	62	stomach	ND	ND	2019
	Nor4	m	62	stomach	ND	ND	2019
	Nor5	f	63	stomach	ND	ND	2019
	Nor6	m	58	GEJ	ND	ND	2019
	Nor7	m	73	stomach	ND	ND	2011
	Nor8	m	70	GEJ	ND	ND	2012
	Nor9	m	71	stomach	ND	ND	2010
	Nor10	m	72	stomach	ND	ND	2017
	Nor11	m	67	GEJ	ND	ND	2011
	Nor12	f	72	stomach	ND	ND	2019
	Nor13	m	59	stomach	ND	ND	2005
	Nor14	m	29	stomach	ND	ND	2013
Validation Samples	Val1	f	84	stomach	ND	0	2019
	Val2	m	47	stomach	ND	0	2010
	Val3	m	56	GEJ	ND	3+	2011
	Val4	m	91	stomach	ND	3+	2019

3.2 H&E staining

For hematoxylin and eosin (H&E) staining, FFPE blocks were cut into 1-4 µm sections using a microtome, mounted on a SuperFrost™ microscope slide and dried at 80°C for 10 min. The staining was performed on a Medite TST 44 autostainer and a robotic cover-slipper covered the tissue afterwards.

3.3 Slide scans

Slides were scanned at 20x or 40x magnification with a M8 microscope and scanner. Images were examined and processed with ViewPoint Light software.

3.4 Immunohistochemistry and *in situ* hybridization

FFPE tissue sections of 1-4 µm thickness were used in all IHC and ISH experiments. All sections were mounted on SuperFrost Plus™ adherent microscope slides.

3.4.1 HER2 immunohistochemistry

The pre-determined HER2-status was re-evaluated for all patients. All HER2 IHC stainings were performed as follows: After drying the samples overnight at 37°C, slides were deparaffinized and rehydrated by a series of washing steps: xylene (3x 5 min), 100% EtOH (2x 2 min), 96% EtOH (2x 2 min), 80% EtOH (2x 2 min), and distilled water (2x 2 min). Antigen retrieval slides were incubated at 95°C for 40 min in Epitope Retrieval Solution (pH 6; 1:10). After cooling down, the tissue slides were washed in distilled water and the tissue area was circled with a hydrophobic barrier pen. Then, the anti-HER2 antibody (1:500, in antibody diluent) was applied and incubated for 30 min at room temperature (RT) in a wet chamber. The antibody solution was removed and the slides were washed in IHC washing buffer. Next, peroxidase-blocking solution was added on the slide and incubated for 7 min at RT, followed by washing in IHC washing buffer. The Dako EnVision solution (anti-mouse-HRP, anti-rabbit-HRP) was applied and incubated for 30 min at RT. The tissue slides were washed in IHC washing buffer before adding 3,3N-Diaminobenzidine Tertrahydrochloride (DAB; 1:50 in DAB substrate buffer) for detection. The tissue section was incubated with the chromogen for 6 min at RT and afterwards immediately transferred into distilled water. Slides were counterstained with hematoxylin for 1 min and rinsed with tap water for 1 min. The tissue was dehydrated in an increasing EtOH series (80% EtOH, 96% EtOH, 2x 100% EtOH; each step 2 min) and xylene (2x 2min). The stained section was covered with PERTEX® mounting medium and a glass coverslip.

The HER2 staining was evaluated by Prof. Dr. Timo Gaiser according to published guidelines [82]. In case of equivocal staining (Dako HER2 Score 2+) additional ISH was performed.

3.4.2 HER2 *in situ* hybridization

To analyze HER2 gene copy number, either SISH or FISH was performed. The FISH-Tissue Implementation Kit was used for HER2 FISH. All buffers and pepsin solution were included. Slides were deparaffinized and rehydrated by a series of washing steps: xylene (2x 5 min), 100% EtOH (5 min), 96% EtOH (5 min), 80% EtOH (5 min), and rinsed with distilled water (2x). For antigen retrieval, the slides were incubated in retrieval buffer (PT1) at 98°C for 15 min. The slides were cooled down and washed in distilled water (2x 1 min). Tissue sections were circled with a diamond pen and subsequently treated with pepsin solution (ES1) for 2 min at 37°C in a hybridizer. The pepsin solution was removed, followed by incubation in wash buffer (WB1) for 5 min at RT. The samples were dehydrated with an increasing EtOH series (80% EtOH, 96% EtOH, 100% EtOH, each step 1 min) and dried at RT. Subsequently, Zyto Light SPEC

CEN17/*ERBB2* Dual Color Probe was applied on the tissue, covered with a cover glass and sealed with fixugum. The samples were kept in the dark until the sealing was dried. Then, probes were hybridized by incubation at 75°C for 10 min followed by incubation at 37°C overnight in a hybridizer. Sealing and cover glass were removed from the tissues followed by two washing steps, each in preheated washing buffer A at 37°C for 5 min. The samples were dehydrated in an increasing EtOH series (80% EtOH, 96% EtOH, 100% EtOH, each step 1 min) and dried at RT in the dark. The tissue was covered with DAPI Vectashield and a cover glass for analysis under an Olympus BX41TF fluorescence microscope with UPlanSApo 60x objective.

For HER2 SISH, the mounted tissue sections were dried at 100°C for 10 min. The procedure was carried out on a VENTANA BenchMark ULTRA autostainer with VENTANA Silver ISH DNP Detection Kit and VENTANA Silver ISH DNP Detection Kit utilizing the VENTANA Her2 Dual ISH DNA probe Cocktail. In the last step, the samples were covered with PERTEX mounting medium and a cover glass for analysis. FISH and SISH evaluation was performed according to published guidelines [82].

3.4.3   HER2 heterogeneity

In addition, the uniformity of HER2 expression in all samples was microscopically evaluated by two board certified pathologists (Prof. Dr. med. Timo Gaiser, Prof. Dr. med. Daniela Hirsch). HER2 heterogeneity was assessed for all staining intensities as described by Motoshima et al. [145]. In brief, samples with HER2 overexpression in >90% of tumor cells were considered HER2 homogenous. Samples with 10-90% of tumor cells showing HER2 overexpression were defined as HER2 heterogeneous.

3.4.4   PD-L1 immunohistochemistry

Tissue sections were dried at 100°C for 10 min before inserting into the VENTANA BenchMark ULTRA autostainer. The PD-L1 antibody (CAL10, 1:50) was used together with the OptiView DAB Detection kit. The tissues were covered with Pertex mounting medium and a cover glass for analysis. Testing was done alongside a tonsil section as "on-slide" positive control.

Interpretation was performed from stained slides by two of the board certified pathologist (Prof. Dr. med. Timo Gaiser; Prof. Dr. med. Daniela Hirsch), who received appropriate training. PD-L1 expression in the tumor cell membrane and membrane and/or cytoplasm of tumor-associated mononuclear inflammatory cells such as lymphocytes and macrophages was scored. The CPS was defined as the total number of tumor cells and immune cells (including

lymphocytes and macrophages) stained with PD-L1 divided by the number of all viable tumor cells, then multiplied by 100.

3.5   Nucleic acid isolation

For NGS and Affymetrix analysis, DNA and RNA of tumor and control samples was extracted. Resection and biopsy specimens were cut into 1-3 and 4-6 10 µm sections, respectively. The sections were placed on an uncoated glass slide and were dried at RT. To guide tumor macrodissection, tumor area was marked on the back of the glass slides. Then, tissue sections were warmed on a heat plate with 45-50°C. Upon melting of the paraffin, the tissue was cut along the marking of the tumor area and was scraped into a tube. Biopsies with high tumor content and normal tissue samples were used completely without dissection.

DNA and RNA were co-isolated using the RecoverAll™ Multi-Sample RNA/DNA Isolation Workflow according to the manufacturer's protocol. The elution volume was 30 µl. Nucleic acid quantity was checked on the Invitrogen™ Qubit™ 3 Fluorometer in high sensitivity mode using the Qubit™ RNA HS Assay Kit Qubit™ or dsDNA HS Assay-Kit.

3.6   Library Prep and Sequencing

All samples were run in duplicates in the library preparation and sequencing process as recommended by Thermo Fisher Scientific. Prior to library preparation, the DNA was treated with Uracil-DNA glycosylase (UDG). For each sample, 20 ng of DNA were mixed with 1000 U UDG and filled up with nuclease-free water to a total volume of 7.5 µl. The mixture was incubated in a thermocycler for 2 min at 37°C followed by 10 min at 50°C and cooled down to 4°C.

After UDG treatment, each sample was filled up to 15 µl with nuclease-free water and was transferred into the first column of an Ion Chef reaction plate. For Oncomine™ Tumor Mutation Load (TML) Assay library preparation, the Ion Chef Instrument was equipped with the reaction plate containing the samples and the Oncomine™ TML assay chef kit including TML primer pools. Run parameters were used as stated in the manufacturer's protocol. The library was diluted to 50 pM and was loaded onto an Ion 540 chip using the Ion Chef instrument. Sequencing was performed on an Ion GeneStudio™ S5 Prime.

For validation of CNV calling, the validation cases were additionally sequenced with the Oncomine comprehensive assay v2. Libraries for DNA and RNA were separately prepared on the Ion Chef instrument according to manufacturer's protocol. The DNA and RNA libraries were mixed in a ratio of 3:1, diluted to 50 pM, and loaded on an Ion 540 Chip using the Ion Chef Instrument. Sequencing was performed on an Ion GeneStudio™ S5 Prime. The data was

analyzed on the Ion Reporter with the Oncomine Comprehensive v2-540-w2.5-DNA and Fusions workflow. The Oncomine Variants filter was applied to review the results.

3.7   Sequencing data analysis

Coordinates of TML panel targets were converted from hg19 to hg38 by liftOver (https://genome.ucsc.edu/cgi-bin/hgLiftOver). Bam files of tumor and unmatched normal samples were downloaded from the IonReporter for analysis of single nucleotide variants (SNVs) and copy number variants (CNVs). The files were converted to fastq files with picard tools and mapped to the human reference genome hg38 (homo sapiens GRCh38.p13, downloaded on January 4th, 2021; [146]) with bwa mem. Afterwards bam files were sorted and indexed with samtools. The normal sample bam files were used to generate a somatic panel of normals (PoN) with mutect2, which was subsequently utilized in somatic mutation calling on tumor files with mutect2 tumor-only mode. The resulting vcf files were filtered for allele frequency (AF) > 0.1 and read depth (DP) > 250 using gatk and vcftools. To reduce false positive calls, duplicate vcf files of each sample were intersected with bfc tools and further annotated with ANNOVAR. For CNV calling, the duplicate bam files were merged per patient and indexed with samtools. Merged tumor and normal bam files were analyzed with ONCOCNV. For amplification and deep deletion CN thresholds equaling or above four and below one were applied, respectively. A CN of three or one was considered as shallow amplification or deletion, respectively. To ensure reproducibility, all steps were implemented into an automated analysis pipeline using snakemake. The pipeline and detailed information are available on GitHub (https://github.com/IPorth/TMLflow).

Silent mutations and mutations with population allele frequency above 5% were excluded. All mutations were visually inspected using the Integrative Genomics Viewer. The TMB was calculated by dividing the number of mutations, including nonsynonymous and frame shift mutations, through the Mb size of the TML panel. The R package Maftools was utilized for visualization of SNV and CNV.

3.8   MSI

To examine the microsatellite status of tumor samples, DNA isolated as described in chapter 3.5 was used in an automatic analysis with an Idylla MSI test according to manufacturer's protocol.

3.9   Affymetrix microarray

Affymetrix microarray experiments, quality control and processing of raw data was performed by Dr. rer. nat. Carolina de la Torre from the NGS core facility of the Medical Faculty Mannheim, University of Heidelberg. Gene expression profiling was performed for 18 patient and 5 normal samples using arrays of GeneChip® Human Transcriptome 2.0 Arrays. Biotinylated antisense cDNA was prepared according to the standard labelling protocol with the GeneChip® WT Plus Reagent Kit and the GeneChip® Hybridization, Wash and Stain Kit. Subsequently, the hybridization on the chip was carried out in a GeneChip Hybridization oven 640. Next, the chip was dyed in the GeneChip Fluidics Station 450 and scanned with a GeneChip Scanner 3000. Pat1 was not included in the Affymetrix experiments because the sample arrived afterwards. A Custom CDF Version 22 with ENTREZ based gene definitions was used to annotate the arrays [147]. The raw fluorescence intensity values were normalized applying quantile normalization and RMA background correction. OneWay-ANOVA was performed to identify differential expressed genes (DEG) using a commercial software package SAS JMP15 Genomics. A false positive rate of a=0.05 with FDR correction was taken as the level of significance.

3.10   Datamining

Publicly available gene expression data sets were obtained from Gene Expression Omnibus (GEO) and the ArrayExpress database. Normalized data of four trastuzumab-resistant and a trastuzumab-sensitive cell line was obtained from GSE77346 [148]. Raw gene expression data from 16 HER2-positive Chinese gastric cancer samples was received from E-MTAB-9990. In addition, inherent published survival and treatment information was used to assign patient groups according to OS [149]. The Shi et al. dataset was normalized by Dr. rer. nat Carsten Sticht (NGS core facility of the Medical Faculty) as described above (Chapter 3.9).

3.11   Gene expression data analysis

3.11.1   Differential gene expression analysis

For differential expression analysis, the R package limma, available on Bioconductor, was used. DEG of the Shi et al. data set were examined for the comparison of survival groups (OS≥12 months vs. OS<12 months). For GSE77346, the comparison trastuzumab-sensitive cells vs. resistant cells was analyzed. All analysis were carried out in unpaired mode.

3.11.2 Pathway activity estimation

Pathway activity was estimated with the R package PROGENy. The DEG between survival groups and normalized gene expression data were used as input. The top 500 pathway sensitive genes were taken into account for calculation of PROGENy scores. Next, enrichment analysis was run with 10000 permutations resulting in normalized enrichment scores

3.11.3 Transcription factor activity estimation

The R package DoRothEA was used determine transcription factor activity. Input data was used as described for PROGENy analysis (Chapter 3.11.2). The regulon database "dorothea_hs" was used to perform transcription factor enrichment analysis.

3.11.4 Immune cell and reactivity analysis

Normalized gene expression data was used as input in all immune cell and activity analyses. ESTIMATE was used for calculation of tumor purity, immune and stromal scores. For investigation of immune cell populations, the webtools xCell (https://xcell.ucsf.edu/) and CIBERSORTx (https://cibersortx.stanford.edu/) were utilized [150,151]. The absolute cell fractions of 22 immune cell types were calculated using the provided signature matrix file. The analysis was run with batch correction in B-mode, quantile normalization and 1000 permutations. The cytolytic activity (CYT) score was determined with the geometric mean of gene expression values for Granzyme A (GZMA) and Perforin 1 (PRF1) [152].

3.12 Statistical analysis

Data is presented as median ± standard deviation. Statistical analysis was performed with GraphPad Prism 9 software. Non-parametric Mann-Whitney U test was utilized to compare continuous variables. Categorical variables were tested with the Fisher's exact test. The relation between data series was calculated with the Spearman correlation coefficient. Progression-free survival was statistically evaluated using Kaplan-Meyer analysis and compared with the Mantel-Haenszel test. Significance was accepted at $p \leq 0.05$ and the significance levels were defined as follows: ns not significant, $*p \leq 0.05$, $**p \leq 0.01$.

4 Results

4.1 Pipeline development for SNV and CNV calling

Thermo Fisher Scientific provides an automated pipeline for SNV analysis of the Oncomine TML panel on the IonReporter platform. However, the pipeline lacks CNV calling and still uses the human reference genome version hg19, while an updated genome version (hg38) is available. Lastly, the IonReporter output format is not directly suitable for further analysis. Thus, I decided to generate a pipeline, which uses the latest reference genome build and includes a CNV calling option. The general criteria for the selection of the software for SNV and CNV calling included the suitability for targeted amplicon sequencing (TAS) data and variant calling on a single tumor sample without matched normal. I chose the workflow manager snakemake for reproducible and scalable data analysis. Compatibility with snakemake was a decisive factor in my software selection process.

4.1.1 CNV caller selection

As stated above, CNV calling is not included in the TML Thermo Fisher Scientific analysis workflow. Therefore, in addition to the general selection criteria, a CNV caller was required to accurately identify *ERBB2* amplifications and provide a numeric copy number per gene in the output file. After conducting a literature search, the CNV callers CNVkit, CovCopCan, IonCopy, CNVPanelizer and ONCOCNV were selected for further testing with TML data from the validation cohort, which included two HER2-negative cases (Val1 and Val2) and two HER2-positive cases (Val3 and Val4).
As control, the samples were analyzed with the Oncomine Comprehensive Assay (OCA) by Thermo Fisher Scientific, which includes CNV calling for a subset of genes including *ERBB2*. For each CNV caller, the number of variants (Figure 6A) as well as the concordance of variants between callers (Figure 6B) were evaluated.
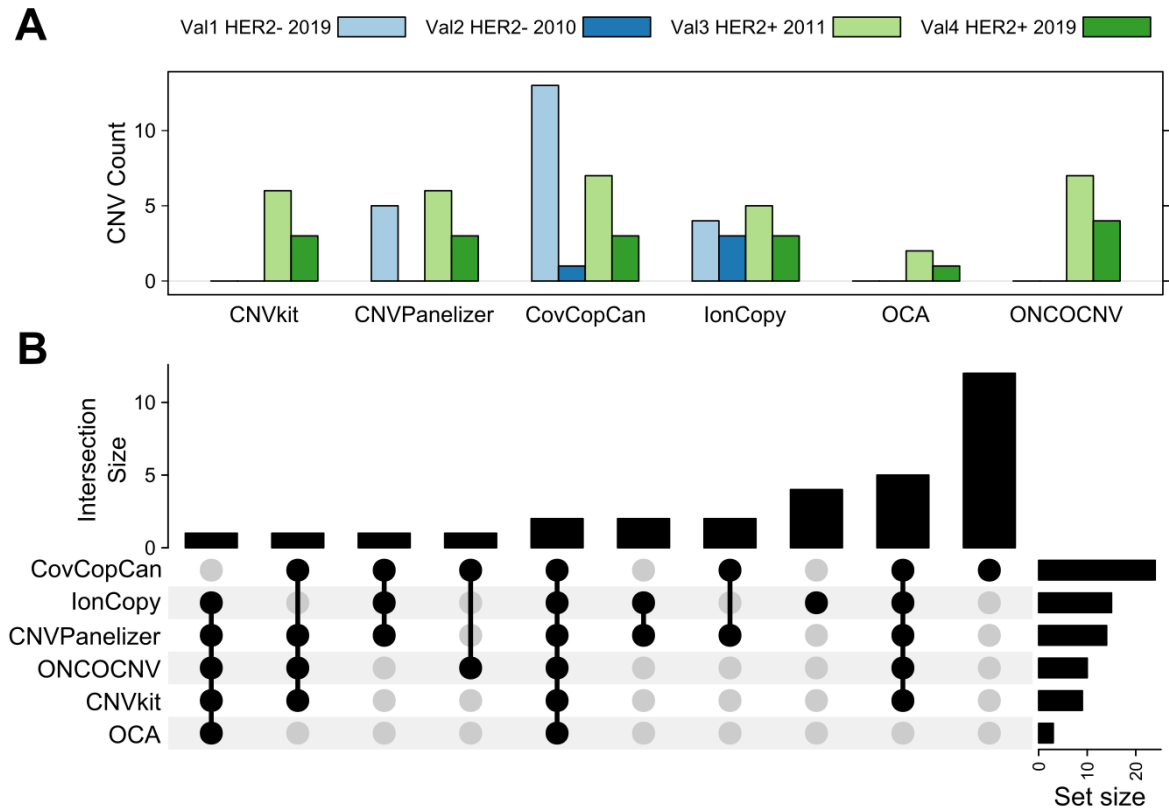
**Figure 6 | CNV caller evaluation with validation cohort**
CNV analysis of the validation cohort with CNV callers CovCopCan, IonCopy, CNVPanelizer, ONCOCNV, CNVkit and OCA. **A:** Sum of CNVs detected per CNV caller and validation sample **B:** Upset plot showing the number of concordant CNVs between different CNV callers (intersection size) as well as the absolute number of CNV calls per caller (set size).
CNV, copy number variant; OCA, Oncomine comprehensive panel;

Among the validation cohort, CovCopCan identified the largest number of variants, detecting 24 CNVs across all cases. Five of the detected variants were unique. However, it did not provide the exact CN for amplifications or deletions and failed to identify the *ERBB2* amplification in Val3, which resulted in its exclusion from further analysis. All other callers identified the *ERBB2* amplification in the HER2-positive cases correctly and did not state an amplified *ERBB2* status in the HER2-negative cases. IonCopy detected 15 CNVs, including 4 unique ones. All remaining variants were confirmed by at least one other caller and no other caller detected unique variants. The TML panel does not target chrY, which causes difficulties in accurate CNV calling on gonosomes. Val1 is the only female representative in the validation cohort. CNVPanelizer and IonCopy detected amplifications on chrX in this case. Additionally, IonCopy called CNVs in Val2, which were not found by any other callers. As a result, CNVPanelizer and IonCopy were also excluded from further analysis.

ONCOCNV and CNVkit where highly concordant and did not detect variants in the HER2-negative cases Val1 and Val2. As correct detection of *ERBB2* copy number status is a main criterion for CNV caller selection, the CNV caller results were compared to *ERBB2* FISH (Figure 7). In addition, the log2-fold CN change detected for the most frequently altered genes

were compared between callers (Figure 7B). The previously excluded CNV callers CNVPanelizer and IonCopy were included for comparison.
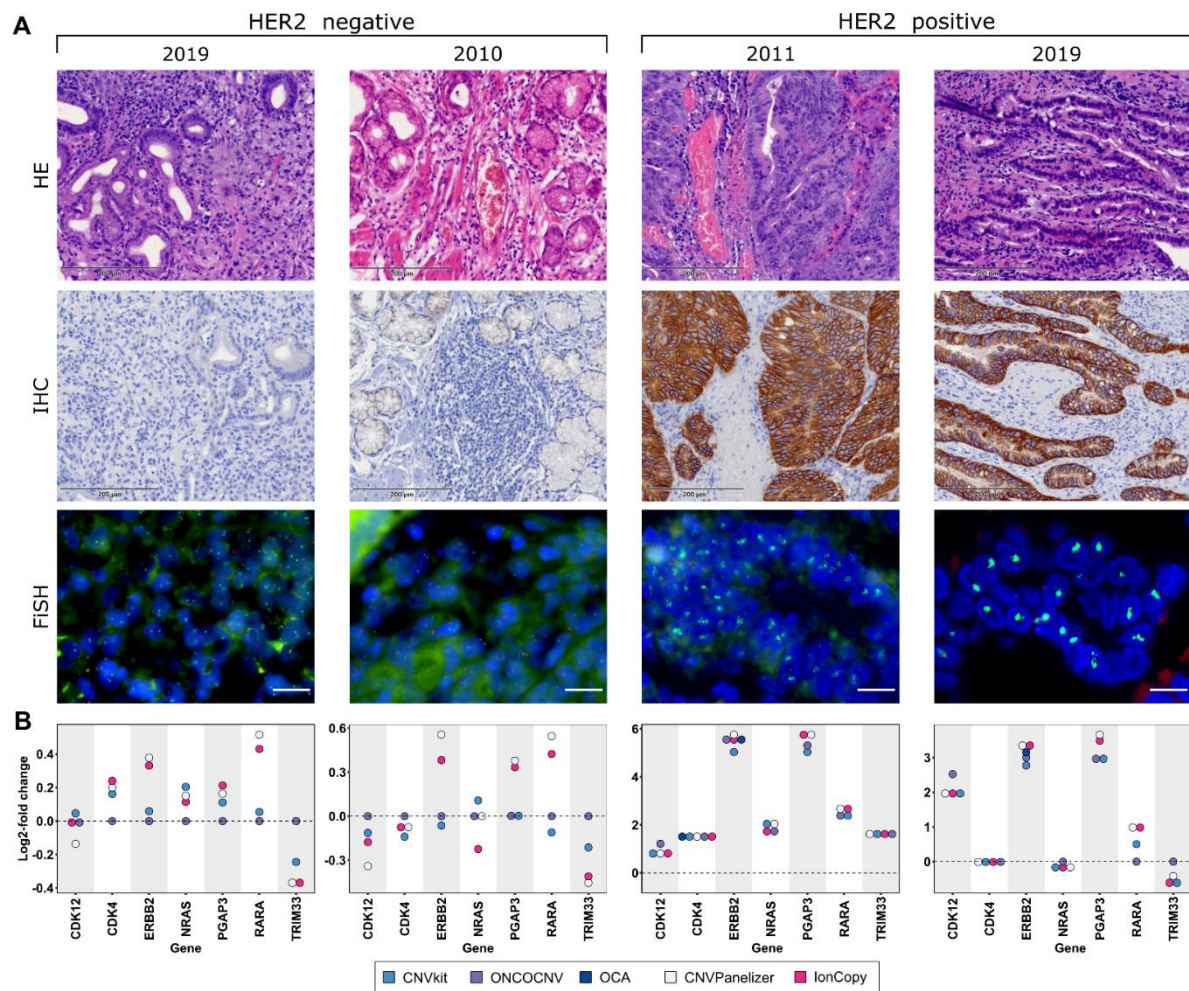
Figure 7 | Evaluation of *ERBB2* amplification in the validation cohort using NGS and FISH
A: Exemplary image of the tumor tissue of the validation samples stained with HE (upper row) and IHC (middle row). Scale bar: 200 µm. Bottom row illustrates the result of fluorescence in-situ hybridization of *ERBB2* and centromer 17. Scale bar: 10 µm. **B:** Results of CNV calling displayed as log2 fold copy number change per gene. Each point corresponds to the log2 fold change CN determined by one of the CNV callers CNVkit, ONCOCNV, OCA, CNVPanelizer or IonCopy

In the HER2-negative, cases Val1 and Val2, the HER2 immunohistochemical staining was scored with IHC score 0 and the FISH evaluation revealed a *ERBB2*/CEP17 ratio of 1.1 and 0.9, respectively. The OCA assay did not detect any amplification in these cases. CNVkit and ONCOCNV estimated log-fold changes of 0.05 and 0 for Val1 and -0.06 and 0 for Val2, respectively. The HER2-positive cases Val3 and Val4 were scored with HER2 IHC score 3+ and the FISH analysis showed a high amplification status, but an exact *ERBB2*/CEP17 ratio could not be determined due to *ERBB2* signal clusters (>20 copies). The CN for *ERBB2* detected by ONCOCNV for Val3 and Val4 were close to the *ERBB2* CN detected by the IonReporter in the OCA panel data, while CNVkit tend to underestimate the *ERBB2* CN in

these cases. In both positive cases, ONCOCNV detected *CDK12* CN log-fold change was higher (1.16 in Val3; 2.5 in Val4) compared to CNVkit, which determined a log-fold change of 0.88 and 1.99 in Val3 and Val4, respectively. For all other genes, the amplifications detected by ONCOCNV and CNVkit were concordant.

CNVkit and ONCOCNV were the top-performing CNV callers among those evaluated based on concordance of CNV calls and absolute CN estimates. CNVkit was originally developed for hybrid-capture sequencing, but it can also be applied for TAS data. The method of CNVkit is based on off-target regions as baseline for CNV calling. In contrast to hybrid-capture panel sequencing, amplicon panel sequencing does not include off-target regions [131]. Thus, the TML data does not have control regions as baseline, which could have had an impact on absolute CN estimates that tended to be lower with CNVkit compared to other CN callers. In contrast, ONCOCNV was specially designed for TAS data and requires normal samples as input to build a baseline for CNV calling. In addition, ONCOCNV's *ERBB2* CN estimation was more consistent with the OCA results. For these reasons, I decided to use ONCOCNV to analyze CNVs.

4.1.2 Selection of SNV caller and calling strategy

There are two main strategies for SNV calling on TAS data. The first strategy involves performing sequencing in replicates and intersecting the SNV calls produced by one caller for each replicate. The second strategy involves using two SNV callers to detect SNVs in the same dataset, and then intersecting the results [153]. Thermo Fisher Scientific recommends running the analysis in duplicates, so the two-caller strategy was applied to merged duplicates to include the complete dataset.

The SNV callers Mutect2, VarDict, VarScan2, SamTools and PipeIT have been reported to be suitable for TAS data [153-155]. However, VarScan2 and PipeIT require a matched normal sample and were therefore excluded. As Ion Torrent sequencing has a high error rate in homopolymer regions, incorporating a PoN was crucial for SNV calling [156,157]. Of the above-mentioned callers, Mutect2 is the only caller that handles a PoN and thus was chosen for the single caller intersection strategy (Figure 8A). The SNV callers Mutect2 and VarDict were found to be an ideal combination for the second strategy and were applied to the merged duplicates of the validation cohort (Figure 8B) [153].

The runtime for both SNV calling strategies was found to be significantly different when applied to the validation cohort. The single-caller intersection strategy with Mutect2 had an average runtime of 5.7 h per sample, while the two-caller intersection on merged samples required an average 16.5 h per sample.
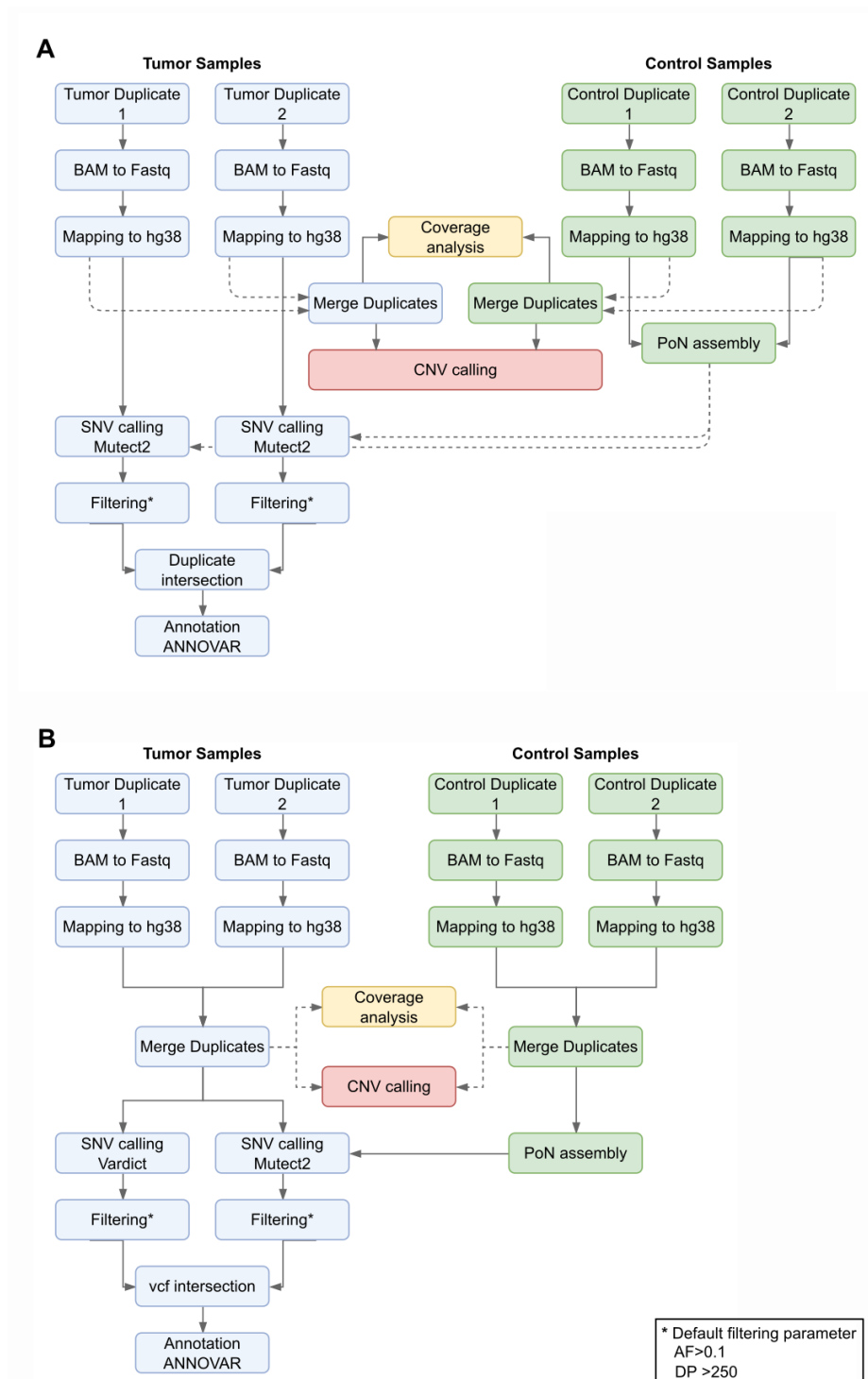
Figure 8 | Single nucleotide variant calling strategies with hg38 for IonReporter target amplicon sequencing data
A: Single-caller intersection strategy. Samples are sequenced in duplicates. Data preparation, single nucleotide variant (SNV) calling with Mutect2 and filtering is performed separately on each tumor sample duplicate (blue). The calling results are intersected and subsequently annotated. Control samples (green) are prepared in the same way as the tumor samples and are used to build a panel of normals (PoN) that is incorporated in tumor SNV calling. Copy number variant (CNV) calling and coverage analysis is performed on duplicates merged after data preparation. **B:** Two SNV caller intersection strategy. The duplicate tumor samples (blue) are prepared separately and then merged into one file. The merged sample is used for CNV calling, coverage analysis and SNV calling with two SNV callers, here Vardict and Mutect2. The SNV calling results of both callers are intersected and annotated. The normal samples (green) are merged after preparation and used as baseline for CNV calling and as PoN in Mutect2 SNV calling.

34

Estimating the runtime of SNV calling for a cohort of 20 samples using the average runtime determined from the validation cohort reveals a SNV calling time of 4.8 days with the single-caller intersection strategy and 13.8 days with the two-caller intersection strategy. Considering hardware availability, the two-caller intersection strategy has limited practicability compared to the single-caller intersection strategy. Thus, the latter was selected for analysis.

After deciding on the final software, a snakemake workflow was built according to Figure 8A. The workflow includes sample preparation and mapping to hg38, CNV calling, coverage analysis, SNV calling with preparation of a PoN, and annotation of SNVs.

The workflow with documentation is available on GitHub (https://github.com/IPorth/TMLflow).

4.1.3   Selection thresholds for read depth and allele frequency

Thresholds for DP and AF had to be set to distinguish sequencing artefacts from true positive SNVs. All cohort samples are formalin-fixed, paraffin-embedded and stored for up to 10 years. Tissue processing and ageing can lead to DNA damage, such as DNA fragmentation and cytosine deamination, which is recognized by the SNV caller as a C>T/G>A nucleotide exchange [158,159]. A common AF threshold used in several studies is 5% and was selected for evaluation [107,160]. However, FFPE-related artefacts have been reported to occur with AF between 1-10% [158]. Therefore, the 10% AF threshold was also tested. The DP threshold was set relative to the sample with the lowest average read depth in the validation cohort, which was Val3 with an average DP of 634. The DP cut-offs evaluated were 500 and 250 and the following AF and DP threshold combinations were tested: AF 5% plus DP 250, AF 5% plus DP 500, and AF 10% plus DP 250. The AF and DP of a variant had to be above the thresholds to be accepted as a true positive SNV.

SNV nucleotide exchange, variant classification and number of variants per sample were evaluated (Figure 9A). The first threshold combination evaluated was AF 5% and DP 250. Mutations were detected in all samples with a median of 10.5 variants per sample, with C>T being the most common nucleotide exchange. Thirteen frameshift mutations were also detected, which occurred mostly in homopolymeric regions likely homopolymer artifacts (Figure 9B). Since the median of 10.5 variants per sample is high in a panel of 409 genes, it is likely that some of the detected mutations are artifacts and more stringent filtering should be applied. Next, the combination of AF 5% plus DP 500 was tested. With this cut-off, no variant was detected in Val3 and the median detected mutation per sample was 1. Although the increased DP threshold reduced frameshift mutations, it was found to be too stringent. Filtering with AF 10% plus DP 250 detected mutations in all samples. Similar to filtering with AF 5% and DP 250, the most common nucleotide exchange was C>T, but fewer frameshift variants were found (6 vs. 10 frameshift variants). Interestingly, more mutations were detected in the 2010

and 2011 samples than in the 2019 samples, which is not surprising and likely caused by artifacts in the aged DNA [158].

Taken together, the AF 10% plus DP 250 filter cutoff was found to be suitable for robust mutation detection in the context of amplicon sequencing of FFPE samples. However, the PoN could not filter all sequencing artifacts in homopolymeric regions, which are interpreted by the SNV caller as frameshift deletions or frameshift insertions (Figure 9B). These frameshifts can occur at an AF above 10% and are therefore difficult to filter. A manual evaluation of frameshift mutations is required.
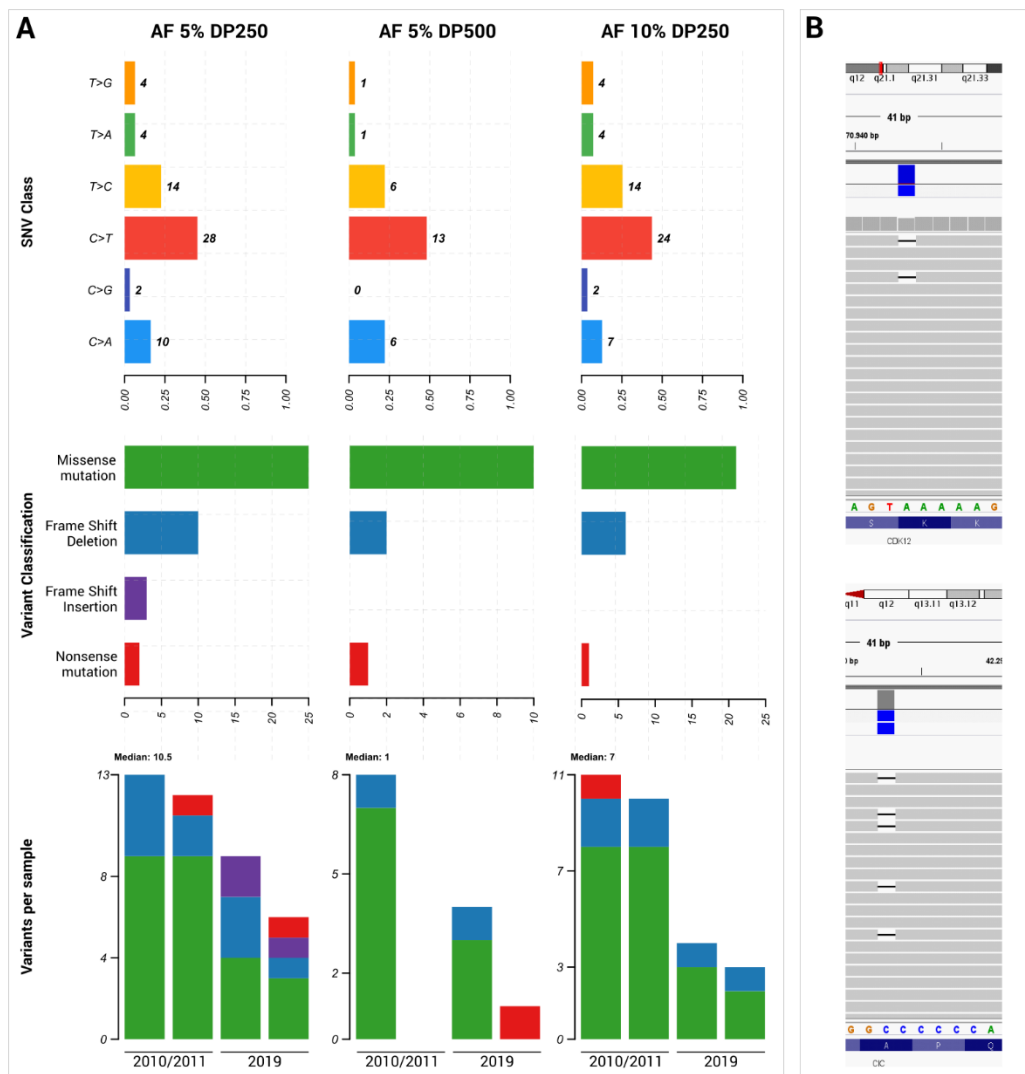
Figure 9 | Evaluation of SNVs detect with varying DP and AF thresholds

A: MAF summary plots showing the frequency of nucleotide exchanges (SNV class), the variant classification as missense mutation (green), frameshift deletion (blue) or insertion (purple) and Nonsense mutation. Variants per sample are shown in the lower row. **B:** IGV screenshot of a frameshift mutation detected in a homopolymeric region. The mutations occurred with an AF of 4.7% and 20% in the upper and lower panel, respectively.

4.2 Patient cohort characteristics

A total of 19 patients with HER2-positive mGEJ/mGEJC from four clinical centers were included in this retrospective study and divided into two groups based on their response to trastuzumab-based therapy: long-term responders (PFS≥12 months, n=7) and short-term responders (PFS<12 months, n=12) (Table 10). The median follow-up duration was 18 months, with a median PFS of 6 months in the short-term responding group and 22 months in the long-term responding group. The patient groups did not show significant differences in tumor location, differentiation, number of metastatic sites, perioperative treatment and HER2 status. However, there was a slight imbalance between the groups in terms of patient age and gender, with all patients in the long-term responder group being male (p=0.2) and the short-term responding group having older patients at diagnosis (p=0.1).

Table 10 | Clinicopathologic characteristics of the retrospective patient cohort, long-term and short-term responder group

| Characteristics	Overall Population (n=19)	Long-Term Responder (n=7)[1]	Short-Term Responder (n=12)[1]	p-value[2]
Age	64 (59, 72)	59 (58, 62)	71 (63, 72)	0.1
Gender				0.2
male	15 (79%)	7 (100%)	8 (67%)	
female	4 (21%)	0 (0%)	4 (33%)	
PFS	9 (4, 19)	22 (19, 40)	6 (4, 9)	<0.001
Location				>0.6
GEJC	10 (53%)	3 (43%)	7 (58%)	
GC	9 (47%)	4 (57%)	5 (42%)	
Differentiation				>0.9
G2	10 (53%)	4 (57%)	6 (45%)	
G3	8 (42%)	3 (43%)	5 (45%)	
unknown	1 (5%)	0	1 (9.1%)	
No. of metastatic sites				0.5
1	7 (37%)	3 (43%)	4 (33%)	
2	9 (47%)	2 (29%)	7 (58%)	
>2	3 (16%)	2 (29%)	1 (8.3%)	
Perioperative Chemotherapy*	4 (21%)	1 (14%)	3 (25%)	>0.9
HER2 Status				>0.9
2+ (ISH positive)	7 (37%)	2 (29%)	5 (36%)	
3+	12 (63%)	5 (71%)	7 (64%)	

[1] n (%); Median (IQR)

[2] Comparison between long-term responder and fast disease progress group were performed with Fisher's exact test or Wilcoxon rank sum test as appropriate

*without trastuzumab

4.3 Evaluation of HER2 status, expression pattern and gene copy number

Patients with locally tested HER2-positive status were included in this retrospective study. The HER2 status was re-evaluated centrally and could be confirmed in 95% (18/19) of the cases. One patient (Pat14) with initially assessed HER2 IHC score 3+ did not show any staining of the remaining tumor cells in the central testing. In addition, an amplification of *ERBB2* could not be detected using FISH. However, this patient was kept in the cohort since the inclusion criterion was HER2-positive status by local testing.
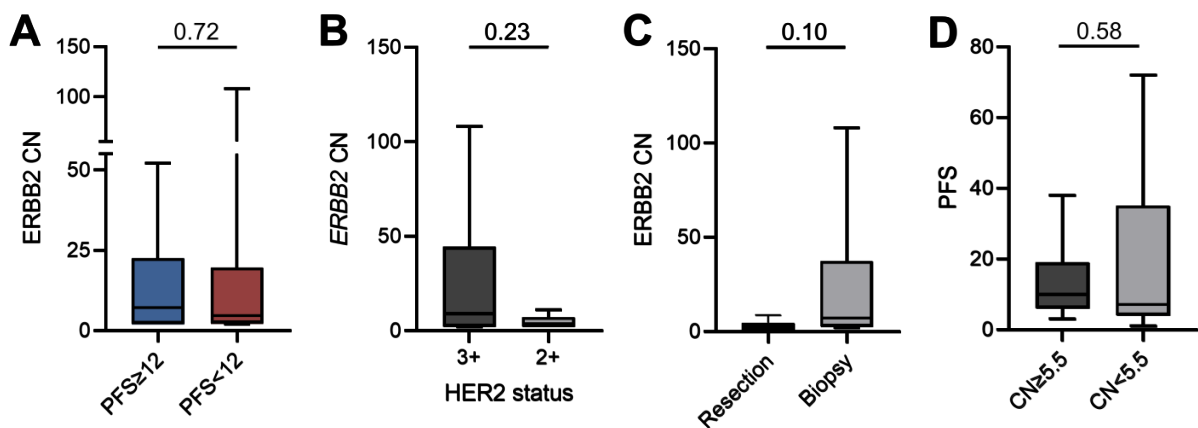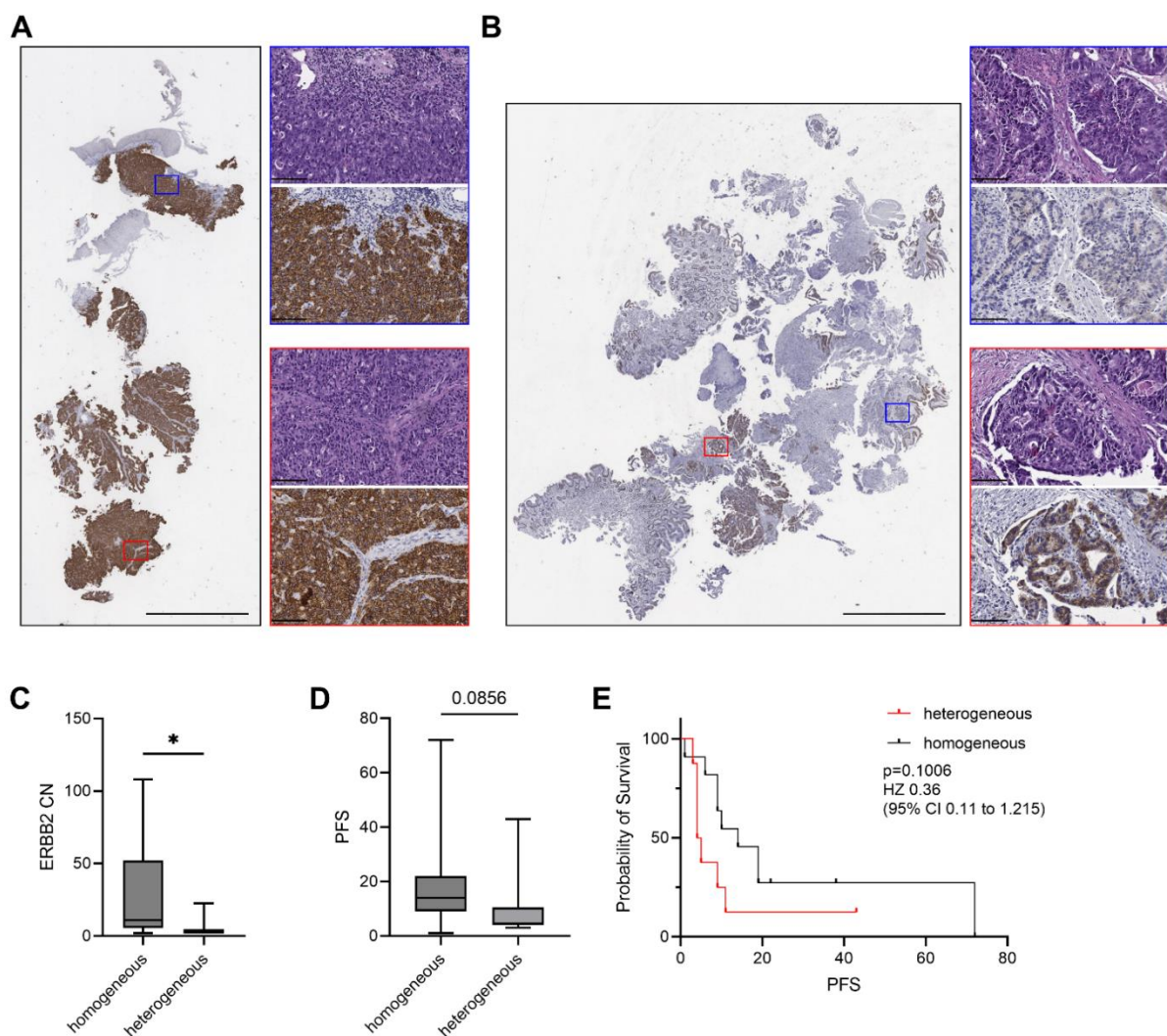

Figure 10 | *ERBB2* copy number and its association with progression-free survival, HER2 immunohistochemistry score and tumor sample specimen
Comparison of *ERBB2* copy number (CN) between **(A)** long-term (PFS≥12 months) and short-term (PFS<12 months) responding patients, **(B)** HER2 status IHC score 3+ and 2+ and **(C)** tumor resection specimen and biopsy. **(D)** The median *ERBB2* CN was used to define an *ERBB2*-high (CN≥5.5) and *ERBB2*-low (CN<5.5) group. The PFS between *ERBB2*-groups was compared.

Using NGS, the *ERBB2* CN was determined for each patient. The long-term responding patient group had a higher median *ERBB2* CN compared to the short-term responding group (median CN 7 vs. 4, p=0.72, Figure 10A). In samples with HER2 IHC score 3+, the *ERBB2* CN was increased but did not reach statistical significance (median CN 9 vs. 3.5, p=0.23, Figure 10B). In addition, *ERBB2* CN was decreased in resection specimens in comparison to biopsies but the trend was not significant (CN 2.75 vs. 7.00, p=0.10; Figure 10C). In literature, the median *ERBB2* CN of a cohort was described as separator between long-term responding and short-term responding patients [108]. Here, an *ERBB2* CN above or below the median was described as *ERBB2*-high or *ERBB2*-low, respectively. In this cohort, the median *ERBB2* CN was 5.5, and patients were assigned to the *ERBB2*-high (CN≥5.5) or *ERBB2*-low (CN<5.5) group accordingly. The median PFS was higher in the *ERBB2*-high group at 10 months compared to 7 months in the *ERBB2*-low group (Figure 10D). The grouping did not reveal a significant difference in PFS (p=0.58). In addition, the *ERBB2*-high status was not significantly associated with improved PFS (HR 0.82, 95% CI 0.27-2.48, p=0.722, Supplementary Figure 2).

Interestingly, although all patients were HER2-positive according to local pathological testing, the *ERBB2* amplification (defined as CN≥4) was only detected by NGS in 57.8% of patients. The discordance between NGS-determined *ERBB2* amplification and IHC-based HER2 status was not associated with PFS (p>0.9).

Heterogeneity in HER2 expression is frequently found in GC and GEJC [161]. Thus, expression pattern of HER2 was visually inspected (Figure 11A and B). A heterogeneous HER2 expression pattern was observed in 42% (8/19) of the samples. In cases with heterogeneous HER2 expression, the median *ERBB2* CN was significantly lower compared to samples with homogenous HER2 expression pattern (CN 2.25 vs. 11.00, p=0.013, Figure 11C). Furthermore, patients with homogenous HER2 expression were associated with higher median

Figure 11 | Association of HER2 expression pattern with *ERBB2* copy number and progression-free survival

Example of homogeneous **(A)** and heterogeneous **(B)** expression pattern of HER2 envisioned by immunohistochemistry. Scale bar: tissue overview 2 mm; zoom 100 µm. **C:** *ERBB2* copy number (CN) compared between homogeneous and heterogeneous expression pattern. **D:** Analysis progression-free survival (PFS) in context of heterogeneous and homogeneous HER2 expression. **E:** Kaplan-Meier curve comparing the survival benefit of patients with different HER2 expression pattern. The Mantel-Haenszel hazard ratio (HR) was applied.

PFS (14 months vs. 4.5 months, p=0.086, Figure 11D) and improved survival (HR 0.36, 95% CI 0.11-1.215, p=0.101, Figure 11E).

Interestingly, a heterogeneous HER2 status was observed in 83% of cases where HER2 status was not confirmed with NGS (p=0.006). No significant association between HER2 expression pattern and clinicopathological features was observed.

Taken together, *ERBB2* CN could not distinguish between trastuzumab long-term and short-term responding patients but improved PFS was associated with homogeneous HER2 expression pattern.

4.4   SNV and CNV analysis

The genomic regions of 406 cancer-associated genes were sequenced with the TML panel and further analyzed using the newly compiled TMLflow pipeline. A mutation was considered a true positive when the DP was over 250 and the AF was above 10%. Genetic alterations in the top 15 mutated genes were detected in 78.95% of the patients (15/19, Figure 12A). The most frequent amplified gene was *ERBB2*, accompanied by *PGAP3*, *CDK12* and *RARA*, which are located on chromosome 17 in proximity to *ERBB2*. *MYC* and *CCNE1* were both amplified in 26% of the patients. Other genes amplified in at least three patients were *RECQL4* and
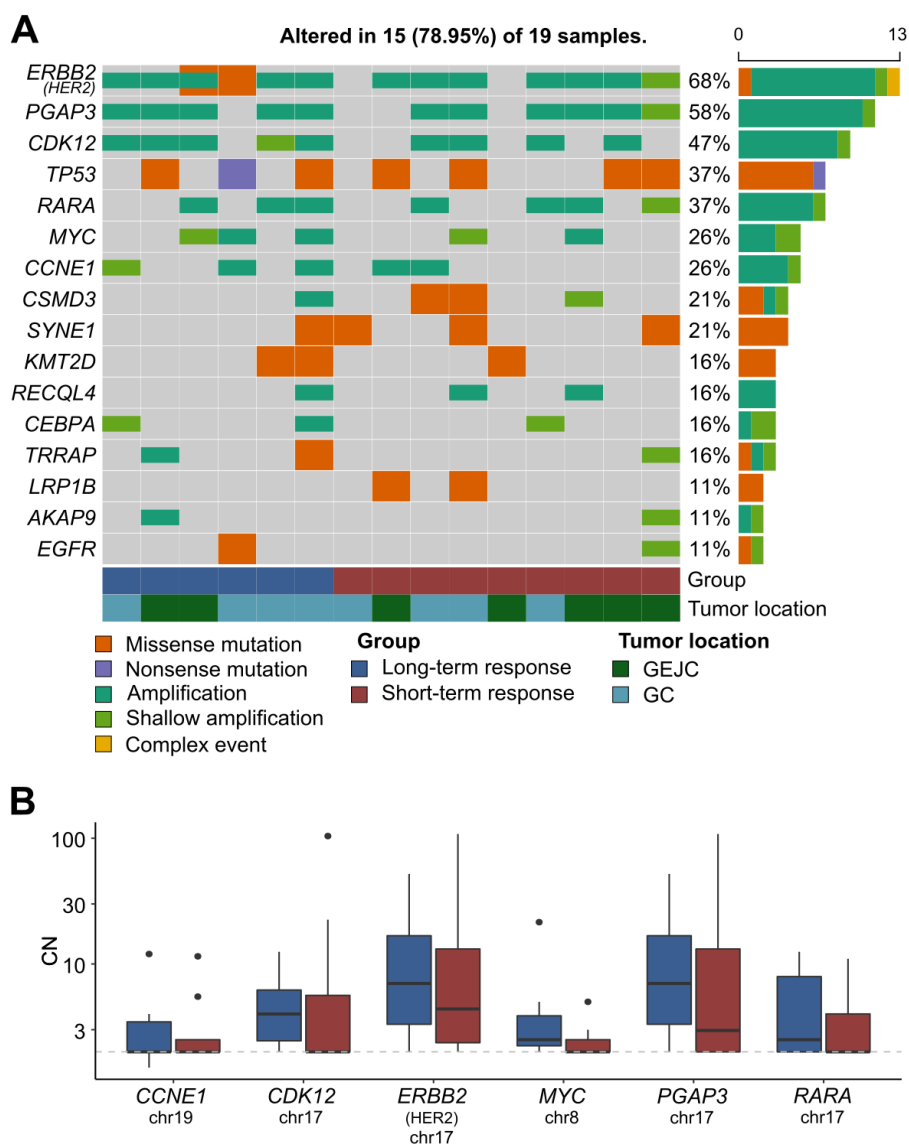
Figure 12 | Distribution of genomic alterations detected by NGS panel sequencing in HER2-positive mGC/mGEJC patients
A: Oncoplot showing genes with molecular alterations in at least two patients of the cohort. **B:** Copy numbers (CN) of genes amplified in a minimum of 25% of patients are compared between long-term (blue) and short-term (red) responding patients.

CEBPA. The CN of genes amplified in at least five patients have been compared between patient groups but no significant difference could be detected (Figure 12B).

Stop-gain and non-synonymous *TP53* mutations were detected in 37% of the patients. These mutations were unique to each patient and were evenly distributed among the patient groups. Other frequently mutated genes included *SYNE1* (21%) and *KMT2D* (16%). As for *TP53*, no mutation was predominant. Mutations in genes involved in ERBB signaling were detected in five patients, three in the long-term and two in the short-term responding group. Two patients in the long-term responding group harbored *ERBB2* mutations. Pat4 was *ERBB2* amplified and presented the *ERBB2* p.V777L mutation with an AF of 76%. The mutation p.P489L in *ERBB2* was found in Pat5 with an AF of 66%. This *ERBB2* mutation was found along with an *EGFR* mutation. In this patient, *ERBB2* amplification was not detected by NGS. One short-term responding patient, Pat19, carried an *EGFR* shallow amplification (CN 3). An *ERBB4* mutation was found in Pat11. Mutations or amplifications in *KRAS* and *PTEN* were not detected in this cohort.

Altogether, several mutations with potential impact on trastuzumab sensitivity were detected but the mutations were equally distributed between patient groups.

4.5   Tumor mutational burden

Using the SNV output of the TMLflow pipeline, the TMB was calculated. None of the patients had a high TMB according to the published threshold of ≥10 mut/Mb [87]. The TMB range in the cohort was 0 - 6.6 mut/Mb and the median TMB was 1.81 mut/Mb. In the patient group with long-term response the median TMB was higher than in the short-term responder group, but the trend was not significant (4.85 mut/Mb vs. 1.82 mut/Mb, p=0.15, Figure 13A). The TMB was significantly associated with tumor location. Tumors with epicenter in the stomach had a
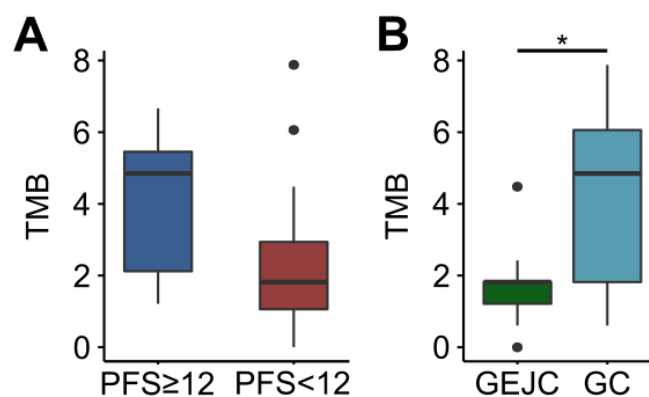
Figure 13 | Association of the tumor mutational burden with PFS and tumor location
**A:** Tumor mutational burden (TMB, mut/Mb) compared between long-term (blue) and short-term responding patients. **B:** TMB of tumors at the gastroesophageal junction (GEJC, green) compared to tumors located in the stomach (GC, light blue)

median TMB of 4.84 while in tumors at the GEJ a median TMB of 1.81 was determined (p=0.049, Figure 13B).

4.6 Analysis of MSI, PD-L1 and immune cell populations

The microsatellite status was determined and all patients of the cohort were MSS. PD-L1 was assessed with IHC as recommended for mGC/mGEJC (Figure 14A)[17]. The PD-L1-positive (CPS≥1) rate in the cohort was 47.3%. The detected CPS values were in general low and PD-L1 expression exclusively occurred in immune cells.
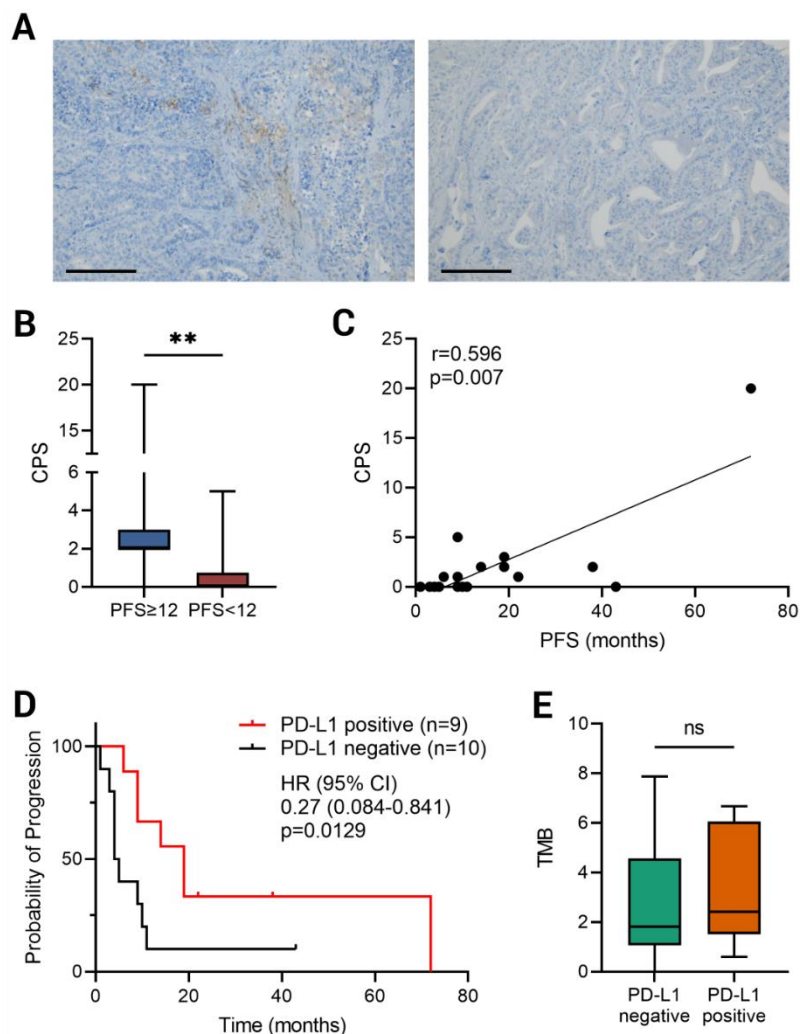
Figure 14 | Relevance of PD-L1 for long-term response to trastuzumab treatment in HER2-positive mGC/mGEJC
A: Exemplary IHC stainings for PD-L1-positive (left) and -negative (right) patients. **B:** PD-L1 combined positive score (CPS) difference between patients with long-term (PFS≥12 months) and short-term (PFS<12 months) response to trastuzumab. **C:** Spearman correlation of PFS and CPS, r is the spearman rank coefficient. **D:** Kaplan-Meier curve comparing the survival benefit of PD-L1-positive (CPS≥1) and -negative patients. The Mantel-Haenszel hazard ratio (HR) was applied. **E:** Tumor mutation burden (TMB, mut/Mb) compared between patients with different PD-L1 status

Long-term responding patients had a significantly higher median CPS than the short-term responders (p=0.005, Figure 14B). Furthermore, a significant correlation between CPS and PFS was observed in the overall patient cohort (r=0.596, p=0.007, Figure 14C). Patients with PD-L1-positive status had an improved PFS (HR 0.27, 95% CI 0.084-0.841, p=0.0129, Figure 14D). Except lower median age at diagnosis (59 years, p=0.024), PD-L1 positivity was not associated with clinicopathological features. In addition, no correlation between TMB and PD-L1 status was observed (Figure 14E).
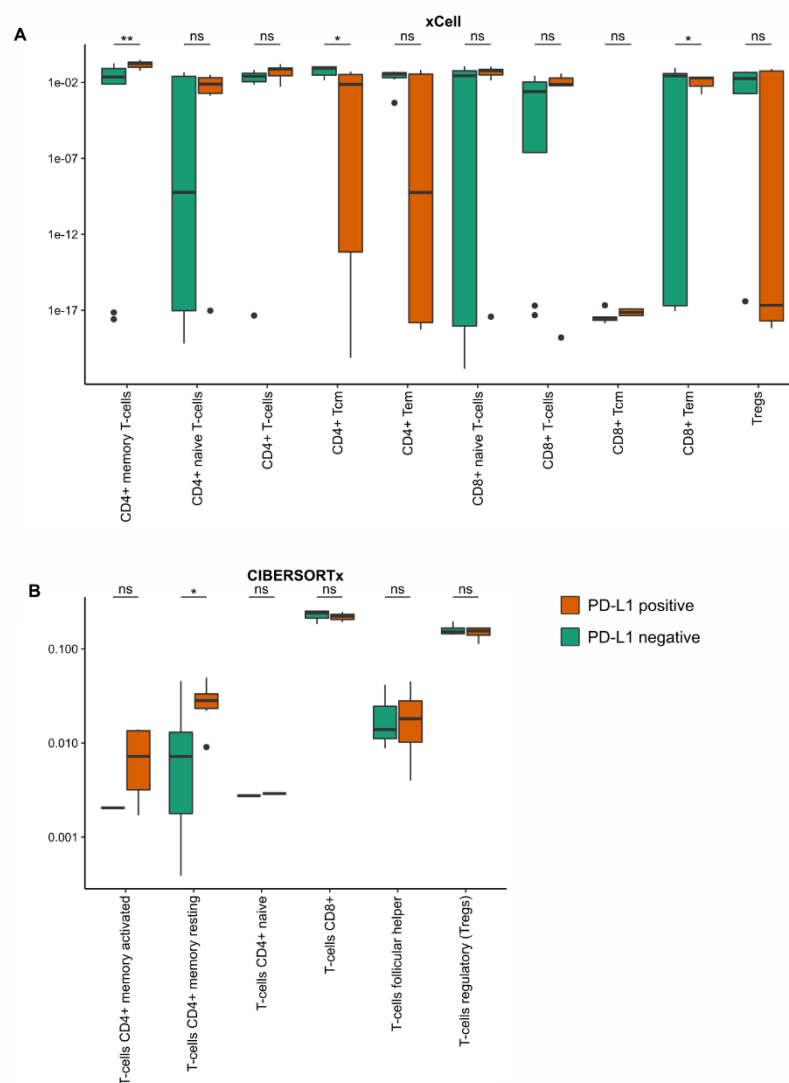
Figure 15 | Relation between of T-cell populations and PD-L1 status
Analysis of T-cell populations of PD-L1-positive (orange) and negative (green) patients by applying **(A)** xCell and **(B)** CIBERSORTx to microarray data

The expression of PD-L1 was only present on immune cells. Thus, Affymetrix gene expression data was used to analyze the composition of immune cells with CIBERSORTx and xCell. In addition, the CYT score was calculated to evaluate the immune cell activity. The comparison of T-cell populations between patient PFS groups showed no significant difference in any

investigated cell types using both analysis methods (Supplementary Figure 1). However, significant alterations in T-cell scores were associated with PD-L1 status. According to xCell analysis, PD-L1-positive patients had higher CD4+ memory T-cell scores (p=0.008, Figure 15A). This finding was confirmed by CIBERSORTx, which detected significantly higher scores for resting CD4+ memory T-cells in the PD-L1-positive patients (p=0.0413, Figure 15B). The activated CD4+ memory T-cells showed a similar trend, but this result did not reach statistical significance (p=0.052). In PD-L1-negative patients, xCell analysis found significantly higher CD4+ central memory (Tcm) and CD8+ effector memory (Tem) T-cell scores (Figure 15A). However, CIBERSORTx could not support this result. The CYT score was significantly increased in the long-term responding patient group (p=0.0245, Figure 16A), but it was not associated with PD-L1 positivity (p=0.1457, Figure 16B)
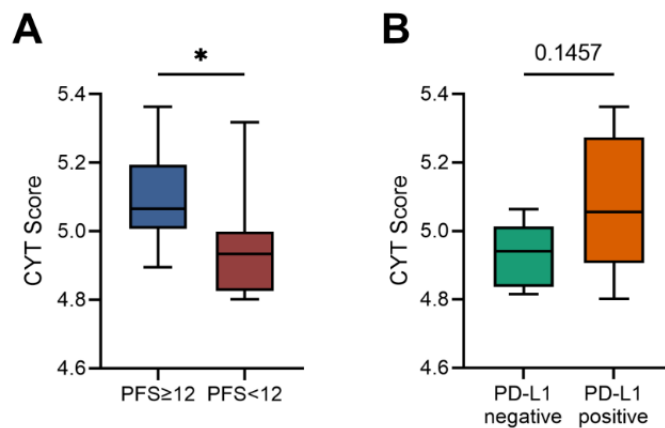
Figure 16 | Analysis of the CYT score in the context of trastuzumab response and PD-L1 status
A: Comparison of the CYT score between trastuzumab long-term and short-term responding patient groups B: Association of CYT score with PD-L1 status

An association of T-cell scores with the PD-L1 groups was observed. Thus, in the next step, correlations between immune population scores and continuous CPS, CYT score and PFS were analyzed using the Spearman rank coefficient (Figure 17). The CYT score was negatively correlated with CD8+ T-cells and positively correlated with CD4+ memory T-cells, however these findings did not reach statistical significance.
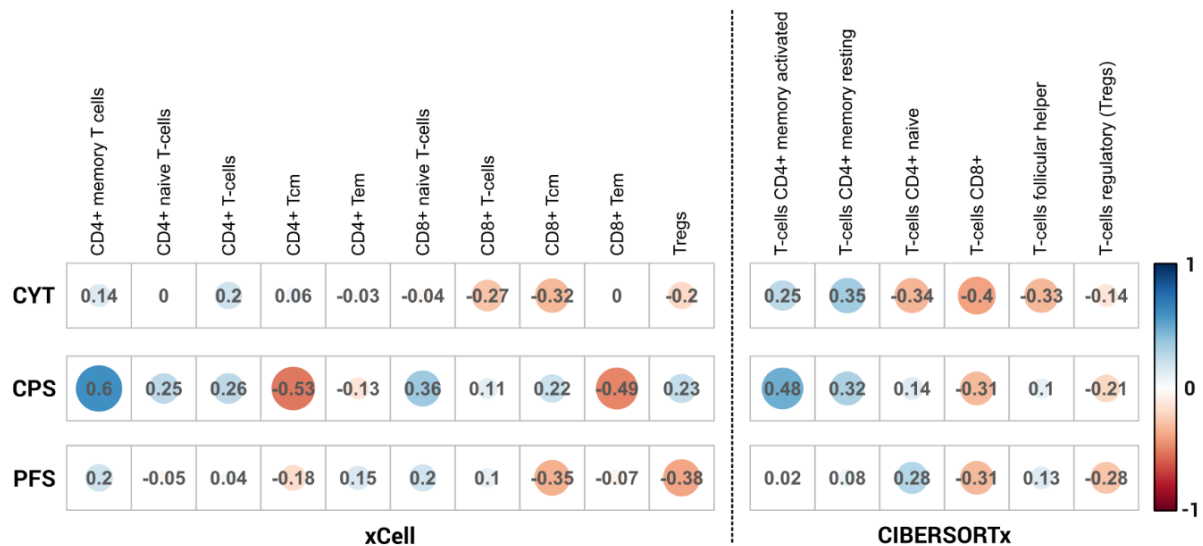
Figure 17 | Spearman correlation of xCell/CIBERSORTx immune cell scores with CPS, CYT score and PFS
Spearman rank coefficient is displayed for correlation each analyzed T-cell type with the cytolytic activity score (CYT), the PD-L1 combined positive score (CPS) and progression-free survival (PFS) under trastuzumab therapy. Red indicates a negative correlation and blue a positive correlation. Size of the circles reflects the strength of correlation.

Several T-cell populations were connected to the CPS. CD4+ T-cells are elevated in PD-L1-positive patients. The analysis reveals a significant correlation between CD4+ memory T-cells and the CPS according to xCell (r=0.601, p=0.008). This association is additionally found by CIBERSORTx. Additionally, the score for activated memory CD4+ T-cell showed a significant positive correlation with the CPS (r=0.4821, p=0.042). Furthermore, resting memory T-cells were also positively associated with CPS, although the trend was not significant. Significant negative correlations were determined between the xCell score CD4+ Tcm and CPS (r=-0.53, p=0.024). In addition, a negative coherence of CD8+ T-effector memory cells (xCell) with CPS was observed (r=-0.488, p=0.039). Weak correlations between PFS and T-cell populations were detected. Different CD8+ and regulatory T-cell scores of xCell and CIBERSORTx were negatively correlated with PFS without reaching statistical significance.

Together, CPS was correlated with improved PFS on trastuzumab-based treatment. In addition, a strong connection between PD-L1 expression and CD4+ memory T-cells was observed.

4.7 Pathway and transcription factor activity analysis

ERBB2 amplification can cause increased activity of MAPK and PI3K/Akt signaling. In this section, the analysis of pathway and transcription factor activity using microarray gene expression data from the retrospective cohort (referred to as the thesis cohort) is described and compared to two publicly available datasets. One dataset, published by Shi et al., includes

microarray data from 16 HER2-positive mGC/mGEJC patients, who received trastuzumab treatment [149]. As in this thesis cohort, patients from Shi et al. were divided into two groups according to OS: Long-term survival (OS≥12 months) and short-term survival (OS<12 months). The other data set, GSE77346, published by Prio et al., comprised microarray data from four cell lines with acquired trastuzumab resistance and one trastuzumab-sensitive cell line which were also analyzed.
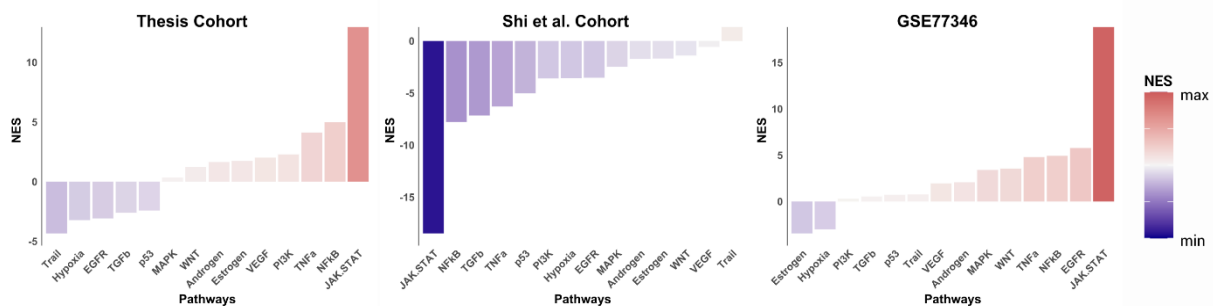

Figure 18 | PROGENy pathway activity prediction in trastuzumab-sensitive cell line and patient samples.
Normalized enrichment scores (NES) of 14 pathways calculated for the comparison of patients with long-term vs. short term response/survival to trastuzumab (Thesis cohort: PFS≥12 months vs. PFS<12 months; Shi et al. cohort: OS≥12 months vs. OS<12 months) and trastuzumab-sensitive vs. resistant cell lines.

The pathway activity analysis revealed contrary activated pathways between the thesis cohort and the Shi et al. cohort (Figure 18). For instance, in the long-term responding patients of the thesis cohort, the JAK-STAT and NFκB pathways were the top activated pathways, whereas they were the most downregulated pathways in long-term surviving patients of the Shi et al. cohort. Furthermore, the Trail pathway, which was the most downregulated pathway in the thesis cohort, was the only upregulated pathway in the Shi et al. cohort. In both data sets, the activity of EGFR, TGFβ, p53 and hypoxia pathways were decreased. The pathway analysis of the trastuzumab-sensitive vs. resistant cell lines agreed with the thesis cohort in terms of the JAK-STAT pathway as most upregulated pathway. Additional pathways exhibiting concordance between the GSE77346 dataset and the thesis cohort included NFκB, TNFα, WNT, MAPK, and androgen signaling, all of which demonstrated increased activity based on PROGENy analysis. However, while EGFR signaling had the second highest enrichment score in the cell line dataset, it was decreased in the patient data.

To determine the activity of transcription factors, I utilized DoRothEA for the comparisons as previously described in the PROGENy analysis. The analysis revealed that the transcription factor E2F4 had the most enhanced activity in both patient cohorts (Figure 19). Additionally, E2F1 and MYC were upregulated in the thesis cohort. STAT2 activity was increased in both

the thesis cohort and trastuzumab-sensitive cells, but downregulated in the Shi et al. cohort. Moreover, the thesis cohort exhibited an overlapping activity of GRHL2 with the cell line data.
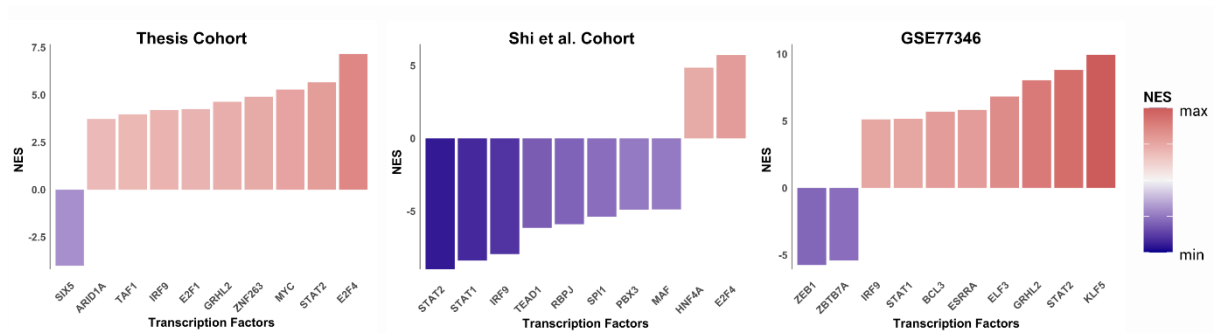
Figure 19 | Top 10 transcription factors with altered activity in patients and cells with response to trastuzumab
Normalized enrichment scores (NES) for top 10 transcription factors with altered activity according to the analysis with DoRothEA. The compared groups for each data set were patients with long-term vs. short term response/survival to trastuzumab (Thesis cohort: PFS≥12 months vs. PFS<12 months; Shi et al. cohort: OS≥12 months vs. OS<12 months) and trastuzumab-sensitive vs. resistant cell lines

Overall, the analysis of the three datasets showed limited concordance in terms of pathway and transcription factor activity. This may be due to the different survival parameters used for grouping in the patient datasets. In this study, the immune cell composition in the tumor microenvironment was found to be associated with trastuzumab response. This could not be recapitulated in the cell line data analyses since tumor cell lines do not contain bystander inflammatory cells.

5 Discussion

Since 2010, the combination of trastuzumab and chemotherapy is the only HER2-targeting first-line treatment approved in Europe for HER2-positive mGC/mGEJC. While this treatment has been shown to improve the survival, outcomes for patients remain generally poor. A group of patients has demonstrated superior survival rates while undergoing trastuzumab therapy. Despite this, the identification of a biomarker for long-term response remains elusive. In this retrospective, multicenter study, I performed a comprehensive analysis to identify biomarkers associated with long-term response to trastuzumab in HER2-positive mGC/mGEJC. Of the routinely assessed biomarkers HER2, PD-L1 and MSI, only PD-L1 CPS was increased in the superior response group. Additionally, PD-L1 positivity was associated with altered T-cell populations, in particular increased CD4+ memory T-cells. Although NGS-determined *ERBB2* CN was not correlated with trastuzumab response, it was associated with the expression pattern of HER2 as the *ERBB2* CN was increased in cases with homogenous HER2 expression. A heterogeneous expression pattern was further associated with inferior PFS on trastuzumab-based treatment. Other genomic alterations in genes of the ERBB signaling pathway and the TMB were not relevant to trastuzumab response in this cohort.

5.1 Challenges and future of HER2 assessment in mGC/mGEJC

The accurate detection of HER2 protein expression and gene amplification is crucial for making treatment decisions in mGC/mGEJC, as a positive HER2 status is required for the addition of trastuzumab to chemotherapy. However, studies evaluating the efficacy of trastuzumab in mGC/mGEJC have shown variable response rates, ranging from 32% to 68%, despite all patients having a HER2-positive status [31,162,163]. In addition, a subset of HER2-positive mGC/mGEJC patients have shown long-term survival on trastuzumab treatment well beyond the median OS reported in the ToGA trial, suggesting that HER2 status alone may not be sufficient to identify patients with long-term response to trastuzumab [79-81].

The current criteria for a positive HER2 status are an IHC score of 3+ or an IHC score of 2+ plus an *ERBB2*:CEP17 ratio ≥2 determined by (F)ISH. However, several studies have evaluated alternative criteria for the HER2 status to improve the identification of trastuzumab-sensitive patients. For instance, an *ERBB2*:CEP17 ratio greater than 4.4 has been proposed to improve the identification of patients with an OS exceeding 12 months [109,110]. These studies also indicated that the level of *ERBB2* amplification, which is reflected by the *ERBB2*:CEP17 ratio, may be relevant to trastuzumab response.

The exact *ERBB2* CN can be quantified with NGS, which could be used as an alternative to ISH methods for detecting *ERBB2* amplification. The concordance between IHC-based HER2 status and NGS-determined *ERBB2* amplification has been analyzed in GC and GEJC, and was found to be highly consistent (87.5-98.4%) [106,108,164]. Patients with discordant results between NGS and IHC-determined HER2 status exhibited shorter PFS and OS [106,108]. NGS has also been used to investigate the relationship between *ERBB2* CN and trastuzumab sensitivity. Several studies found a strong positive correlation between level of *ERBB2* CN and PFS on trastuzumab-based treatment [85,106-108]. High-level *ERBB2* amplification was associated with superior response to trastuzumab, and attempts have been made to set a cut-off to define the *ERBB2*-high patient group. The median *ERBB2* CN, the upper quantile of the *ERBB2* CN, or a receiver-operator curve were utilized in different studies to determine the *ERBB2*-high threshold [85,106-108]. Each study found an improved response to trastuzumab in the *ERBB2*-high group. However, none of the applied *ERBB2* CN thresholds used have been validated in another cohort.

In the presented work, I evaluated the HER2 status, the ERBB2 CN and HER2 expression pattern in relation of trastuzumab response. In contrast to the literature, the *ERBB2* CN was not found to be positively correlated with PFS. In addition, using the median *ERBB2* CN to define the *ERBB2*-high patient group did not discriminate between patients with long and short-term responses to trastuzumab. The HER2 status was confirmed by NGS in only 63% of the patients. However, the high discordance between NGS-determined *ERBB2* amplification and IHC-based HER2 status was not associated with a worse outcome on trastuzumab treatment, as might have been expected from the literature [106,108]. As heterogeneity is frequently found in GC and has been previously described to cause difficulties in accurate *ERBB2* CN detection by NGS, this is likely to be the reason for the strong discordance in HER2 status between the two detection methods [90-92,108,164]. Indeed, the HER2 expression pattern was heterogeneous in 42% of the cases and this was associated with significantly lower *ERBB2* CN. Moreover, a homogenous HER2 expression pattern was further correlated with improved response to trastuzumab, which is consistent with previous studies [91,92]. In addition to the HER2 expression pattern, the tumor sample type may impact *ERBB2* CN detection, as resection specimens tend to have lower *ERBB2* CN than biopsies. Even if the tumor area of the resection specimen has been macro-dissected for DNA extraction prior to sequencing, contamination with non-tumor cells is higher than in biopsies and can affect the interpretation of the sequencing data.

In conclusion, this study found that the *ERBB2* CN alone when determined by NGS is not a reliable predictor of trastuzumab response. Instead, the HER2 expression pattern was identified as an important marker for response to trastuzumab. Furthermore, NGS-determined

ERBB2 CN should be interpreted with caution, as tumor heterogeneity and the type of tumor sample may affect the accuracy of the result.

5.2   Genetic predictors for trastuzumab response in mGC and mGEJC

The mutational landscape of GC has been extensively studied. *TP53* was the most frequently mutated gene in GC, occurring in 59-61.6% of GC and 81.4% of GEJC patients [160,165]. Furthermore, mutations in *TP53* were correlated with *ERBB2* amplification [160,165]. Genetic alterations such as SNV and CNV co-occurring with *ERBB2* alterations have been discussed to contribute to primary resistance to trastuzumab treatment in mGC/mGE. Most studies focus on mutations in genes associated with ERBB signaling like *EGFR*, *KRAS, MYC* and *PI3K* [86,107,166]. The influence of a mutation or amplification in one of these genes on trastuzumab response is controversial. For instance, in a study by Shimozaki et al., *KRAS* mutations were associated with worse PFS and OS on trastuzumab therapy but *KRAS* amplification was not correlated with survival [167]. In contrast, other studies found *KRAS* amplifications in patients with poor response to trastuzumab, but could not confirm the relevance of *KRAS* mutations [107]. Another study found no association between *KRAS* genetic alterations to survival or response to trastuzumab [115,168]. In addition to genes related to RTK signaling, amplification of *CCNE1*, which is involved in the cell cycle, has been associated with shorter survival in HER2-positive mGC patients on trastuzumab-based treatment [115]. The impact of genetic alterations in individual genes on the efficacy of trastuzumab is difficult to evaluate. However, a combination of mutated genes was shown to predict the response to trastuzumab treatment. For instance, Hino et al. found that co-amplifications of genes in the RTK pathway have been linked with survival on trastuzumab [107].

The AMNESIA study also proposed that a panel of five genes might be able to identify patients with primary resistance to trastuzumab. An SNV in *EGFR*, *KRAS*, *PTEN*, *PI3K* and *MET* or a CNV in *EGFR*, *KRAS* or *MET* was found in 55% of trastuzumab-resistant patients. These genetic alterations were not found in trastuzumab-sensitive patients [86]. The relevance of the AMNESIA panel mutations for HER2 targeting was further highlighted in a re-evaluation of the JACOB trial, where patients with AMNESIA mutations had an inferior OS [169].

In this study, I used panel sequencing to evaluate the effect of SNVs and CNVs on trastuzumab response and found that they had a limited impact on trastuzumab response. In the cohort, SNVs were most frequently detected in *TP53*, as described in the literature [160,165]. The *TP53* mutations occurred at a frequency of 37%, which is lower than the reported mutation rates [160,165]. Although genetic alterations associated with resistance in the literature were detected in this cohort, no mutated gene occurred exclusively in the long-term responding patient group. Of the genes in the AMNESIA panel, only *EGFR* was genetically altered in two

patients, but only one of these patients had a short-term response to trastuzumab. In addition, mutations and amplifications in other RTK pathway genes were equally distributed between long-term and short-term responders.

A possible explanation for the low mutation frequency in our cohort could be that mutations were missed due to the stringent variant filtering applied in the analysis. The AF had to be greater than 10% to accept a mutation. Published studies either used a lower AF threshold of 5% or did not report the threshold [86,107,115]. However, the stringent thresholds in the present study were chosen to call SNVs with high reliability since our samples were compromised due to DNA damages caused by formalin fixation and high block age. Another reason for potentially missing relevant mutations is that a single tumor sample was analyzed in the present study. According to literature, 53.2 - 91.3% of tumor mutations may be missed in a single sample analysis due to the genetic heterogeneity of GC, which could lead to an underestimation of the relevance of a mutation [170]. Finally, the sequencing analysis in the present analysis was limited to 409 genes and it cannot be excluded that mutations in other genes are relevant in the context of HER2-positive mGC/mGEJC.

Overall, mutations and genetic alterations in genes associated with poor response to trastuzumab in the literature did not show prognostic relevance in this study. Furthermore, the analysis did not reveal any new associations of mutations with trastuzumab response.

5.3   *ERBB2* somatic mutations in long-term responding patients

Somatic *ERBB2* mutations, which are rare in HER2-positive cancers, were detected in two patients with long-term responses to trastuzumab [112,113]. This is in contrast to what has been described in the literature, where *ERBB2* mutations are predominantly linked to trastuzumab resistance [107,171,172]. One of the patients with a PFS of 19 months carried the *ERBB2* p.V777L mutation, which is located in the tyrosine kinase domain and was previously reported in a HER2-positive mGC patient who had a poor PFS on trastuzumab-based therapy (PFS 2 months) [107]. The p.V777L mutation has also been associated with primary resistance to trastuzumab in breast cancer [173]. In contrast, this mutation has been found to mediate trastuzumab response in HER2-negative metastatic breast cancer patients [174]. Therefore, the effect of the *ERBB2* p.V777L variant on trastuzumab sensitivity remains unclear, and it could be speculated that genomic co-alterations may have modulated the anticipated effect of the mutation on trastuzumab response in this case.

The other *ERBB2* mutation detected was p.P489L and is located in the extracellular domain. This mutation was not related with trastuzumab response in HER2-positive mGC/mGEJC so far, but it has been associated with improved trastuzumab sensitivity in acute myeloid

leukemia [175]. In the patient with the p.P489L mutation, *ERBB2* was not amplified according to NGS analysis.

In addition to the domain in which the HER2 mutation is located, AF appears to play a role in its impact on trastuzumab response. Previous research has shown that a high AF of *ERBB2* mutations correlates with a reduced response to trastuzumab in HER2-positive mGC/mGEJC [107]. However, in this cohort, both *ERBB2* mutations with high AF (>60%) were detected in patients with a PFS of more than 12 months. This suggests that the effect of the *ERBB2* mutations discovered in this study may be less significant for trastuzumab sensitivity than initially expected from literature.

5.4   TMB as biomarker for trastuzumab response

In addition to single mutations, there is an increasing interest in the potential of TMB as a biomarker for response to therapy. While most studies have focused on the relationship between TMB and immunotherapy in HER2-negative cancers, some reports have proposed that TMB may also be important for trastuzumab response in GC [87,123,176,177].

In this study, I analyzed TMB to evaluate its relevance for trastuzumab response in mGC/mGEJC. Although the result did not reach statistical significance, a trend was observed that patients with a long-term response to trastuzumab had a higher TMB, which is consistent with the literature [87,176]. However, that the previous study by Kim et al. only investigated the relationship between TMB and trastuzumab response in mGC. In the presented study, TMB was associated with tumor location. The TMB was lower in GEJC than in the GC, which is consistent with the literature, where a median TMB of 6.6 was reported for GC and 1.8 for GEJC [178,179].

It is important to note that TMB assessment is highly depending on the types of mutations included. In this study, non-synonymous and frameshift mutations were included in the TMB calculation, and strict selection thresholds for somatic mutations were used (AF > 10%, DP > 250). However, these filtering criteria neglect low-frequency mutations, which may have led to an underestimation of TMB in this cohort. Moreover, the AF and DP thresholds used to filter somatic mutations are often not reported in TMB studies, but they may introduce bias into TMB estimation [180].

Although the results of this study tend to support the potential of the TMB as a biomarker of trastuzumab response, a definitive conclusion cannot be drawn due to the variability of TMB calculation. Further studies using consistent TMB assessment criteria are required to fully evaluate the relevance of TMB as a predictor of response to HER2-targeting treatment.

5.5 Relevance of PD-L1 for response of HER2-positive mGC and mGEJC to trastuzumab

PD-L1 is an immune checkpoint protein and the ligand of the programed death protein 1 (PD-1). PD-L1 and PD-1 are commonly expressed on immune cells like macrophages and activated T-cells [181]. The binding of PD-L1 to PD1 regulates immune response by reducing cytokine secretion and lytic activity of T-cells. PD-L1 overexpression in tumor cells is a potential mechanism of immune evasion [182]. In 2021, the EMA approved the addition of immunotherapies, nivolumab/pembrolizumab, to chemotherapy as first-line therapy for tumors with PD-L1 expression in tumor and/or immune cells [17]. As a result, PD-L1 expression is now evaluated in clinical diagnostics in addition to HER2 assessment. PD-L1 and HER2 expression co-occur in 25-85% of GC/GEJ patients [75,183-187]. The prognostic relevance of PD-L1 and HER2 positivity (PD-L1+/HER2+) on GC patient survival has been evaluated in the literature with conflicting results. Lian et al. reported improved survival for PD-L1+/HER2+ GC patients compared to PD-L1-/HER2+ patients [183]. In contrast, Lv et al. associate PD-L1+/HER2+ with poor survival and suggested that these patients are unlikely to respond to immunotherapies [185]. However, this was disproved by the KEYNOTE-811 trial where the combination of pembrolizumab, trastuzumab and chemotherapy led to improved response rates compared to treatment with trastuzumab and chemotherapy [184].

In this study, I investigated the impact of PD-L1 expression on trastuzumab response in HER2-positive mGC/mGEJC patients. The results revealed that PD-L1 positive patients (CPS≥1) had a significantly improved PFS on trastuzumab-based therapy compared to PD-L1 negative patients, supporting the findings by Lian et al. [183]. PD-L1 positivity was defined as CPS≥1, which is consistent with several other studies [184,188,189]. Interestingly, in this work it was observed that the cut-off for PD-L1 positivity was less relevant as a positive correlation of CPS with PFS was detected, highlighting the robustness of the results and independence of chosen thresholds. The location of PD-L1 expression can be an additional important factor. It was reported in literature that PD-L1 expression on tumor cells is associated with improved survival in GC [190]. In contrast, PD-L1 expression was exclusively detected on immune cells and correlated with improved PFS in the presented study. Moreover, the analysis of T-cell populations revealed increased CD4+ memory T-cells in PD-L1-positive patients, while CD8+ T-cell scores were increased in PD-L1 negative patients. The correlations between T-cell populations, PD-L1 positivity, and GC clinical outcome are contradicting in literature. In contrast to the presented study, PD-L1 expression has been associated with increased presence of CD8+ T-cells and favorable outcome in literature [191-193]. However, a study by Thompson et al. reported a correlation between CD8+ T-cells and worse PFS and OS in PD-

L1 positive GC and GEJC, which is consistent with the presented results [194]. Studies analyzing CD8+ T-cells in context of PD-L1 expression mostly do not evaluate the presence of other immune cell types like CD4+ memory T-cells [191-193]. Although high numbers of CD4+ memory T-cells are associated with improved clinical outcome in GC, the relationship of high CD4+ memory T-cells in PD-L1 positive patients and survival on trastuzumab in HER2-positive mGC/mGEJC has not been reported yet [195].

Overall, a positive correlation between CPS and PFS was observed in this study, highlighting the relevance of PD-L1 assessment for HER2-targeting treatment in HER2-positive mGC/mGEJC. Furthermore, the results suggest a potential biological mechanism involving an increased presence of CD4+ memory T-cells. However, due to treatment heterogeneity, the design of the study and the limited sample size it cannot definitely be concluded if PD-L1 is a prognostic or predictive factor in the context of trastuzumab.

5.6   Outlook

In this work, I was able to show an association between PD-L1 CPS and PFS in HER2-positive mGC/mGEJC patients treated with trastuzumab-based therapy. In addition, immune cell population analysis revealed an increase in CD4+ memory T-cells in PD-L1 positive patients. Furthermore, heterogeneity in the HER2 expression pattern was correlated with decreased NGS-determined *ERBB2* CN and inferior PFS on trastuzumab-containing therapy. However, this was a hypothesis-generating study with a small sample size, and further validation in a larger cohort is required to verify the findings.

PD-L1 expression was associated with altered T-cell populations in this cohort. However, the immune cell population analysis was conducted using a computational approach with bulk microarray data. It would be of interest to confirm these findings in an experimental approach like IHC staining for immune cell markers. In addition, new techniques like spatial transcriptomics on FFPE sections could give insights into the distribution of CD4+, CD8+ and PD-L1 expressing cells in the tumor microenvironment on a single-cell level and further correlate the findings with pathological annotations. An alternative approach could be to use digital pathology to evaluate the extent of tumor infiltrating lymphocytes.

This study suggests that HER2 heterogeneity and PD-L1 expression are relevant factors in the long-term response of HER2-positive mGC/mGEJC to trastuzumab treatment. However, evaluating HER2 expression pattern remains challenging due to the absence of a standardized scoring system for the assessment of HER2 heterogeneity. In this study, a binary classification system based on microscopic evaluation of the HER2 IHC was used to rate the HER2 expression as either homogenous or heterogeneous. Quantification of HER2-positive tumor cells could provide an additional informative value for trastuzumab treatment response. Digital

pathology may offer a solution for consistent HER2 expression evaluation by training a neuronal network for exact quantification of HER2-positive tumor cells. Besides heterogeneity in protein expression, it would be of interest to investigate the genomic heterogeneity and clonal composition of the tumor in relation to treatment response. However, the sequencing technique used in this study was not broad enough to allow clonal reconstruction with reasonable confidence and resolution. In addition, a single sample was sequenced which provides limited information about tumor heterogeneity. To analyze the clonal composition of tumors and its impact on trastuzumab sensitivity, a sequencing approach covering a larger genomic area would have to be performed for clonal tracking, ideally with multiple tumor samples and augmenting single cell data.

Lastly, all evaluated samples were taken prior to trastuzumab treatment. Analyzing the impact of trastuzumab treatment on the clonal composition of the tumor, the strength and location of PD-L1 expression, and presence immune cells could provide valuable insights.

Altogether, this study underlines the relevance of HER2 heterogeneity and PD-L1 expression for long-term response of HER2-positive mGC/mGEJC to trastuzumab. The results indicate that multiple factors are involved in treatment response. However, further analysis in a larger cohort is required to confirm these findings.

6 Summary

Gastric cancer is the fifth most prevalent cancer type, with the fourth highest cancer-related mortality worldwide. Since 2010, the HER2-targeting agent trastuzumab has been approved as a first-line therapy in combination with chemotherapy for HER2-positive advanced/metastatic gastric or gastroesophageal junction cancer. However, despite improvement of overall survival through trastuzumab treatment, the survival remains low with only about one year. However, a subgroup of patients with long-term response to trastuzumab has been observed in small studies and case reports. Genetic alterations and the level of HER2 gene amplification have been proposed to identify patients with trastuzumab long-term response. Despite this, a biomarker for superior response to trastuzumab remains elusive.

This study aimed to identify a biomarker that could distinguish between HER2-positive gastric cancer patients with long-term and short-term response to trastuzumab plus chemotherapy.

FFPE tumor samples and follow-up data of 19 patients with HER2-positive advanced/metastatic gastric or gastroesophageal junction cancer who underwent trastuzumab-containing therapy were retrospectively collected from four German clinical centers. The patients were divided into long-term (n=7) and short-term responding groups (n=12) according to progression-free survival on trastuzumab-containing therapy (PFS≥12 months vs. PFS<12 months). A comprehensive genetic and gene expression analysis was performed. In addition, established biomarkers HER2, PD-L1 and MSI were analyzed.

An automated analysis pipeline was developed to detect genetic alterations such as somatic single nucleotide variants and copy number alterations. The copy number of the HER2 gene, ERBB2, could not distinguish between trastuzumab long-term and short-term response in gastric cancer patients. However, two somatic non-synonymous mutations were detected in ERBB2, and both mutations occurred in patients with long-term response to trastuzumab. Other genetic alterations and the tumor mutational burden were not correlated with response to trastuzumab. The HER2 protein expression pattern was also evaluated, and the results showed that patients with homogeneous HER2 expression pattern had improved progression-free survival on trastuzumab-containing therapy.

Evaluation of the biomarker PD-L1 revealed a higher PD-L1 combined positive score in long-term responding patients, and a positive correlation between PD-L1 combined positive score and PFS in the overall study population. PD-L1 positivity, defined as a combined positive score ≥1, was associated with improved PFS on trastuzumab-based treatment. Furthermore, using bioinformatics methods, increased PD-L1 combined positive scores could be associated with a higher level of CD4+ memory T-cells.

In conclusion, genetic alterations and the tumor mutational burden were not correlated with response to a trastuzumab-containing therapy, while a homogeneous HER2 protein expression pattern and PD-L1 combined positive score were identified as potential biomarkers for improved progression-free survival. The findings highlight the clinical relevance of PD-L1 for the treatment of HER2-positive advanced gastric and gastroesophageal adenocarcinoma.

7 References

1. Sung, H., Ferlay, J., Siegel, R.L., et al. (2021). Global Cancer Statistics 2020: GLOBOCAN Estimates of Incidence and Mortality Worldwide for 36 Cancers in 185 Countries. CA Cancer J Clin *71*, 209-249.
2. Morgan, E., Arnold, M., Camargo, M.C., et al. (2022). The current and future incidence and mortality of gastric cancer in 185 countries, 2020-40: A population-based modelling study. EClinicalMedicine *47*, 101404.
3. Randi, G., Ben, E., Carvalho, R., et al. (2018). European Cancer Information System web-application: analysing and visualising European cancer data. European Journal of Public Health *28*, cky214.189.
4. Arnold, M., Ferlay, J., van Berge Henegouwen, M.I., et al. (2020). Global burden of oesophageal and gastric cancer by histology and subsite in 2018. Gut *69*, 1564-1571.
5. Wang, S., Zheng, R., Arnold, M., et al. (2022). Global and national trends in the age-specific sex ratio of esophageal cancer and gastric cancer by subtype. Int J Cancer *151*, 1447-1461.
6. Thrift, A.P., and El-Serag, H.B. (2020). Burden of Gastric Cancer. Clin Gastroenterol Hepatol *18*, 534-542.
7. Song, Z., Wu, Y., Yang, J., et al. (2017). Progress in the treatment of advanced gastric cancer. Tumour Biol *39*, 1010428317714626.
8. Zentrum für Krebsregisterdaten (2022). Magenkrebs (Magenkarzinom). https://www.krebsdaten.de/Krebs/DE/Content/Krebsarten/Magenkrebs/magenkrebs_node.html.
9. American Society of Clinical Oncology (ASCO) (2023). Stomach Cancer: Statistics. https://www.cancer.net/cancer-types/stomach-cancer/statistics.
10. Katai, H., Ishikawa, T., Akazawa, K., et al. (2018). Five-year survival analysis of surgically resected gastric cancer cases in Japan: a retrospective analysis of more than 100,000 patients from the nationwide registry of the Japanese Gastric Cancer Association (2001-2007). Gastric Cancer *21*, 144-154.
11. Suzuki, H., Oda, I., Abe, S., et al. (2016). High rate of 5-year survival among patients with early gastric cancer undergoing curative endoscopic submucosal dissection. Gastric Cancer *19*, 198-205.
12. Maconi, G., Manes, G., and Porro, G.B. (2008). Role of symptoms in diagnosis and outcome of gastric cancer. World J Gastroenterol *14*, 1149-1155.
13. Ferro, A., Peleteiro, B., Malvezzi, M., et al. (2014). Worldwide trends in gastric cancer mortality (1980-2011), with predictions to 2015, and incidence by subtype. Eur J Cancer *50*, 1330-1344.
14. Derakhshan, M.H., Arnold, M., Brewster, D.H., et al. (2016). Worldwide Inverse Association between Gastric Cancer and Esophageal Adenocarcinoma Suggesting a Common Environmental Factor Exerting Opposing Effects. Am J Gastroenterol *111*, 228-239.
15. Machlowska, J., Baj, J., Sitarz, M., et al. (2020). Gastric Cancer: Epidemiology, Risk Factors, Classification, Genomic Characteristics and Treatment Strategies. Int J Mol Sci *21*.
16. McColl, K.E.L. (2019). What is causing the rising incidence of esophageal adenocarcinoma in the West and will it also happen in the East? J Gastroenterol *54*, 669-673.
17. Lordick, F., Carneiro, F., Cascinu, S., et al. (2022). Gastric cancer: ESMO Clinical Practice Guideline for diagnosis, treatment and follow-up. Ann Oncol.
18. Enzinger, P.C., and Mayer, R.J. (2003). Esophageal cancer. N Engl J Med *349*, 2241-2252.
19. Cancer Genome Atlas Research, N., Analysis Working Group: Asan, U., Agency, B.C.C., et al. (2017). Integrated genomic characterization of oesophageal carcinoma. Nature *541*, 169-175.

20. Siewert, J.R., and Stein, H.J. (1998). Classification of adenocarcinoma of the oesophagogastric junction. Br J Surg *85*, 1457-1459.

21. Leitlinienprogramm Onkologie (Deutsche Krebsgesellschaft, D.K., AWMF) (2019). S3-Leitlinie Magenkarzinom, Langversion 2.0, 2019 AWMF Registernummer: 032/009OL, http://www.leitlinienprogramm-onkologie.de/leitlinien/magenkarzinom/ , (abgerufen am: 12.07.2021). http://www.leitlinienprogramm-onkologie.de/leitlinien/magenkarzinom/.

22. Rice, T.W., Patil, D.T., and Blackstone, E.H. (2017). 8th edition AJCC/UICC staging of cancers of the esophagus and esophagogastric junction: application to clinical practice. Ann Cardiothorac Surg *6*, 119-130.

23. Lauren, P. (1965). The Two Histological Main Types of Gastric Carcinoma: Diffuse and So-Called Intestinal-Type Carcinoma. An Attempt at a Histo-Clinical Classification. Acta Pathol Microbiol Scand *64*, 31-49.

24. Yao, Q., Qi, X., and Xie, S.H. (2020). Sex difference in the incidence of cardia and non-cardia gastric cancer in the United States, 1992-2014. BMC Gastroenterol *20*, 418.

25. Polom, K., Marano, L., Marrelli, D., et al. (2018). Meta-analysis of microsatellite instability in relation to clinicopathological characteristics and overall survival in gastric cancer. Br J Surg *105*, 159-167.

26. Wang, H.B., Liao, X.F., and Zhang, J. (2017). Clinicopathological factors associated with HER2-positive gastric cancer: A meta-analysis. Medicine (Baltimore) *96*, e8437.

27. Kaneko, S., and Yoshimura, T. (2001). Time trend analysis of gastric cancer incidence in Japan by histological types, 1975-1989. Br J Cancer *84*, 400-405.

28. Pyo, J.H., Ahn, S., Lee, H., et al. (2016). Clinicopathological Features and Prognosis of Mixed-Type T1a Gastric Cancer Based on Lauren's Classification. Ann Surg Oncol *23*, 784-791.

29. Nagtegaal, I.D., Odze, R.D., Klimstra, D., et al. (2020). The 2019 WHO classification of tumours of the digestive system. Histopathology *76*, 182-188.

30. Al-Batran, S.E., Homann, N., Pauligk, C., et al. (2019). Perioperative chemotherapy with fluorouracil plus leucovorin, oxaliplatin, and docetaxel versus fluorouracil or capecitabine plus cisplatin and epirubicin for locally advanced, resectable gastric or gastro-oesophageal junction adenocarcinoma (FLOT4): a randomised, phase 2/3 trial. Lancet *393*, 1948-1957.

31. Bang, Y.J., Van Cutsem, E., Feyereislova, A., et al. (2010). Trastuzumab in combination with chemotherapy versus chemotherapy alone for treatment of HER2-positive advanced gastric or gastro-oesophageal junction cancer (ToGA): a phase 3, open-label, randomised controlled trial. Lancet *376*, 687-697.

32. Shitara, K., Van Cutsem, E., Bang, Y.J., et al. (2020). Efficacy and Safety of Pembrolizumab or Pembrolizumab Plus Chemotherapy vs Chemotherapy Alone for Patients With First-line, Advanced Gastric Cancer: The KEYNOTE-062 Phase 3 Randomized Clinical Trial. JAMA Oncol *6*, 1571-1580.

33. Janjigian, Y.Y., Shitara, K., Moehler, M., et al. (2021). First-line nivolumab plus chemotherapy versus chemotherapy alone for advanced gastric, gastro-oesophageal junction, and oesophageal adenocarcinoma (CheckMate 649): a randomised, open-label, phase 3 trial. Lancet *398*, 27-40.

34. Obermannova, R., Alsina, M., Cervantes, A., et al. (2022). Oesophageal cancer: ESMO Clinical Practice Guideline for diagnosis, treatment and follow-up. Ann Oncol *33*, 992-1004.

35. Popescu, N.C., King, C.R., and Kraus, M.H. (1989). Localization of the human erbB-2 gene on normal and rearranged chromosomes 17 to bands q12-21.32. Genomics *4*, 362-366.

36. Yarden, Y., and Sliwkowski, M.X. (2001). Untangling the ErbB signalling network. Nat Rev Mol Cell Biol *2*, 127-137.

37. Kennedy, S.P., Hastings, J.F., Han, J.Z., et al. (2016). The Under-Appreciated Promiscuity of the Epidermal Growth Factor Receptor Family. Front Cell Dev Biol *4*, 88.

38. Guy, P.M., Platko, J.V., Cantley, L.C., et al. (1994). Insect cell-expressed p180erbB3 possesses an impaired tyrosine kinase activity. Proc Natl Acad Sci U S A *91*, 8132-8136.

39. Carraway, K.L., 3rd, and Cantley, L.C. (1994). A neu acquaintance for erbB3 and erbB4: a role for receptor heterodimerization in growth signaling. Cell *78*, 5-8.

40. Pinkas-Kramarski, R., Soussan, L., Waterman, H., et al. (1996). Diversification of Neu differentiation factor and epidermal growth factor signaling by combinatorial receptor interactions. EMBO J *15*, 2452-2467.

41. Yarden, Y., and Pines, G. (2012). The ERBB network: at last, cancer therapy meets systems biology. Nat Rev Cancer *12*, 553-563.

42. Riese, D.J., 2nd, Gallo, R.M., and Settleman, J. (2007). Mutational activation of ErbB family receptor tyrosine kinases: insights into mechanisms of signal transduction and tumorigenesis. Bioessays *29*, 558-565.

43. Seshacharyulu, P., Ponnusamy, M.P., Haridas, D., et al. (2012). Targeting the EGFR signaling pathway in cancer therapy. Expert Opin Ther Targets *16*, 15-31.

44. Garrett, T.P., McKern, N.M., Lou, M., et al. (2003). The crystal structure of a truncated ErbB2 ectodomain reveals an active conformation, poised to interact with other ErbB receptors. Mol Cell *11*, 495-505.

45. Tzahar, E., Waterman, H., Chen, X., et al. (1996). A hierarchical network of interreceptor interactions determines signal transduction by Neu differentiation factor/neuregulin and epidermal growth factor. Mol Cell Biol *16*, 5276-5287.

46. Di Fiore, P.P., Pierce, J.H., Kraus, M.H., et al. (1987). erbB-2 is a potent oncogene when overexpressed in NIH/3T3 cells. Science *237*, 178-182.

47. Hudziak, R.M., Schlessinger, J., and Ullrich, A. (1987). Increased expression of the putative growth factor receptor p185HER2 causes transformation and tumorigenesis of NIH 3T3 cells. Proc Natl Acad Sci U S A *84*, 7159-7163.

48. Liu, Y., Ma, L., Liu, D., et al. (2014). Impact of polysomy 17 on HER2 testing of invasive breast cancer patients. Int J Clin Exp Pathol *7*, 163-173.

49. Tapia, C., Glatz, K., Novotny, H., et al. (2007). Close association between HER-2 amplification and overexpression in human tumors of non-breast origin. Mod Pathol *20*, 192-198.

50. Kurebayashi, J. (2001). Biological and clinical significance of HER2 overexpression in breast cancer. Breast Cancer *8*, 45-51.

51. Sakai, K., Mori, S., Kawamoto, T., et al. (1986). Expression of epidermal growth factor receptors on normal human gastric epithelia and gastric carcinomas. J Natl Cancer Inst *77*, 1047-1052.

52. Takenaka, M., Hanagiri, T., Shinohara, S., et al. (2011). The prognostic significance of HER2 overexpression in non-small cell lung cancer. Anticancer Res *31*, 4631-4636.

53. Luo, H., Xu, X., Ye, M., et al. (2018). The prognostic value of HER2 in ovarian cancer: A meta-analysis of observational studies. PLoS One *13*, e0191972.

54. Baretton, G., Kreipe, H.H., Schirmacher, P., et al. (2019). HER2 testing in gastric cancer diagnosis: insights on variables influencing HER2-positivity from a large, multicenter, observational study in Germany. Virchows Arch *474*, 551-560.

55. Van Cutsem, E., Bang, Y.J., Feng-Yi, F., et al. (2015). HER2 screening data from ToGA: targeting HER2 in gastric and gastroesophageal junction cancer. Gastric Cancer *18*, 476-484.

56. Kunz, P.L., Mojtahed, A., Fisher, G.A., et al. (2012). HER2 expression in gastric and gastroesophageal junction adenocarcinoma in a US population: clinicopathologic analysis with proposed approach to HER2 assessment. Appl Immunohistochem Mol Morphol *20*, 13-24.

57. Allgayer, H., Babic, R., Gruetzner, K.U., et al. (2000). c-erbB-2 is of independent prognostic relevance in gastric cancer and is associated with the expression of tumor-associated protease systems. J Clin Oncol *18*, 2201-2209.

58. Fendly, B.M., Winget, M., Hudziak, R.M., et al. (1990). Characterization of murine monoclonal antibodies reactive to either the human epidermal growth factor receptor or HER2/neu gene product. Cancer Res *50*, 1550-1558.

59. Junttila, T.T., Akita, R.W., Parsons, K., et al. (2009). Ligand-independent HER2/HER3/PI3K complex is disrupted by trastuzumab and is effectively inhibited by the PI3K inhibitor GDC-0941. Cancer Cell *15*, 429-440.

60. Arnould, L., Gelly, M., Penault-Llorca, F., et al. (2006). Trastuzumab-based treatment of HER2-positive breast cancer: an antibody-dependent cellular cytotoxicity mechanism? Br J Cancer *94*, 259-267.

61. Yuki, S., Shinozaki, K., Kashiwada, T., et al. (2020). Multicenter phase II study of SOX plus trastuzumab for patients with HER2(+) metastatic or recurrent gastric cancer: KSCC/HGCSG/CCOG/PerSeUS 1501B. Cancer Chemother Pharmacol *85*, 217-223.

62. Gong, J., Liu, T., Fan, Q., et al. (2016). Optimal regimen of trastuzumab in combination with oxaliplatin/ capecitabine in first-line treatment of HER2-positive advanced gastric cancer (CGOG1001): a multicenter, phase II trial. BMC Cancer *16*, 68.

63. Miura, Y., Sukawa, Y., Hironaka, S., et al. (2018). Five-weekly S-1 plus cisplatin therapy combined with trastuzumab therapy in HER2-positive gastric cancer: a phase II trial and biomarker study (WJOG7212G). Gastric Cancer *21*, 84-95.

64. Hegewisch-Becker, S., Moorahrend, E., Kröning, H., et al. (2012). Trastuzumab (TRA) in combination with different first-line chemotherapies for treatment of HER2-positive metastatic gastric or gastroesophageal junction cancer (MGC): Findings from the German noninterventional observational study HerMES. Journal of Clinical Oncology *30*, 4065-4065.

65. Fu, X., Zhang, Y., Yang, J., et al. (2018). Efficacy and safety of trastuzumab as maintenance or palliative therapy in advanced HER2-positive gastric cancer. Onco Targets Ther *11*, 6091-6100.

66. Gurbuz, M., Akkus, E., Sakin, A., et al. (2022). Trastuzumab +/- Capecitabine Maintenance After the First-Line Treatment of HER2-Positive Advanced Gastric Cancer: Retrospective Observational Real-Life Data of Turkish Oncology Group. J Gastrointest Cancer *53*, 282-288.

67. Li, Q., Lv, M., Jiang, H., et al. (2020). A prospective observational study on the optimal maintenance strategy in HER2-positive advanced gastric cancer treated with trastuzumab-based therapy. J Cancer Res Clin Oncol *146*, 287-295.

68. Oh, D.Y., and Bang, Y.J. (2020). HER2-targeted therapies - a role beyond breast cancer. Nat Rev Clin Oncol *17*, 33-48.

69. Lewis Phillips, G.D., Li, G., Dugger, D.L., et al. (2008). Targeting HER2-positive breast cancer with trastuzumab-DM1, an antibody-cytotoxic drug conjugate. Cancer Res *68*, 9280-9290.

70. Thuss-Patience, P.C., Shah, M.A., Ohtsu, A., et al. (2017). Trastuzumab emtansine versus taxane use for previously treated HER2-positive locally advanced or metastatic gastric or gastro-oesophageal junction adenocarcinoma (GATSBY): an international randomised, open-label, adaptive, phase 2/3 study. Lancet Oncol *18*, 640-653.

71. Ogitani, Y., Aida, T., Hagihara, K., et al. (2016). DS-8201a, A Novel HER2-Targeting ADC with a Novel DNA Topoisomerase I Inhibitor, Demonstrates a Promising Antitumor Efficacy with Differentiation from T-DM1. Clin Cancer Res *22*, 5097-5108.

72. Shitara, K., Bang, Y.J., Iwasa, S., et al. (2020). Trastuzumab Deruxtecan in Previously Treated HER2-Positive Gastric Cancer. N Engl J Med *382*, 2419-2430.

73. Koessler, T., Alsina, M., Arnold, D., et al. (2022). ESMO Congress 2021: highlights from the EORTC gastrointestinal tract cancer group's perspective. ESMO Open *7*, 100392.

74. Daiichi-Sankyo (2022). ENHERTU® Approved in the EU for Patients with Previously Treated HER2 Positive Advanced Gastric Cancer.

75. Janjigian, Y.Y., Oh, D.-Y., Rha, S.Y., et al. (2022). Dose-escalation and dose-expansion study of trastuzumab deruxtecan (T-DXd) monotherapy and combinations in patients (pts) with advanced/metastatic HER2+ gastric cancer (GC)/gastroesophageal junction adenocarcinoma (GEJA): DESTINY-Gastric03. Journal of Clinical Oncology *40*, 295-295.

76. Franklin, M.C., Carey, K.D., Vajdos, F.F., et al. (2004). Insights into ErbB signaling from the structure of the ErbB2-pertuzumab complex. Cancer Cell *5*, 317-328.

77. Tabernero, J., Hoff, P.M., Shen, L., et al. (2023). Pertuzumab, trastuzumab, and chemotherapy in HER2-positive gastric/gastroesophageal junction cancer: end-of-study analysis of the JACOB phase III randomized clinical trial. Gastric Cancer 26, 123-131.

78. Hecht, J.R., Bang, Y.J., Qin, S.K., et al. (2016). Lapatinib in Combination With Capecitabine Plus Oxaliplatin in Human Epidermal Growth Factor Receptor 2-Positive Advanced or Metastatic Gastric, Esophageal, or Gastroesophageal Adenocarcinoma: TRIO-013/LOGiC--A Randomized Phase III Trial. J Clin Oncol 34, 443-451.

79. Ilhan-Mutlu, A., Taghizadeh, H., Beer, A., et al. (2018). Correlation of trastuzumab-based treatment with clinical characteristics and prognosis in HER2-positive gastric and gastroesophageal junction cancer: A retrospective single center analysis. Cancer Biol Ther 19, 169-174.

80. Schade, S., Koenig, U., Mekolli, A., et al. (2022). Cure Is Possible: Extensively Metastatic HER2-Positive Gastric Carcinoma with 5 years of Complete Remission after Therapy with the FLOT Regimen and Trastuzumab. Case Rep Gastroenterol 16, 80-88.

81. Puhr, H.C., and Ilhan-Mutlu, A. (2020). A case report on the long-term survival of a patient with HER2-positive metastatic gastric adenocarcinoma and a short review of the current literature. memo - Magazine of European Medical Oncology 13, 453-458.

82. Ruschoff, J., Hanna, W., Bilous, M., et al. (2012). HER2 testing in gastric cancer: a practical approach. Mod Pathol 25, 637-650.

83. Lordick, F., Al-Batran, S.E., Dietel, M., et al. (2017). HER2 testing in gastric cancer: results of a German expert meeting. J Cancer Res Clin Oncol 143, 835-841.

84. Kaito, A., Kuwata, T., Tokunaga, M., et al. (2019). HER2 heterogeneity is a poor prognosticator for HER2-positive gastric cancer. World J Clin Cases 7, 1964-1977.

85. Zhang, L., Hamdani, O., Gjoerup, O., et al. (2022). ERBB2 Copy Number as a Quantitative Biomarker for Real-World Outcomes to Anti-Human Epidermal Growth Factor Receptor 2 Therapy in Advanced Gastroesophageal Adenocarcinoma. JCO Precis Oncol 6, e2100330.

86. Pietrantonio, F., Fuca, G., Morano, F., et al. (2018). Biomarkers of Primary Resistance to Trastuzumab in HER2-Positive Metastatic Gastric Cancer Patients: the AMNESIA Case-Control Study. Clin Cancer Res 24, 1082-1089.

87. Kim, H.R., Ahn, S., Jo, H., et al. (2021). The Impact of Tumor Mutation Burden on the Effect of Frontline Trastuzumab Plus Chemotherapy in Human Epidermal Growth Factor Receptor 2-Positive Advanced Gastric Cancers. Front Oncol 11, 792340.

88. Hanahan, D., and Weinberg, R.A. (2011). Hallmarks of cancer: the next generation. Cell 144, 646-674.

89. Saito, T., Kondo, C., Shitara, K., et al. (2015). Comparison of intratumoral heterogeneity of HER2 expression between primary tumor and multiple organ metastases in gastric cancer: Clinicopathological study of three autopsy cases and one resected case. Pathol Int 65, 309-317.

90. Haffner, I., Schierle, K., Raimundez, E., et al. (2021). HER2 Expression, Test Deviations, and Their Impact on Survival in Metastatic Gastric Cancer: Results From the Prospective Multicenter VARIANZ Study. J Clin Oncol 39, 1468-1478.

91. Yagi, S., Wakatsuki, T., Yamamoto, N., et al. (2019). Clinical significance of intratumoral HER2 heterogeneity on trastuzumab efficacy using endoscopic biopsy specimens in patients with advanced HER2 positive gastric cancer. Gastric Cancer 22, 518-525.

92. Wakatsuki, T., Yamamoto, N., Sano, T., et al. (2018). Clinical impact of intratumoral HER2 heterogeneity on trastuzumab efficacy in patients with HER2-positive gastric cancer. J Gastroenterol 53, 1186-1195.

93. Zhang, Q., Yu, T., Zhao, Z., et al. (2022). Temporal heterogeneity of HER2 expression in metastatic gastric cancer: a case report. World J Surg Oncol 20, 157.

94. Seo, S., Ryu, M.H., Park, Y.S., et al. (2019). Loss of HER2 positivity after anti-HER2 chemotherapy in HER2-positive gastric cancer patients: results of the GASTric cancer HER2 reassessment study 3 (GASTHER3). Gastric Cancer 22, 527-535.

95. Pietrantonio, F., Caporale, M., Morano, F., et al. (2016). HER2 loss in HER2-positive gastric or gastroesophageal cancer after trastuzumab therapy: Implication for further clinical research. Int J Cancer *139*, 2859-2864.

96. Cancer Genome Atlas Research, N. (2014). Comprehensive molecular characterization of gastric adenocarcinoma. Nature *513*, 202-209.

97. Cristescu, R., Lee, J., Nebozhyn, M., et al. (2015). Molecular analysis of gastric cancer identifies subtypes associated with distinct clinical outcomes. Nat Med *21*, 449-456.

98. Lei, Z., Tan, I.B., Das, K., et al. (2013). Identification of molecular subtypes of gastric cancer with different responses to PI3-kinase inhibitors and 5-fluorouracil. Gastroenterology *145*, 554-565.

99. Ye, Y., Yang, W., Ruan, X., et al. (2022). Metabolism-associated molecular classification of gastric adenocarcinoma. Front Oncol *12*, 1024985.

100. Li, T., Chen, X., Gu, M., et al. (2020). Identification of the subtypes of gastric cancer based on DNA methylation and the prediction of prognosis. Clin Epigenetics *12*, 161.

101. Cappello, F., Angerilli, V., Munari, G., et al. (2022). FFPE-Based NGS Approaches into Clinical Practice: The Limits of Glory from a Pathologist Viewpoint. J Pers Med *12*.

102. Samorodnitsky, E., Jewell, B.M., Hagopian, R., et al. (2015). Evaluation of Hybridization Capture Versus Amplicon-Based Methods for Whole-Exome Sequencing. Hum Mutat *36*, 903-914.

103. Chen, H., Luthra, R., Goswami, R.S., et al. (2015). Analysis of Pre-Analytic Factors Affecting the Success of Clinical Next-Generation Sequencing of Solid Organ Malignancies. Cancers (Basel) *7*, 1699-1715.

104. Delio, M., Patel, K., Maslov, A., et al. (2015). Development of a Targeted Multi-Disorder High-Throughput Sequencing Assay for the Effective Identification of Disease-Causing Variants. PLoS One *10*, e0133742.

105. Malone, E.R., Oliva, M., Sabatini, P.J.B., et al. (2020). Molecular profiling for precision cancer therapies. Genome Med *12*, 8.

106. Janjigian, Y.Y., Sanchez-Vega, F., Jonsson, P., et al. (2018). Genetic Predictors of Response to Systemic Therapy in Esophagogastric Cancer. Cancer Discov *8*, 49-58.

107. Hino, K., Nishina, T., Kajiwara, T., et al. (2022). Association of ERBB2 Copy Number and Gene Coalterations With Trastuzumab Efficacy and Resistance in Human Epidermal Growth Factor Receptor 2-Positive Esophagogastric and Gastric Cancer. JCO Precis Oncol *6*, e2200135.

108. Stein, S.M., Snider, J., Ali, S.M., et al. (2021). Real-world association of HER2/ERBB2 concordance with trastuzumab clinical benefit in advanced esophagogastric cancer. Future Oncol *17*, 4101-4114.

109. Gomez-Martin, C., Plaza, J.C., Pazo-Cid, R., et al. (2013). Level of HER2 gene amplification predicts response and overall survival in HER2-positive advanced gastric cancer treated with trastuzumab. J Clin Oncol *31*, 4445-4452.

110. Ock, C.Y., Lee, K.W., Kim, J.W., et al. (2015). Optimal Patient Selection for Trastuzumab Treatment in HER2-Positive Advanced Gastric Cancer. Clin Cancer Res *21*, 2520-2529.

111. Shin, J.W., Kim, S., Ha, S., et al. (2019). The HER2 S310F Mutant Can Form an Active Heterodimer with the EGFR, Which Can Be Inhibited by Cetuximab but Not by Trastuzumab as well as Pertuzumab. Biomolecules *9*.

112. Park, S., Ahn, S., Kim, D.G., et al. (2022). High Frequency of Juxtamembrane Domain ERBB2 Mutation in Gastric Cancer. Cancer Genomics Proteomics *19*, 105-112.

113. Wen, W., Chen, W.S., Xiao, N., et al. (2015). Mutations in the Kinase Domain of the HER2/ERBB2 Gene Identified in a Wide Variety of Human Cancers. J Mol Diagn *17*, 487-495.

114. Wang, S., Zhao, Y., Song, Y., et al. (2022). ERBB2D16 Expression in HER2 Positive Gastric Cancer Is Associated With Resistance to Trastuzumab. Front Oncol *12*, 855308.

115. Lee, J.Y., Hong, M., Kim, S.T., et al. (2015). The impact of concomitant genomic alterations on treatment outcome for trastuzumab therapy in HER2-positive gastric cancer. Sci Rep *5*, 9289.

116. Chalmers, Z.R., Connelly, C.F., Fabrizio, D., et al. (2017). Analysis of 100,000 human cancer genomes reveals the landscape of tumor mutational burden. Genome Med *9*, 34.
117. Buttner, R., Longshore, J.W., Lopez-Rios, F., et al. (2019). Implementing TMB measurement in clinical practice: considerations on assay requirements. ESMO Open *4*, e000442.
118. Allgauer, M., Budczies, J., Christopoulos, P., et al. (2018). Implementing tumor mutational burden (TMB) analysis in routine diagnostics-a primer for molecular pathologists and clinicians. Transl Lung Cancer Res *7*, 703-715.
119. Jardim, D.L., Goodman, A., de Melo Gagliato, D., et al. (2021). The Challenges of Tumor Mutational Burden as an Immunotherapy Biomarker. Cancer Cell *39*, 154-173.
120. Goodman, A.M., Kato, S., Bazhenova, L., et al. (2017). Tumor Mutational Burden as an Independent Predictor of Response to Immunotherapy in Diverse Cancers. Mol Cancer Ther *16*, 2598-2608.
121. Palmeri, M., Mehnert, J., Silk, A.W., et al. (2022). Real-world application of tumor mutational burden-high (TMB-high) and microsatellite instability (MSI) confirms their utility as immunotherapy biomarkers. ESMO Open *7*, 100336.
122. McGrail, D.J., Pilie, P.G., Rashid, N.U., et al. (2021). High tumor mutation burden fails to predict immune checkpoint blockade response across all cancer types. Ann Oncol *32*, 661-672.
123. Kim, J., Kim, B., Kang, S.Y., et al. (2020). Tumor Mutational Burden Determined by Panel Sequencing Predicts Survival After Immunotherapy in Patients With Advanced Gastric Cancer. Front Oncol *10*, 314.
124. Owada-Ozaki, Y., Muto, S., Takagi, H., et al. (2018). Prognostic Impact of Tumor Mutation Burden in Patients With Completely Resected Non-Small Cell Lung Cancer: Brief Report. J Thorac Oncol *13*, 1217-1221.
125. Wang, F., Wei, X.L., Wang, F.H., et al. (2019). Safety, efficacy and tumor mutational burden as a biomarker of overall survival benefit in chemo-refractory gastric cancer treated with toripalimab, a PD-1 antibody in phase Ib/II clinical trial NCT02915432. Ann Oncol *30*, 1479-1486.
126. FDA (2020). FDA approves pembrolizumab for adults and children with TMB-H solid tumors https://www.fda.gov/drugs/drug-approvals-and-databases/fda-approves-pembrolizumab-adults-and-children-tmb-h-solid-tumors.
127. Wang, P., Chen, Y., and Wang, C. (2021). Beyond Tumor Mutation Burden: Tumor Neoantigen Burden as a Biomarker for Immunotherapy and Other Types of Therapy. Front Oncol *11*, 672677.
128. Fu, M., Huang, Y., Peng, X., et al. (2022). Development of Tumor Mutation Burden-Related Prognostic Model and Novel Biomarker Identification in Stomach Adenocarcinoma. Front Cell Dev Biol *10*, 790920.
129. Wang, K., Li, M., and Hakonarson, H. (2010). ANNOVAR: functional annotation of genetic variants from high-throughput sequencing data. Nucleic Acids Res *38*, e164.
130. Li, H., and Durbin, R. (2009). Fast and accurate short read alignment with Burrows-Wheeler transform. Bioinformatics *25*, 1754-1760.
131. Talevich, E., Shain, A.H., Botton, T., et al. (2016). CNVkit: Genome-Wide Copy Number Detection and Visualization from Targeted DNA Sequencing. PLoS Comput Biol *12*, e1004873.
132. Derouault, P., Chauzeix, J., Rizzo, D., et al. (2020). CovCopCan: An efficient tool to detect Copy Number Variation from amplicon sequencing data in inherited diseases and cancer. PLoS Comput Biol *16*, e1007503.
133. McKenna, A., Hanna, M., Banks, E., et al. (2010). The Genome Analysis Toolkit: a MapReduce framework for analyzing next-generation DNA sequencing data. Genome Res *20*, 1297-1303.
134. Robinson, J.T., Thorvaldsdottir, H., Wenger, A.M., et al. (2017). Variant Review with the Integrative Genomics Viewer. Cancer Res *77*, E31-E34.

135. Boeva, V., Popova, T., Lienard, M., et al. (2014). Multi-factor data normalization enables the detection of copy number aberrations in amplicon sequencing data. Bioinformatics *30*, 3443-3450.
136. Danecek, P., Bonfield, J.K., Liddle, J., et al. (2021). Twelve years of SAMtools and BCFtools. Gigascience *10*.
137. Molder, F., Jablonski, K.P., Letcher, B., et al. (2021). Sustainable data analysis with Snakemake. F1000Res *10*, 33.
138. Ritchie, M.E., Phipson, B., Wu, D., et al. (2015). limma powers differential expression analyses for RNA-sequencing and microarray studies. Nucleic Acids Res *43*, e47.
139. Schubert, M., Klinger, B., Klunemann, M., et al. (2018). Perturbation-response genes reveal signaling footprints in cancer gene expression. Nat Commun *9*, 20.
140. Garcia-Alonso, L., Holland, C.H., Ibrahim, M.M., et al. (2019). Benchmark and integration of resources for the estimation of human transcription factor activities. Genome Res *29*, 1363-1375.
141. Yoshihara, K., Shahmoradgoli, M., Martinez, E., et al. (2013). Inferring tumour purity and stromal and immune cell admixture from expression data. Nat Commun *4*, 2612.
142. Mayakonda, A., Lin, D.C., Assenov, Y., et al. (2018). Maftools: efficient and comprehensive analysis of somatic variants in cancer. Genome Res *28*, 1747-1756.
143. Gu, Z., Eils, R., and Schlesner, M. (2016). Complex heatmaps reveal patterns and correlations in multidimensional genomic data. Bioinformatics *32*, 2847-2849.
144. Budczies, J., Pfarr, N., Romanovsky, E., et al. (2018). Ioncopy: an R Shiny app to call copy number alterations in targeted NGS data. BMC Bioinformatics *19*, 157.
145. Motoshima, S., Yonemoto, K., Kamei, H., et al. (2018). Prognostic implications of HER2 heterogeneity in gastric cancer. Oncotarget *9*, 9262-9272.
146. Schneider, V.A., Graves-Lindsay, T., Howe, K., et al. (2016). Evaluation of GRCh38 and de novo haploid genome assemblies demonstrates the enduring quality of the reference assembly. bioRxiv, 072116.
147. Dai, M., Wang, P., Boyd, A.D., et al. (2005). Evolving gene/transcript definitions significantly alter the interpretation of GeneChip data. Nucleic Acids Res *33*, e175.
148. Piro, G., Carbone, C., Cataldo, I., et al. (2016). An FGFR3 Autocrine Loop Sustains Acquired Resistance to Trastuzumab in Gastric Cancer Patients. Clin Cancer Res *22*, 6164-6175.
149. Shi, W., Zhang, G., Ma, Z., et al. (2021). Hyperactivation of HER2-SHCBP1-PLK1 axis promotes tumor cell mitosis and impairs trastuzumab sensitivity to gastric cancer. Nat Commun *12*, 2812.
150. Newman, A.M., Steen, C.B., Liu, C.L., et al. (2019). Determining cell type abundance and expression from bulk tissues with digital cytometry. Nat Biotechnol *37*, 773-+.
151. Aran, D., Hu, Z., and Butte, A.J. (2017). xCell: digitally portraying the tissue cellular heterogeneity landscape. Genome Biol *18*, 220.
152. Wakiyama, H., Masuda, T., Motomura, Y., et al. (2018). Cytolytic Activity (CYT) Score Is a Prognostic Biomarker Reflecting Host Immune Status in Hepatocellular Carcinoma (HCC). Anticancer Res *38*, 6631-6638.
153. Karimnezhad, A., Palidwor, G.A., Thavorn, K., et al. (2020). Accuracy and reproducibility of somatic point mutation calling in clinical-type targeted sequencing data. BMC Med Genomics *13*, 156.
154. Wang, Q., Kotoula, V., Hsu, P.C., et al. (2019). Comparison of somatic variant detection algorithms using Ion Torrent targeted deep sequencing data. BMC Med Genomics *12*, 181.
155. Garofoli, A., Paradiso, V., Montazeri, H., et al. (2019). PipeIT: A Singularity Container for Molecular Diagnostic Somatic Variant Calling on the Ion Torrent Next-Generation Sequencing Platform. J Mol Diagn *21*, 884-894.
156. Liu, L., Li, Y., Li, S., et al. (2012). Comparison of next-generation sequencing systems. J Biomed Biotechnol *2012*, 251364.
157. Merriman, B., Ion Torrent, R., Team, D., et al. (2012). Progress in ion torrent semiconductor chip based sequencing. Electrophoresis *33*, 3397-3417.

158. Wong, S.Q., Li, J., Tan, A.Y., et al. (2014). Sequence artefacts in a prospective series of formalin-fixed tumours tested for mutations in hotspot regions by massively parallel sequencing. BMC Med Genomics *7*, 23.

159. Do, H., and Dobrovic, A. (2009). Limited copy number-high resolution melting (LCN-HRM) enables the detection and identification by sequencing of low level mutations in cancer biopsies. Mol Cancer *8*, 82.

160. Cai, H., Jing, C., Chang, X., et al. (2019). Mutational landscape of gastric cancer and clinical application of genomic profiling based on target next-generation sequencing. J Transl Med *17*, 189.

161. Grillo, F., Fassan, M., Sarocchi, F., et al. (2016). HER2 heterogeneity in gastric/gastroesophageal cancers: From benchside to practice. World J Gastroenterol *22*, 5879-5887.

162. Kurokawa, Y., Sugimoto, N., Miwa, H., et al. (2014). Phase II study of trastuzumab in combination with S-1 plus cisplatin in HER2-positive gastric cancer (HERBIS-1). Br J Cancer *110*, 1163-1168.

163. Gravalos, C., Gomez-Martin, C., Rivera, F., et al. (2011). Phase II study of trastuzumab and cisplatin as first-line therapy in patients with HER2-positive advanced gastric or gastroesophageal junction cancer. Clin Transl Oncol *13*, 179-184.

164. Ross, D.S., Zehir, A., Cheng, D.T., et al. (2017). Next-Generation Assessment of Human Epidermal Growth Factor Receptor 2 (ERBB2) Amplification Status: Clinical Validation in the Context of a Hybrid Capture-Based, Comprehensive Solid Tumor Genomic Profiling Assay. J Mol Diagn *19*, 244-254.

165. Wood, A.C., Zhang, Y., Mo, Q., et al. (2022). Evaluation of Tumor DNA Sequencing Results in Patients with Gastric and Gastroesophageal Junction Adenocarcinoma Stratified by TP53 Mutation Status. Oncologist *27*, 307-313.

166. Sanchez-Vega, F., Hechtman, J.F., Castel, P., et al. (2019). EGFR and MET Amplifications Determine Response to HER2 Inhibition in ERBB2-Amplified Esophagogastric Cancer. Cancer Discov *9*, 199-209.

167. Shimozaki, K., Shinozaki, E., Yamamoto, N., et al. (2023). KRAS mutation as a predictor of insufficient trastuzumab efficacy and poor prognosis in HER2-positive advanced gastric cancer. J Cancer Res Clin Oncol *149*, 1273-1283.

168. Kim, J., Fox, C., Peng, S., et al. (2014). Preexisting oncogenic events impact trastuzumab sensitivity in ERBB2-amplified gastroesophageal adenocarcinoma. J Clin Invest *124*, 5145-5158.

169. Pietrantonio, F., Manca, P., Bellomo, S.E., et al. (2023). HER2 Copy Number and Resistance Mechanisms in Patients with HER2-positive Advanced Gastric Cancer Receiving Initial Trastuzumab-based Therapy in JACOB Trial. Clin Cancer Res *29*, 571-580.

170. Rocken, C., Amallraja, A., Halske, C., et al. (2021). Multiscale heterogeneity in gastric adenocarcinoma evolution is an obstacle to precision medicine. Genome Med *13*, 177.

171. Jiao, X.D., Liu, K., Wu, Y., et al. (2021). HER2 Splice Site Mutation c.1899-1G>A as the Potential Acquired Resistance to Trastuzumab in a Patient with HER2-Positive Gastric Adenocarcinoma. Oncologist *26*, 717-721.

172. Kong, X., Zhang, K., Wang, X., et al. (2019). Mechanism of trastuzumab resistance caused by HER-2 mutation in breast carcinomas. Cancer Manag Res *11*, 5971-5982.

173. Hirotsu, Y., Nakagomi, H., Amemiya, K., et al. (2017). Intrinsic HER2 V777L mutation mediates resistance to trastuzumab in a breast cancer patient. Med Oncol *34*, 3.

174. Lei, L., Ye, W.W., Zheng, L.F., et al. (2019). A significant response to a combination of trastuzumab and vinorelbine in HER2-negative metastatic breast cancer with HER2 V777L mutation. Onco Targets Ther *12*, 2931-2936.

175. Joshi, S.K., Keck, J.M., Eide, C.A., et al. (2020). ERBB2/HER2 mutations are transforming and therapeutically targetable in leukemia. Leukemia *34*, 2798-2804.

176. Hu, C.T., Zhou, Y.C., Zu, L.D., et al. (2021). High tumor mutation burden in a patient with metastatic gastric cancer sensitive to trastuzumab: a case report. Ann Palliat Med *10*, 5846-5852.

177. Lee, K.W., Van Cutsem, E., Bang, Y.J., et al. (2022). Association of Tumor Mutational Burden with Efficacy of Pembrolizumab+/-Chemotherapy as First-Line Therapy for Gastric Cancer in the Phase III KEYNOTE-062 Study. Clin Cancer Res *28*, 3489-3498.

178. Sha, D., Jin, Z., Budczies, J., et al. (2020). Tumor Mutational Burden as a Predictive Biomarker in Solid Tumors. Cancer Discov *10*, 1808-1825.

179. Lin, Y., Luo, Y., Sun, Y., et al. (2020). Genomic and transcriptomic alterations associated with drug vulnerabilities and prognosis in adenocarcinoma at the gastroesophageal junction. Nat Commun *11*, 6091.

180. Makrooni, M.A., O'Sullivan, B., and Seoighe, C. (2022). Bias and inconsistency in the estimation of tumour mutation burden. BMC Cancer *22*, 840.

181. Han, Y., Liu, D., and Li, L. (2020). PD-1/PD-L1 pathway: current researches in cancer. Am J Cancer Res *10*, 727-742.

182. Jiang, X., Wang, J., Deng, X., et al. (2019). Role of the tumor microenvironment in PD-L1/PD-1-mediated tumor immune escape. Mol Cancer *18*, 10.

183. Lian, J., Zhang, G., Zhang, Y., et al. (2022). PD-L1 and HER2 expression in gastric adenocarcinoma and their prognostic significance. Dig Liver Dis *54*, 1419-1427.

184. Janjigian, Y.Y., Kawazoe, A., Yanez, P., et al. (2021). The KEYNOTE-811 trial of dual PD-1 and HER2 blockade in HER2-positive gastric cancer. Nature *600*, 727-730.

185. Lv, H., Zhang, J., Sun, K., et al. (2020). Expression of Human Epidermal Growth Factor Receptor-2 Status and Programmed Cell Death Protein-1 Ligand Is Associated With Prognosis in Gastric Cancer. Front Oncol *10*, 580045.

186. Beer, A., Taghizadeh, H., Schiefer, A.I., et al. (2020). PD-L1 and HER2 Expression in Gastroesophageal Cancer: a Matched Case Control Study. Pathol Oncol Res *26*, 2225-2235.

187. Attia, S., Abd El Hafez, A., Abdel-Aziz, A., et al. (2022). Prognostic Value of PD-L1 Immunohistochemical Marker in Gastric Carcinoma and Its Correlation with HER2 Status. Asian Pac J Cancer Prev *23*, 1433-1444.

188. Bang, Y.J., Kang, Y.K., Catenacci, D.V., et al. (2019). Pembrolizumab alone or in combination with chemotherapy as first-line therapy for patients with advanced gastric or gastroesophageal junction adenocarcinoma: results from the phase II nonrandomized KEYNOTE-059 study. Gastric Cancer *22*, 828-837.

189. Muro, K., Chung, H.C., Shankaran, V., et al. (2016). Pembrolizumab for patients with PD-L1-positive advanced gastric cancer (KEYNOTE-012): a multicentre, open-label, phase 1b trial. Lancet Oncol *17*, 717-726.

190. Angell, H.K., Lee, J., Kim, K.M., et al. (2019). PD-L1 and immune infiltrates are differentially expressed in distinct subgroups of gastric cancer. Oncoimmunology *8*, e1544442.

191. Wang, Y., Zhu, C., Song, W., et al. (2018). PD-L1 Expression and CD8(+) T Cell Infiltration Predict a Favorable Prognosis in Advanced Gastric Cancer. J Immunol Res *2018*, 4180517.

192. Ito, S., Masuda, T., Noda, M., et al. (2020). Prognostic Significance of PD-1, PD-L1 and CD8 Gene Expression Levels in Gastric Cancer. Oncology *98*, 501-511.

193. Kwak, Y., Koh, J., Park, Y., et al. (2020). Differential prognostic impact of CD8(+) T cells based on human leucocyte antigen I and PD-L1 expression in microsatellite-unstable gastric cancer. Br J Cancer *122*, 1399-1408.

194. Thompson, E.D., Zahurak, M., Murphy, A., et al. (2017). Patterns of PD-L1 expression and CD8 T cell infiltration in gastric adenocarcinomas and associated immune stroma. Gut *66*, 794-801.

195. Ning, Z.K., Hu, C.G., Huang, C., et al. (2020). Molecular Subtypes and CD4(+) Memory T Cell-Based Signature Associated With Clinical Outcomes in Gastric Cancer. Front Oncol *10*, 626912.

8 Supplement
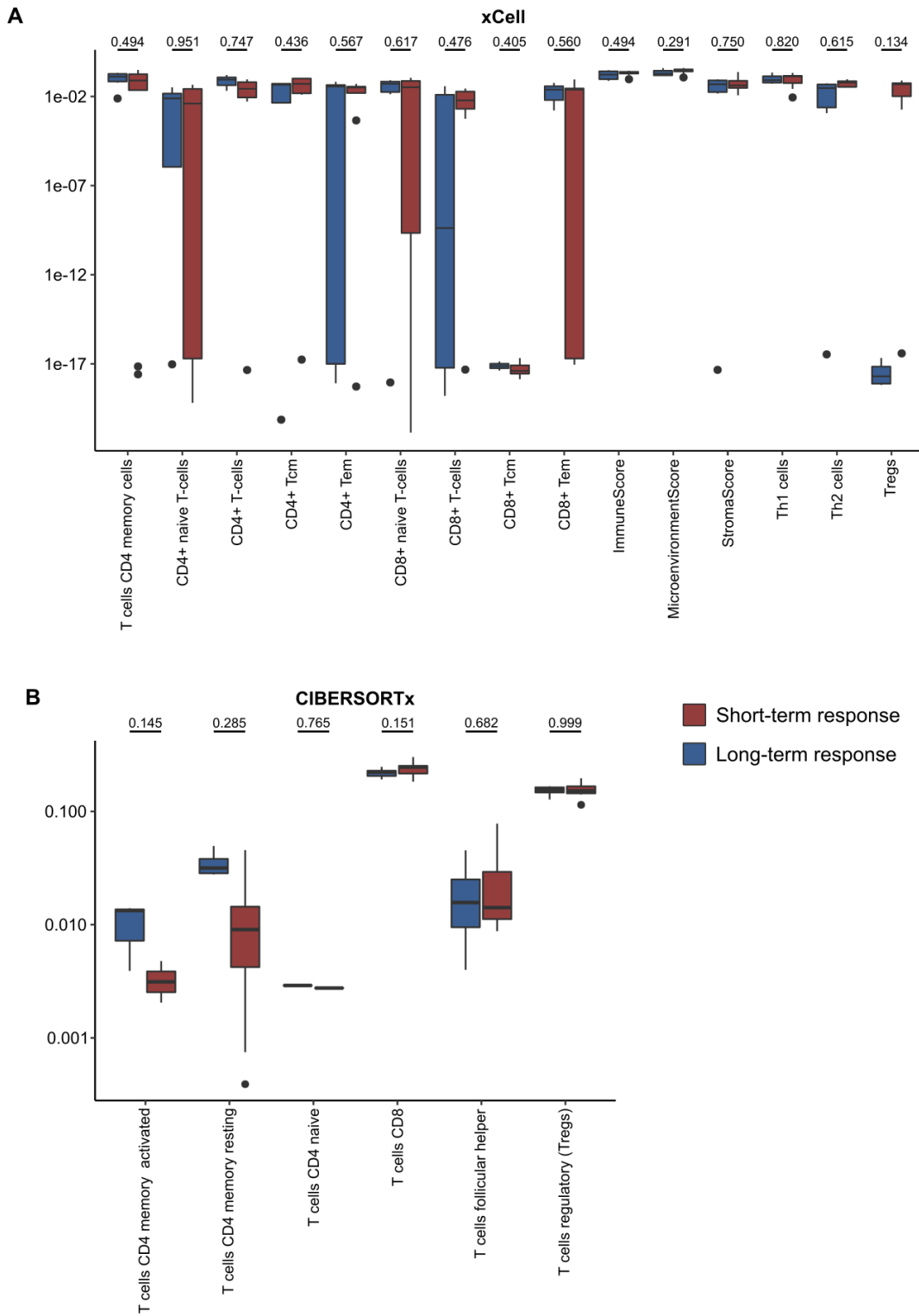
Supplementary Figure 1 | **Comparison of T-cell scores between patients with long-term (blue) and short-term response (red) using A) xCell and B) CIBERSORTx**
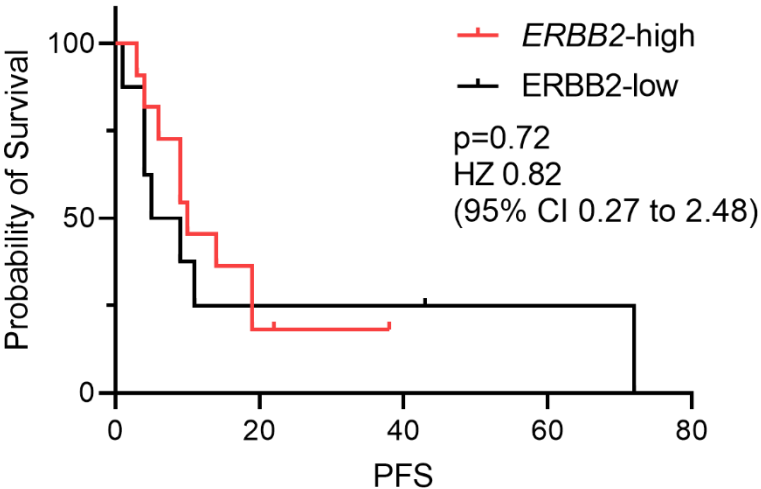
Supplementary Figure 2 | Survival analysis of ERBB2-high and ERBB2-low patients
Kaplan-Meier curve comparing the survival benefit of ERBB2-high and ERBB2-low patients. The ERBB2-high group is defined by an *ERBB2* CN ≥ 5.5. The Mantel-Haenszel hazard ratio (HR) was applied.

Supplementary table 1 | Sample overview with clinical characteristics and therapy details

5FU: 5-fluorouracil; CTx: chemotherapy; FLO: 5FU/leucovorin/oxaliplatin; FLOT: 5FU/leucovorin/oxaliplatin/docetaxel; GEJ: gastroesophageal junction; ND: not determined; PLF: cisplatin/leucovorin/5FU;

	Patient ID	Gender	Age at diagnosis	Location	PFS	HER2 status	PD-L1 status	Trastuzumab + CTx	Duration (days)	Trastuzumab maintenance	Duration (days)
Long-term responder	Pat1	m	59	GEJ	72	3+	positive	PLF + Trastuzumab	190	Trastuzumab mono	2011
	Pat2	m	45	stomach	38	2+	positive	FLOT + Trastuzumab	222	Trastuzumab mono	0
	Pat3	m	56	GEJ	19	3+	positive	FLOT/FLT + Trastuzumab	183	5FU + Trastuzumab / Trastuzumab mono	378
	Pat4	m	61	GEJ	19	2+	positive	FLOT/FLO + Trastuzumab	161	5FU + Trastuzumab	434
	Pat5	m	62	stomach	43	3+	negative	FLOT/FLO + Trastuzumab	177	5FU + Trastuzumab	769
	Pat6	m	59	stomach	14	3+	positive	FLOT/FLT + Trastuzumab	222	5FU + Trastuzumab	197
	Pat7	m	74	stomach	22	3+	positive	FLOT + Trastuzumab	145	5FU + Trastuzumab / Trastuzumab mono	496
Short-term responder	Pat8	m	73	stomach	4	2+	negative	FLOT/FLO + Trastuzumab	92	5FU + Trastuzumab	56
	Pat9	m	70	GEJ	9	3+	negative	FLO + Trastuzumab	113	5FU + Trastuzumab	43
	Pat10	m	71	stomach	4	3+	negative	FLO + Trastuzumab	111	5FU + Trastuzumab	21
	Pat11	m	72	stomach	10	3+	negative	FLO + Trastuzumab	111	5FU + Trastuzumab	ND
	Pat12	m	67	GEJ	5	2+	negative	FLOT + Trastuzumab	42	Trastuzumab mono	84
	Pat13	m	77	stomach	4	3+	negative	FLO + Trastuzumab	44	5FU + Trastuzumab	77
	Pat14	f	75	GEJ	11	3+	negative	FLO + Trastuzumab	84	5FU + Trastuzumab / Trastuzumab mono	196
	Pat15	f	72	stomach	6	2+	positive	FLOT + Trastuzumab	14	5FU + Trastuzumab	15
	Pat16	m	51	GEJ	9	3+	positive	FLOT + Trastuzumab	140	5FU + Trastuzumab	125
	Pat17	m	59	GEJ	3	3+	positive	FLO + Trastuzumab	84	Trastuzumab mono	21
	Pat18	f	59	GEJ	9	2+	negative	FLOT + Trastuzumab	43	Trastuzumab mono	190
	Pat19	f	64	GEJ	1	2+	negative	FLO + Trastuzumab	42	Trastuzumab mono	0
Control Samples	Nor1	m	61	stomach	ND	ND	ND	ND	ND	ND	ND
	Nor2	f	61	stomach	ND	ND	ND	ND	ND	ND	ND
	Nor3	m	62	stomach	ND	ND	ND	ND	ND	ND	ND
	Nor4	m	62	stomach	ND	ND	ND	ND	ND	ND	ND
	Nor5	f	63	stomach	ND	ND	ND	ND	ND	ND	ND

9 Curriculum Vitae

PERSONAL DETAILS

Name and first name:	Isabel Porth
Date of birth:	29th June 1993
Place of birth:	Darmstadt (Germany)

_____

EDUCATION

2003 – 2012	Eleonorenschule Darmstadt
15.06.2012	Abitur (1.4)

_____

ACADEMIC EDUCATION

WS 2012/2013	University of Heidelberg, Heidelberg Bachelor of Science Molecular Biotechnology Thesis: Synthesis and characterization of a localizable, fluorescent calcium indicator for live cell application
31.08.2015	Bachelor of Science (2.1)
10/2015 – 04/2019	Master of Science Molecular Biotechnology University of Heidelberg
2018 – 04/2019	Thesis: "Synthetic astrocyte-specific promoter for AAV-mediated gene expression"
04.04.2019	Master of Science (1.1)
Since 02/2020	Doctoral studies

10 Acknowledgement